Universidade de Lisboa

Faculdade de Ciências

Departamento de Física

Design and Fabrication by Inkjet Printing of Electrodes for Electromyography

João Pedro Alves Martins

Dissertação

Mestrado Integrado em Engenharia Biomédica e Biofísica

Engenharia Clínica e Instrumentação Médica

Setembro 2013

Universidade de Lisboa

Faculdade de Ciências

Departamento de Física

Design and Fabrication by Inkjet Printing of Electrodes for Electromyography

João Pedro Alves Martins

Dissertação orientada por

Dr. Ana Teresa Pereira
Prof. Dr. Hugo Ferreira

Mestrado Integrado em Engenharia Biomédica e Biofísica

Engenharia Clínica e Instrumentação Médica

Setembro 2013

Resumo

A utilização de impressoras de jacto de tinta (*inkjet printers*) tem dado um enorme contributo na indústria electrónica reduzindo as dimensões dos componentes e introduzindo processos de fabricação mais rápidos e menos dispendiosos. Uma das grandes vantagens deste método de fabricação é a facilidade de *design* dos circuitos, a deposição de materiais directamente no substrato sem haver contacto, a sobreposição de desenhos impressos e a versatilidade de materiais utilizados, tirando o maior partido das suas características.

Duas formas de tirar partido das funcionalidades de uma impressora *inkjet*, em engenharia biomédica, é, por um lado, desenvolver circuitos eléctricos desenhados especialmente para aquisição de sinais fisiológicos. Esses circuitos, aliados às capacidades da impressão por jacto de tinta, poderão resultar em electrónica flexível com materiais com elevada biocompatibilidade, promovendo desta forma uma próxima interacção com o corpo humano. Por outro lado, as aplicações da impressora *inkjet* podem levar ao desenvolvimento de eléctrodos impressos enquadrando-os no conceito de pele electrónica, isto é, integrar dispositivos electrónicos utilizando características da pele humana (flexibilidade, extensibilidade e compatibilidade). Assim, o principal objectivo deste trabalho é fabricar, utilizando esta técnica, eléctrodos com a capacidade de medir sinais electromiográficos dos músculos responsáveis pelo movimento da mão e dedos. A fim de utilizar as potencialidades da tecnologia *inkjet*, os eléctrodos devem obter medições congruentes do ponto de visto fisiológico e devem se mostrar vantajosos face aos, já convencionais, eléctrodos descartáveis.

A finalidade da construção destes eléctrodos deverá preencher a carência que os eléctrodos convencionais possuem, de não serem flexíveis e de não serem utilizados durante largos períodos de tempo. As vantagens extraídas de eléctrodos impressos poderão ainda ser mais vastas não só a nível económico, pela construção de eléctrodos *low-cost*, mas também a nível de desempenho, biocompatibilidade e *design*, com o desenvolvimento de eléctrodos finos, *paper-like* e passiveis de acoplarem circuitos electrónicos também impressos.

O desenvolvimento do trabalho apresentou uma variedade de tarefas, com inicio na aprendizagem dos conceitos e métodos de funcionamento da impressora *Fujifilm Dimatrix 2831 Materials Printer*. Esta impressora, utilizada para obtenção de todos os eléctrodos e circuitos aqui referidos, possui uma tecnologia *drop-on-deman* coordenada por material piezoeléctrico, conseguindo uma resolução até $\sim$5 μm. As voltagens induzidas a este material tem um enorme impacto na formação das gotas de tinta, e por isso a uma boa qualidade de impressão. No entanto, outros factores como a viscosidade

da tinta e a tensão de superfície também desempenham importantes papeis para aumento da qualidade de impressão.

As tarefas seguintes incluíram a optimização dos procedimentos para tratamento dos substratos de forma a que a deposição da tinta de prata fosse óptima. Os substratos utilizados neste trabalho foram: papel fotográfico, biocelulose e polidimetilsiloxano (PDMS). Também os métodos de impressão tiveram que ser optimizados controlando a velocidade e a direcção da deposição das gotas de tinta. Uma vez que foi apenas utilizado um tipo de tinta prata, uma dispersão de nanoparticulas de prata, foi utilizada a mesma velocidade de deposição das gotas, 10 m/s com temperatura do tinteiro constante, de 30°C. Por fim, houve necessidade de melhorar o processo de sinterização que visa a remoção do solvente e outras substâncias presentes na tinta de prata, e que tem enorme impacto na resistividade final do padrão impresso. Um bom processo de sinterização faz com que as nanoparticulas de prata tenham um forte contacto entre elas, aumentando consideravelmente a conductividade do material. Para este fim, foi testada a sinterização térmica padrão e introduzida um novo método, a sinterização eléctrica cuja aplicação de uma diferença de potencial permite a passagem de corrente eléctrica gerando calor localmente.

Para impressão de eléctrodos, os seus *designs* foram adaptados às características dos materiais, sendo que, por exemplo, para materiais mais flexíveis foram implementadas conexões serpenteadas entre pequenos eléctrodos. Para outros substratos, como o papel fotográfico, foi optado um *design* semelhante ao dos eléctrodos convencionais para obter melhor termo de comparação. Já para aplicação de sinterização eléctrica, optou-se por um design que consiste num único filamento para que seja possível a aplicação de uma diferença de potencial em ambas as extremidades. Durante o aperfeiçoamento dos eléctrodos, foi elaborado uma série de estudos acerca das características dos mesmos (resistividade e impedância) e as suas medições foram comparadas com os resultados obtidos, em condições semelhantes, aos eléctrodos tipicamente utilizados em ambiente clínico. Como resultados de medições de sinais electrocardiográficos, os eléctrodos impressos em papel fotográfico mostraram-me vantajosos quanto à morfologia do traçado, pois o termo de comparação foi similar aos obtidos por eléctrodos convencionais. No estudo de sinais electromiográficos, os eléctrodos impressos em biocelulose e papel fotográfico tiveram taxas de sinal-ruído abaixo das obtidas pelos tradicionais eléctrodos de uso clínico. Ainda assim, os dados dos eléctrodos impressos podem ser utilizados para captação de sinais fisiológicos pois foi possível demonstrar a extracção de informações acerca do movimento dos músculos esqueléticos e cardíaco. Contudo, não foi possível a obtenção de sinais fisiológicos utilizando eléctrodos impressos em PDMS. Devido a

uma fraca adesão da tinta de prata à superfície do substrato, a tinta era removida do eléctrodo quando havia contacto entre o eléctrodo e a pele.

Tarefas intermédias incluíram a impressão de pequenos circuitos electrónicos, nomeadamente um circuito impresso cuja principal função é a leitura e tratamento (amplificação e filtragem) de sinais electrocardiográficos. Dois outros circuitos, mais simples, foram impressos: um díodo emissor de luz e um sensor de luz. Todas as pistas de condução de ambas as camadas foram impressas com prata em papel fotográfico e os componentes electrónicos foram colados com cola de prata. A optimização deste processo poderá trazer enormes vantagens pela possibilidade de construção de circuitos electrónicos flexíveis e finos com eléctrodos incorporados.

Por fim, a última tarefa inclui processamento de sinal a qual inclui a implementação de algoritmos em ambiente *MatLab* para extracção de movimentos dos músculos do antebraço. Com a informação extraída por três movimentos distintos da mão foi provado que os eléctrodos impressos podem ser usados para posterior reconhecimento de padrões. A distinção dos três movimentos foi feita com sucesso, sobretudo para os eléctrodos impressos em biocelulose e para os eléctrodos de baixa resistividade em papel fotográfico.

Este trabalho também abriu portas para investigações futuras em que mais substratos e tintas podem ser testadas e mais componentes podem ser integrados aos já aqui desenvolvidos. Desta forma, a tecnologia *inkjet* pode contribuir com a sua versatilidade para a inovação nos campos electrofisiologia e das interacções homem-máquina.

Abstract

Inkjet technology has advantages as a fabrication method when compared to other conventional procedures. Inkjet technology allows the deposition of several materials directly with non contact with it, mask-less and the possibility of printing over a previous printed pattern [1]. Due its versatility of inks (conductive, polymers and organic) and substrates, direct deposition of materials with high precision ($\sim$5 μm) using simple methods, this technique shows a high potential as a fabrication method. Despite the wide range of applications of inkjet printing in electronics, a lack of intend for printing devices for collecting biosignals. The subject of the work presented was the first step towards the development of a inkjet device for a close contact with skin for collecting biosignals.

One way to apply the functionalities of an inkjet printer, in biomedical engineering, is developing printed electrodes introducing electronic skin concept, i.e., implement electronic devices using features of electronic skin (flexibility, extensibility and compatibility). Thus, the major goal of this work was develop, using this technique, electrodes capable of measuring electromyographic signals from the forearm's muscles responsible to move hand and fingers. In order to use the potentials of inkjet technology, these electrodes must obtain congruent measurements and should prove advantageous when compared to the standard electrodes. The versatility of inkjet printing allowed to print electrodes, using a inkjet printer DMP-2831, onto substrates that included photographic paper, biocellulose and PDMS and test the performance of different designs: standard flat discs, spiked, filamentary and serpentine array of small electrodes.

This thesis presents the development of tasks that includes the design and choice of materials, optimization of printing and sintering procedures, printing electronic circuits and ends with signal processing. During the optimization of the electrodes measurements of resistivity and impedance were performed to understand the behaviour and characteristics of them. Finally, a linear discriminant analysis was used to successfully distinguish between three hand movements.

Acknowledgements

It is my pleasure to acknowledge all the persons that made this work possible and permitted me to carry it until the end with the same enthusiasm.

Firstly, I would like to express my sincere gratitude to my supervisors Ana Teresa Pereira and Hugo Ferreira for the continuous support, their availability to teach, patience, motivation, enthusiasm, and immense knowledge. Their guidance helped me through all the time of this work.

I would like to acknowledge Prof. Luís Alcácer, Ana Luísa, João Bastos, Tânia Braz, Graça Brotas and all members of Organic Electronics Group, Instituto de Telecomunicações, by making me feel at home from the first day, for their scientific and technological teaching and because their friendship made work easier. My thanks also goes to André Lourenço, Hugo Silva and Ana Priscila from Pattern and Image Analysis Group, Instituto de Telecomunicações, for their enthusiasm and belief in my work.

I would like to acknowledge my family, my parents Maria José and Lidio, my brother Edgar and my grandmother, Maria for always being present my entire life. To my parents in law, Fernando and Manuela, for their practical help and comprehension. Last but not least, I finish by thanking to the love of my life, Joana, for her unconditional support and encouragement.

I would like to acknowledge to FCT for partly funding this work with the following project reference PTDC/CTM/102144/2008.

Contents

List of Figures

List of Tables

Chapter 1

Introduction

1.1 Inkjet Technology

Nowadays, the standard fabrication procedures of electric circuits, as screen printing, photolithography and electrotyping use masks techniques to create different regions on the substrates: conductive and non conductive regions. Those techniques might have disadvantages in terms of efficiency because are slow procedures with, sometimes, the use of several different materials with a high waste of materials that are deposited; environmental whereas some procedures require the usage of polluting solvents to mask removal. Conventional techniques have lack of simplicity of the entire procedure [2], and lack of application of organic electronics where the compatibility between solvents for the photoresist and the materials that is being deposited is critical. Even simpler techniques like transfer printing require previous procedures as lithography to build the molds.

Therefore was a need to create a simpler fabrication procedure in which a conductive material deposition with a certain shape and dimension directly on a substrate: *inkjet printing*.

Since the invention of the letterpress with movable lead type, printing technology has kept up the development of computerized information. This technological breakthrough lead to the abandonment of physical printing masters or printing plates for every type of information to be produced. Therefore conventional printing had key disadvantages as large financial and time investments to produce printing masters and complex working steps [3].

Unlike conventional printing technology, digital printing didn't need pre-manufactured masters or a significant impact force on the substrate to transmit information. The

solution for the non use of printing masters was achieved by an accurate positioning of a small volume of a liquid droplet directly on the substrate [3].Today, inkjet technology is a familiar method for printing text and images onto porous surfaces like paper, directly from computer software, as a sort of writing [4].

Using the same principle as the graphic arts industry, electronic print technology adopted a similar way to deposit different materials onto different substrates besides paper [5]. This free-form fabrication method has been used for building three-dimensional structures and has being explored as a way of printing electrical and optical devices [6].The inkjet is a material's conservation and deposition technique only used for liquid phase materials, where the solute is either dissolved or dispersed in a solvent. The versatility of material inkjet allows the use of organic (polymers, proteins or nucleic acids) and inorganic inks (silver, gold,...) which can be used to develop electronic devices. The printer's versatility allied to the simplicity of the procedures ensures a great technology for developing either electronic and non electronic devices.

The possibility of printing materials using inkjet technology brought several advantages to the manufacturing procedures conventional used, such as photo-lithography and transfer printing. Comparing with those standard techniques for patterning thin films or bulk substrates with high precision, some differences stand out. The appeal of inkjet technology lies in being a non contact printing which implies a lesser risk of material's contamination, it is a mask-less approach which makes an intuitive procedure, a low temperature process and an addictive procedure, i.e., it is possible to print over a previous printed pattern [5].

Inkjet material deposition printers had the same basic principle of digital printing namely the absence or presence of information at each pixel of the picture (computer data), enabling the deposition of material on a specific localization on a substrate [3]. For these reason, direct write allows the use of thin and flexible substrates but also stiff materials. However, the need for a versatile inkjet technology for forming multilayer devices raises the number of materials problems that before were not applied [6], such as surface tension or the hydrophobicity of the substrate's surface.

The versatility of printer continues on designs because the structures' designs are made digitally allowing to change it with ease and instantly. Designs could be made with small dimensions to build, for instance, micro-structures but also large patterns with several centimetres. Material inkjet printers have compatibility with low and large printing areas so is easy to scale patterns to a large area manufacturing. Another attractive feature is the low cost procedure due to the reduction of wasted materials. This feature is implicit on how the printer works because ink's droplets are only deposited where

	Photolitography	Shadow Mask	Micro-contact Printing	Inkjet Printing
Cost	Extremely high	Low	Medium	Low
Area	Extremely small	Large	Medium	Large
Efficiency	Low	High	High	High
Temperature	High	Low	Medium	Low and high
Mask	Needed	Needed	Needless	Needless
Resolution	Extremely high	Low	High	High
Compatibility with polymer	Bad	Good	Bad	Excellent
Flexibility	Bad	Bad	Bad	Good, digital lithography
Compatibility with Roll to roll	Bad	Medium	Good	Good
Material consuming	Large	Medium	Low	Low
Environment	Clean room, vibration isolation	Low	Medium	Low
Process	Multi-step	Multi-step	Multi-step	All in one
Mode of action	Non contact	Contact	Contact	Non contact

TABLE 1.1: Comparison between patterning techniques [4].

programmed to, whereas in lithography processes the material is deposited over the entire area of the substrate and then removed in the areas where is not desired.

The possibility of printing materials using inkjet technology brought several advantages to the manufacturing procedures conventional used, such as photo-lithography, transfer printing, shadow masks or micro contacted printing (see Table 1.1). The capability of inkjet printing provides a high potential for simplification of fabrication process with small costs.

The main process of inkjet printing involves ink's storing on a cartridge before the ejection of an exact quantity of ink throw a noozle. Although this is the main principle of function, inkjet printing technology can be classified into two major working processes: continuous inkjet (CIJ) and drop on demand (DoD) technology (see Figure 1.1). Each working process has several minor categories which are classified according to the principle used to produce droplets. [7].

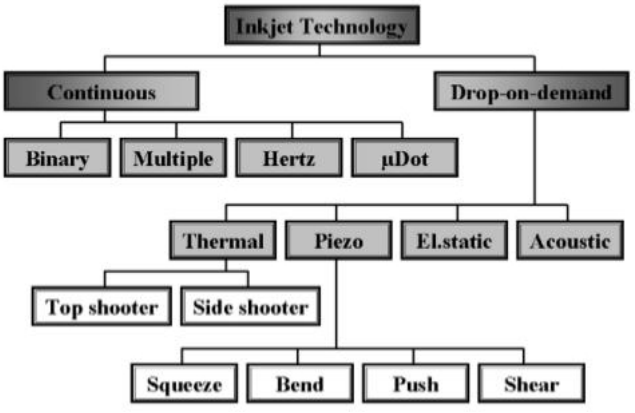

FIGURE 1.1: Classification of inkjet printing technologies [7].

1.1.1 Continuous inkjet

As the name of inkjet category implies, the continuous inkjet (CIJ) process starts by forming ink drops from a continuously flowing jet of ink that is driven from a nozzle. The process starts with a high-pressure pump that directs liquid ink from a reservoir forcing the liquid to leave throw a nozzle as a form of jet (see Figure 1.2). Imposing a regular disturbance with a defined frequency causes the jet to break up into small ink drops and a uniform stream of drops is produced. If there is no regular disturbance with, for instance, a piezoelectric transducer, small perturbations at a particular wavelength begin to grow and naturally develop along the jet causing the jet to break up. If not controlled, the break up point and the size of formed drops are unpredictable therefore useless. Some parameters are important to calculate the break up point, since it is proportional to nozzle diameter, jet velocity, ink density and ink viscosity [8].

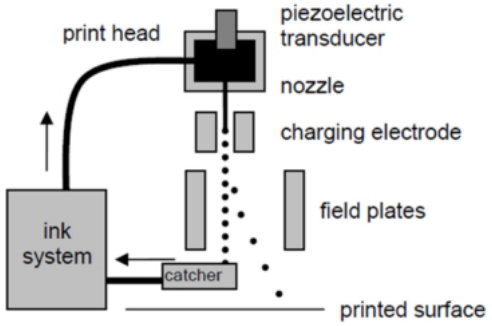

FIGURE 1.2: Schematic diagram of a single-jet of continuous inkjet printer [8].

During a controlled break up of jet, certain drops from the stream are selected individually for printing inducing electrical charge by having an electrode nearby held at an appropriate potential. When a positive voltage is applied to the charge electrode, the induced charge is retained on the drop resulting in the drops taking a negative charge proportional to the voltage applied [8].

Then the drops pass through a fixed electric field causing a deflection of the charged drop according to their charge while the uncharged drops are captured for reuse. That is the reason why is commonly used electrically conducting ink on CIJ technology. The degree of the drop deflection is determined by the electric field strength which in turn depends on the voltage applied and the distance between the field plates. This way, is produced one line of the image to be printed. By moving the substrate, several lines are successively printed forming the desired image or text. In a more complex system, more jets can be couple to obtain a faster printing [7].

Currently, this type of printing is used to apply some information, as batch codes, dates or product names on individual packages and product on a production line. Yet,

continuous inkjet printing is not used in print electronics as the recycling process after exposure to the environment might result in contamination of the ink [3]. The major advantages are the high speed printing and the existence of a relative long distance between print head and the substrate. From a mechanical point of view, this technique is also advantageous because the risk of clogging the nozzle is too remote due to the continuously flow of ink through it, which allows the use of volatile solvents that dry faster. Finally, CIJ has also the advantage of being able to be used with non-planar geometry substrates. [3].

Although CIJ is a very mature technique and widely used in industry, has troubles fabricating very delicate and high resolution patterns. The main problem is the creation of undesired satellite drops when the continuous jet is breaking up. Is common to find smaller, satellite drops that, depending on inks characteristics, either recombine with the main drop or be deflected to unwanted places causing poor printing resolution or even printing failure. To fix this, attempts to deliberately create and use the satellite drops for high resolution patterning [8].

1.1.2 Drop on demand

Instead of continuously firing drops it is also possible to create drops only when an actuation pulse is provided, the drop-on-demand (DoD)system. Major advantages of DoD printers over CIJ printers include the fact that there is no need for complicated hardware for break up the jet, charging electrodes, deflection plates, capture and re-circulation systems and high pressure pumps. That is a reason why DoD technology in the form of inkjet printing has demonstrated a rapid growth during the last two decades [9].

Drop-on-demand print heads usually have an array of nozzles each of which ejects ink drops only when are required, reducing the fluid's waste and contamination. An actuator creates a rapid change in the cavity volume and initiates an impulse that propagates pushing a drop of fluid outwards through the nozzle (see Figure 1.3). For the drop overcome the decelerating action of ambient air, its velocity must be few meters per second which depends directly on the amount of kinetic energy transferred [8]. Even so, the entire process of forming drops is in some ways simpler and more intuitive than CIJ system.

Although other methods have been explored, the two most common means to trigger the ejection of fluid is using a heater pad (thermal inkjet) and using the distortion of a piezoelectric elements (piezoelectric inkjet).

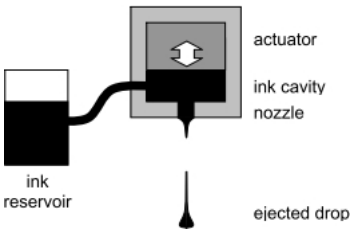

FIGURE 1.3: Schematic diagram of a drop-on-demand print head [8].

1.1.2.1 Thermal inkjet

A thermal inkjet print head typically contain a series of nozzles where behind each exists a tiny firing chamber where the ink ejection process occurs. Each firing chamber consists of a substrate, typically a silicon substrate, a thin film heating resistor, made of tantalum aluminum ($TaAl$) by photolitography, ink barriers and a nozzle [10].

Various conductive and insulation layers as well as a resistive layer generating heat are patterned into the substrate. When a few microseconds pulse of electric current passes through the resistive layer, it rapidly heats up raising the plate temperature to about 300^oC [6]. This heat energy causes the boiling of the ink forming a bubble of vapour, which results in the formation and ejection of a drop. As the bubble continues to expand and fill the chamber, ink in the chamber is driven out of the nozzle, forming a droplet. After, approximately 10 to 20 μs, the bubble collapses, and the drop of ink is detached from nozzle plate. Then, through a channel new ink enters the chamber refilling it and the procedure is repeated to form a new droplet [7].

The inks are usually water-based and must have a volatile component to form the bubble, otherwise droplet ejection cannot occur. The main problem is to avoid clogging of the nozzle by dried ink. For this reason, the range of ink solvents that could be used in thermal inkjet are less broader then piezoelectric inkjet. Also the high temperature can cause damage to either the ink or the materials around the firing chamber. To minimize chamber's damage and because the heater layer is normally very fragile, other layers are patterned on top of the heater in order to protect it from thermal and mechanical damage by bubble collapse [3].

1.1.2.2 Piezoelectric inkjet

A piezoelectric inkjet system, as the name implies, uses a piezoelectric material, as actuator, to convert applied externally electrical energy into mechanical deformation of an ink chamber. Behind each nozzle is a piezoelectric material, typically lead zirconium titanate (PZT), instead of a heating element. A chamber filled with a fluid is contracted

due to the displacement of the walls in response to application of an external voltage. The result of a sudden volume change are pressure waves that begin to propagating throughout the capillary [11].

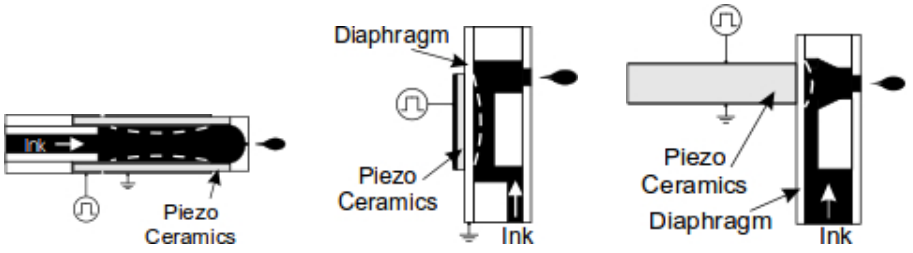

(a) Squeeze (b) Push (c) Bend

FIGURE 1.4: Three types of piezoelectric inkjet.

Depending on the piezoelectric deformation mode, this type of technology can be classified into four types: squeeze, shear, push and bend. The squeeze mode was the first to be invented and the tubes with a diameter of about 1 mm are radially polarized [7]. When it is desired to have a droplet ejected, a short time voltage pulse is applied and the contraction of the transducer is made radially. The result is a smaller tube that squeezes the ink and a droplet is expelled. Push and bend modes have the same principle, in both the electric field is generated between the electrodes parallel to the polarization of the piezoelectric material. Applying a voltage to the piezoelectric plate results in a contraction of the plate thereby causing the diaphragm to bend inwardly into the pressure chamber. This bending, once more, applies pressure on the fluid inside the chamber forcing the droplet to come out. In a similar way, in push mode is applied a voltage that expand the piezoelectric material towards the nozzle. The piezoelectric material push a thin diaphragm, to prevent undesirable interaction between the actuator and the ink, which pushes the ink through the orifice [7]. In a shear mode system, the electric field is designed to be perpendicular to the piezoelectric material. If the electric field is applied parallel to the poling field, then the piezoelectric material reacts in extension mode, i.e., the material lengthness in one dimension and shortness in the other. This was the principle to push and bend mode. But if the electric field is applied perpendicular to the poling field, the piezoelectric material reacts in a shear mode which allows a change in only one dimension. This is the main operation principle of print heads in a shear mode [12].

The base plate of this print heads contains multiple ink channels in which metal electrodes are deposited on the upper half of both sides of the channel wall. A cover plate is bonded on the upper surface of the walls, and a nozzle plate is bonded on the front surface of the substrat, and the ink is stored in a common chamber. When an electrical

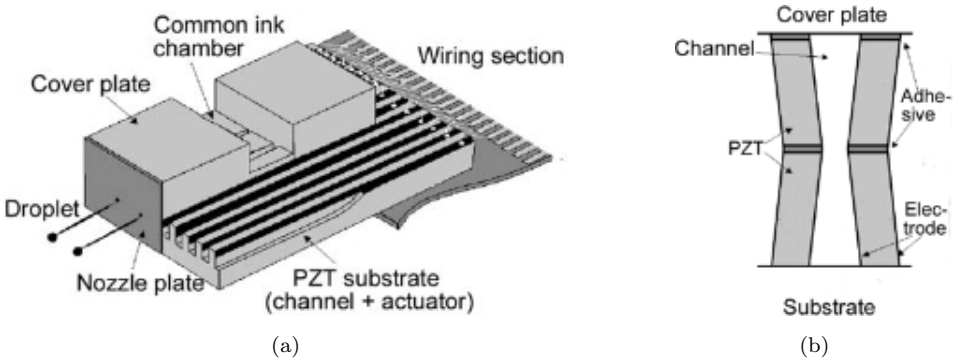

FIGURE 1.5: Piezoelectric inkjet with shear mode. (a) Scheme of a piezoelectric inkjet print head with shear mode. (b) Cross section of a channel (PZT). [13].

field is applied in the direction orthogonal to the polarization of the piezoelectric material, PZT are deformed increasing the channel volume which makes the ink enter the channel. After the generation of the pressure wave, it is propagated between nozzles and the common chamber, changing the pressure consecutively along the channel. When the negative pressure reaches the peak, the voltage is applied in the direction in which the channel volume is decreased. At this point, pressure inside the channel is greater than atmospheric pressure and a droplet is ejected [13].

In short, the size and velocity of the drop ejected from the nozzle is controlled by piezoelectric materials which are linearly dependent of the voltage. However, fluids properties, namely, ink viscosity could be a limiting factor because the ejection of the drop depends of shock waves that propagate through the ink.

Inkjet images are normally formed by printing several drops at discrete localizations on the substrate. The minimum space between two drops determine the resolution of the printer [8]. Printing thin lines or small dots is limited by the size of the drop, which depends on jetting conditions, the ink, the substrate and nozzle diameter. Intrinsic printer properties has influence on the final look of the printed structure, especially when very small dimensions are required (few micrometers). One important property for every type of inkjet is the nozzle dimension. Intuitively, the nozzle diameter should be the minimum diameter of the drop. The decrease of this component diameter could be possible and advantageous causing an increase of resolution, but would be disadvantageous because it would involve more complicated fabrication processes, thereby increasing the cost. Further, smaller nozzles are easier to clog causing a reduction of reliability and repeatability of all jetting process [5].

After leaving the nozzle, the droplet falls, at last, under action of gravity and air resistance until it reach the substrate. Finally, the drop of ink spreads on the substrate and starts to dry due to solvent evaporation [5]. During the spreading until the final form

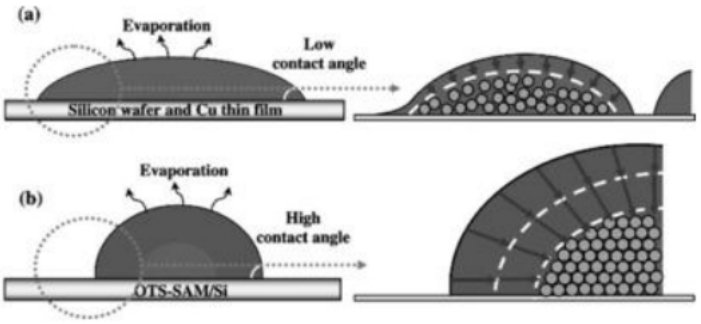

FIGURE 1.6: Scheme of an ink drop behaviour in contact with (a) a hydrophilic surface and (b) extremelly hidrophobic surface [11].

of the printed droplet, drop motion is conditioned by two main factors: surface tension forces and, once more, ink viscosity. Substrate characteristics might also interfere in final printed drop dimensions, since in a hydrophobic surface the drop spreads much less than in a hydrophilic surface (see Figure 1.6). The combination between these two factors dictate the final form and dimension of the printed droplet [11].

1.2 Electrodes

Bioelectric phenomena, associated to several physiological processes, are related with electric conductivity mechanisms which involves ions as charge transporters. Therefore, to measure a physiological signal is necessary an interaction with those ionic charges and translate them to electric current for further processing by the electronic components. This function is performed by the electrode, which allows the interaction between electrons on the electrode and the solution that contains the ions present in the body [14]. The interaction between the two elements allowing the transference of charge is made through oxidation-reduction reactions, operating as half of a galvanic cell [15].

The ions from the body contained in the solution are, mostly, cations thereby oxidate in the presence of electrode's metal, which means that the ions loose electrons and return to the solution with a positive charge. When there is contact, the metal becomes reduced due to the early release of electrons. Consequently, on the surface of the electrode is, at this moment, a positive charge solution due to the loss of electrodes and a negative charge metal due to the gain of electrons. Therefore, a difference of potential was formed. This voltage is a characteristic of the metal on the surface of the electrode [14].

From an electrochemistry point of view, electrodes are included into two major categories: polarizable and non-polalarizable. Ideally, polarizable electrodes allow the passage of current between the solution and the electrode by means of a variation on charge

distribution of the solution near the electrode. This option cannot be perfect for measuring physiological signals, like electromyography (EMG), because there are almost always motion of muscles, therefore causing possible motion of the electrode relative to the surface. If electrode motion occurs with respect to the surface, there will be a variation on charge distribution on the interface between both [14]. According to the polarizable electrodes theory, a variation of charge distribution may induce a difference of potential on the electrode due to motion and not from the desired physiological signal. This mistake is known as motion artefact and is more likely to occur using polarizable electrodes [15].

On the other hand, the non-polarizable electrodes category, allow the passage of current between the electrolytic solution and the electrode's metal without changing the charge distribution of the solution nearby the electrode. Although the theory is applied to perfect electrodes, it is possible to develop more or less polarizable electrodes using only different materials [14].

Among non-polarizable electrodes, the silver-silver chloride ($Ag/AgCl$) stands out. They are typically used in clinical environment for physiological processes monitoring as EMG, electrocardiography (ECG) and electroencephalography (EEG). This type of electrode consists of bulk silver coated by silver chloride. When exposed to light, some silver chloride from the top layer can be reduced to silver, however not all is reduced, thereby a thin stable layer is formed between the bulk silver and the $AgCl$ coating [14]. Besides the non-polarizable behaviour, it was shown that Ag-$AgCl$ electrodes have less electronic noise at low frequencies compared to an equivalent silver electrode, without the $AgCl$ coating [16].

Beyond electrochemistry characterization of electrodes, is important to understand the intrisic electric characteristics of the electrode system. On previous studies [16–19] is possible to understand the electric circuit behind the electrode is composed by a resistor and a capacitor in parallel. Is likely that this two components represent an electrode. As mentioned before, it is necessary the existence of two layers of charges (solution and electrode) which represents a capacitor, and the resistor represents the losses on the passage between the two layers. These studies brought a new concept of electronic circuit concept which in conclusion is a RC circuit. This conclusion emerged by the refutation of a resistor in series with a capacitor would translate on an infinite resistance at low frequencies and, therefore, was rejected [20].

The theory developed in the last years indicate that each component of an entire system, skin (epidermis and dermis) and electrode (electrode plus solution), can be represented with ionic and electric characteristics.

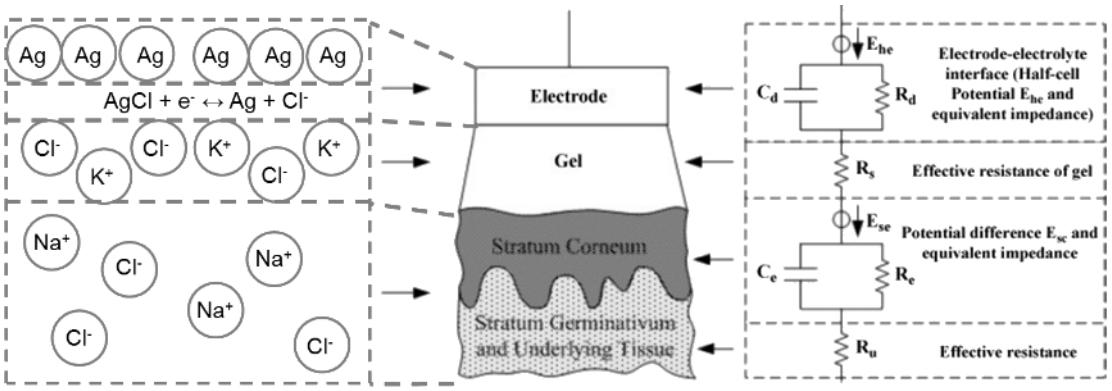

FIGURE 1.7: Scheme of the layers involved on the interaction electrode-skin. On the left, ionic characteristics. On the right, electronic characteristics [21].

One important point on the electronic representation of an electrode lies on the fact that the impedance changes with the signal frequency which can be caused by the types of materials used and the thickness of the AgCl layer. With low frequencies the impedance should be high and stable (due to the resistor), however from a certain frequency the impedance should decrease due to the capacitive component [20].

1.2.1 Conventional electrodes

Throughout time there has been a concern to optimize the electrodes in a way to perform more reliable measurements and closest to the physiological processes. The better way to improve electrode performance was optimizing the electric properties which can be made in two ways. The first, more intuitive, is decreasing only the resistance value of the equivalent circuit obtaining passive electrodes. The second is increasing both capacitive and resistive component, active electrodes. [21].

The first option of decreasing the resistive component of the entire system is done daily in clinical environment when the standard wet electrodes are used for measuring EMG, ECG or EEG. These electrodes are, typically, disks of a conductor material, usually silver, with the previous mentioned top layer made of silver chloride. Yet, another layer is added: an electrolytic gel. The function of the electrolytic gel is, precisely, minimize the impedance that exists between the electrode system and the skin system (surface plus deeper layers). This gel is a potassium chloride or sodium chloride solution which operates as an intermediate between the electrode and skin, maximizing the contact. However, the great disadvantage of these type of electrodes is that they can not be used for a long period of time [21].

Another type of electrodes are those called active or dry electrodes. These electrodes may be either resistively or capacitively coupled to the skin. This type of electrodes

did not require any type of electrolytic gel as an intermediate therefore the value of the resistive component is greater than the previous ones but have a higher inherent noise level. Unlikely the wet electrodes, dry electrodes are mostly non-polarizable whereas their applications are directed to long term measurements, typically, cardiac measurements that expect few chest moves. However, its reliability may decrease because their dielectric properties are susceptible to change with the presence of perspiration and the erosion of the dielectric substance. For these type of electrodes, the materials used to built them are iridium oxide, platinum or aluminium. In an attempt to replace the gel, is sometimes used a spongy and viscous material that serves the same purpose but is not as effective [14]. Most of active electrodes contain a high input impedance electronics amplifier in the same housing as the detection surfaces.

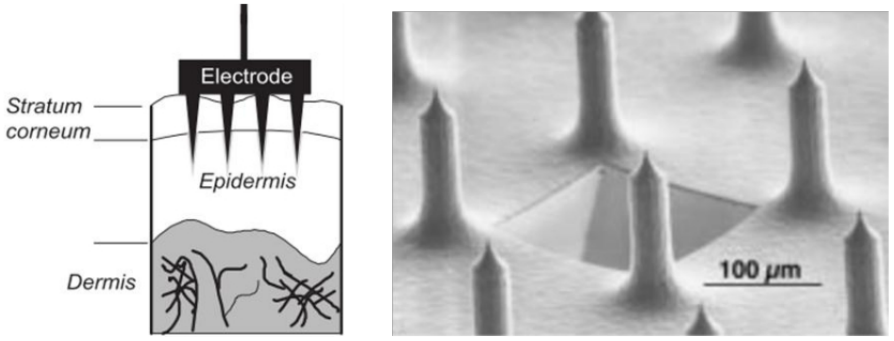

(a) (b)

FIGURE 1.8: Spiked electrodes. (a) Representative scheme of the spiked electrodes on the skin [22]. (b) SEM photo of the needles of spiked electrodes [23].

Yet, there is another type of electrodes that try to reduce the resistance to improve their performance. The main objective was to abdicate of electrolytic gel, like the dry electrodes, but benefit with the low impedance of the wet electrodes. The solution were the three dimension (3D) or spiked electrodes. This type of electrodes have, as their main advantage, the design. On the surface that have contact with the skin, is placed needles with length enough to achieve the most resistive layer of the skin, the *stratum corneum*. Typically, these needles have a length of approximately 100 μm, however, is not a standard value neither for every person or every anatomic regions of the same person. This is, obviously a disadvantage because if the needles are too short, the *stratum corneum* is not overpassed. Nevertheless, if the needles are excessively long, can cause discomfort or even pain [22].

Another options to improve the performance of electrodes are being explored nowadays. Although contradictory, the signals collected by electrodes could be good if the resistance on skin-electrode interface is infinite. It was shown that this technique is great for reception of low noise signals. What happens is that this electrodes have a extra capacitive component which allows the collection of physiological signals if the contact

between the electrode and and skin is not consistent or even interrupted. These electrodes are, today, commercialize to general public because are incorporated into clothing and sport accessories to keep the athletes monitoring throughout the physical exercise [21]. The electric properties of several type of electrodes are in Figure 1.9.

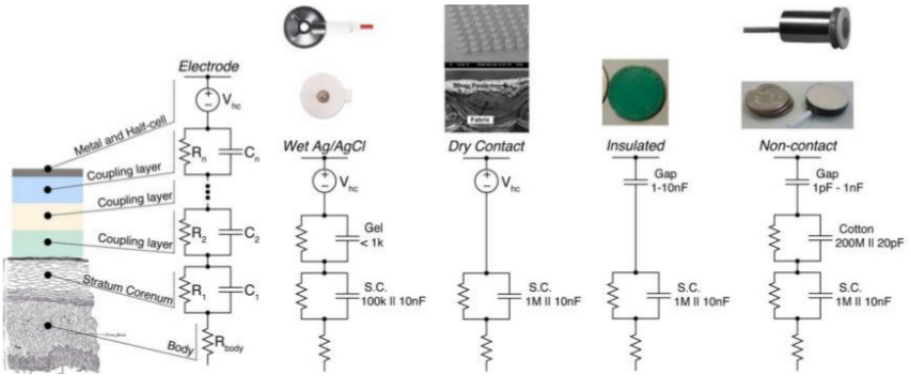

FIGURE 1.9: Electric properties of the electrode-skin interface for several types of electrodes including, from right to left, standard wet Ag-AgCl electrodes, dry electrodes, capacitive electrodes with contact and without contact [21].

Although the diversity of electrodes fabricated and their applications, a lack of using a new approach to obtain new types of electrodes with different physical characteristics, like the concept of electronic skin.

1.3 State-of-Art of non conventional electrodes

The concept of electronic skin started with the idea to integrate electronic devices into substrates with human skin characteristics. The concept was initially developed for robotic applications, an attempt to give the touch capability to hand prostheses using several pressure sensors [24]. However, the applications of the concept could go beyond robotics.

The first group developing the concept of electronic skin [25], created a new approach to the interface between physiological measurements and stimulation and the skin. In order to overtake the most traditional designs and their limitations, they produced a new approach to group electrodes, sensors, electronic components, energy supply and connectivity into thin and flexible membranes.

The device flexibility was achieved, partly, due to substrate selection but also to the serpentine shape of components and sensors. The membrane in which the components are into is kept by two other protective membranes with equal thickness. In order to the device not cause discomfort to the user, the membranes were developed to be thin, light, adaptable and with an adequate adhesion to natural skin [24].

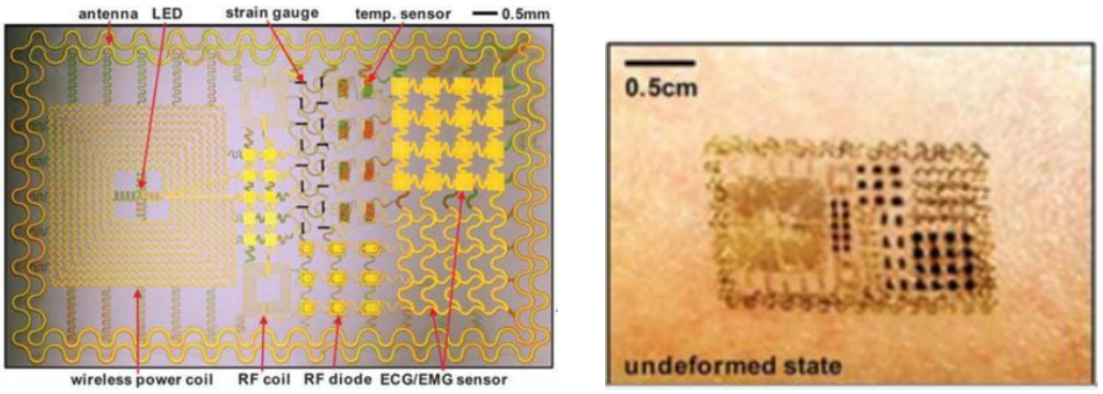

(a) (b)

FIGURE 1.10: Electronic skin developed by [24]. (a) Scheme of electronic skin with several components on a flexible substrate. (b) The entire system on it normal state in contact with skin.

The researcher team, [25], has accomplished the integration of multifunctional sensors (such as temperature, strain, and electro physiological) microscale light-emitting diodes (LEDs), active and passive circuit elements (such as transistors, diodes, and resistors), wireless power coils, and devices for radio frequency (RF) communications (such as high-frequency inductors, capacitors, oscillators, and antennae), all integrated on the surface of a thin (∼30 mm), gas-permeable elastomeric sheet based on a modified polyester. The active elements use established electronic materials, such as silicon and gallium arsenide, in the form of curved filamentary. The result is a high-performance system that offers reversible, elastic responses to large strain deformations that are orders of magnitude smaller than those possible with conventional electronics or even with recently explored flexible/stretchable device technologies. These mechanical characteristics lead to robust adhesion to the skin via Van der Waals forces alone, without any mechanical fixturing hardware or adhesive tapes [25].

Electronics in this form were also integrated directly with commercial temporary transfer tattoos as a substrate alternative to polyester or polyvinyl acetate (PVA). The electronic skin was configured for measuring ECG, EMG, and EEG in conformal, skin-mounted modes without conductive gels or penetrating needles providing important, system-level demonstrations. All materials that come into direct contact with the skin (gold, polyimide, and polyester) are biocompatible. The devices were used for up to 24 hours or more on neck, forehead, cheek and chin and showed no degradation or irritation to the skin. The result of ECG recordings from the chest revealed high-quality signals with information on all phases of the heartbeat, including rapid depolarization of the cardiac wave, and the associated QRS complex [25].

However the fabrication process, transfer printing, of the entire system is quite complex and have several phases. The transfer-printing fabrication approach has proved to be

viable and low-cost in this demonstration, which will greatly facilitate the practical clinical use of the electronic skin. Nevertheless transfer printing is based on molds construction which are made by lithography procedures [26]. Besides, the skin electronic device has flexible transistors for signal amplification so to built this components, was used an additional process similar to the first [27].

For that reason, the use of a simpler technique like inkjet printing to build a complex system as the mentioned could bring some advantages. Many groups have been trying to develop almost the same components on the electronic skin but separately. At least one research group tried to implement electrodes on a flexible substrate using inkjet technology. They reported a high performance and stable inkjet printed stretchable silver electrodes on wave structured elastomeric substrate. They deposited conductive silver directly on a ultraviolet ozone treated polydimethylsiloxane (PDMS) substrates having vertical wavy structures. The ultraviolet ozone treatment and intentionally roughness surface improved adhesion between silver ink and PDMS surface. The group optimized inkjetting conditions to obtain well deposited silver electrodes by controlling the cartridge temperature, ink drop velocity and drop spacing (resolution) [28].

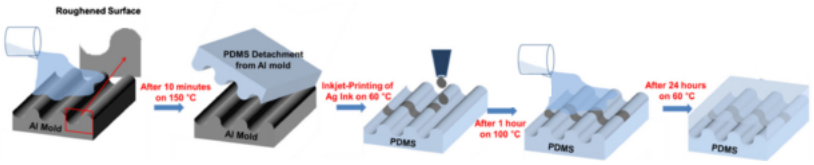

FIGURE 1.11: Fabrication process scheme of the inkjet printed stretchable silver electrodes by Chung et al. [28].

The group [28] compared the method of printing silver ink on PDMS with and without wavy structure, concluding that the adhesion and stretching performance were much improved when the substrates with wavy structures were introduce. They also concluded that increasing the number of printings, thick and low resistance metal electrodes can be obtained. However, depositing too thick metal films on a compliant substrate typically show poor stretchability. The procedure consisted in roughing intentionally the PDMS by roughing first the aluminium mold with wavy patterns with period and amplitude of 200 μm using a wire-electro discharging machine. Then, two times printed silver electrodes having width 1 mm and length of 20 mm and thickness of 1.6 μm shows sheet resistance of 0.44 Ω/sq after sinterization process at 100°C on a hot plate during 1h. The inkjet printed stretchable silver electrodes showed good stretchable performance at low to high speed strain stress and good stability [28].

1.4 Electromyography

Electrophysiology is the study of the electrical properties of biological cells and tissues which involves measurements of voltage change or electric current, named biopotentials. The origins of these biopotentials can be traced at the cellular level and the electric potential across a cell membrane is the result of different ionic concentrations that exist inside and outside the cell. The semipermeable membrane separates high concentrations of potassium ion and low concentration of, mostly, sodium ions inside and outside the cell. Some of the cells in the body are excitable and produce an action potential, which results from a rapid flux of ions across the cell membrane in response to an electric stimulation or transient change in the electric gradient of the cell. The electric excitation of cells generates currents in the surrounding volume conductor manifesting itself as potentials in the body.

Many organs in the body such as muscles, heart, brain and eyes manifest their function through electric activity, generating biopotentials capable of being measured. The heart, for instance, produces a signal called electrocardiogram, the brain produces a signal called electroencephalogram, eye movements results in a signal called electrooculogram and the activity of the muscles, such as contractions and relaxation produces an electromyogram.

Electromyography (EMG) is an experimental technique concerned with the development, recording and analysis of myoelectric signals. It provides easy access to physiological processes that cause the muscle to generate force, produce movement and accomplish the countless functions which allow us to interact with the world around us. The EMG signal is the electrical manifestation of the neuromuscular activation associated with a contracting muscle. The signal represents the current generated by the ionic flow across the membrane of the muscle fibers that propagates through the intervening tissues to reach the detection surface of an electrode located in the environment. It is a complicated signal that is affected by the anatomical and physiological properties of muscles and the control scheme of the nervous system, as well as the characteristics of the instrumentation used to detect and observe it.

In order to understand the EMG signal, it is necessary to appreciate some fundamental aspects of physiology. Muscle fibers are innervated in groups called motor units, which when activated generate a motor unit action potential. The activation from the central nervous system is repeated continuously for as long as the muscle is required to generate force. This continued activation generates motor unit action potential trains. These trains from the concurrently active motor units superimpose to form the EMG signal. As the excitation from the central nervous system increases to generate greater force in

the muscle, a greater number of motor units are recruited and the firing rates of all the active motor units increases.

The most fundamental functional unit of a muscle is called the motor unit. The electrical signal that emanates from the activation of the muscle fibers of a motor unit that are in the detectable surrounding area of an electrode is called the motor unit action potential (MUAP) which constitutes the fundamental unit of the EMG signal. Many factors may influence the shape of the MUAP like:

- the relative geometrical relationship of the detection surfaces of the electrode and the muscles fibers of the motor unit in the surrounding area;
- the relative position of the region where the nerve branches contact the muscle fibers;
- the size of the muscle fibers cause the amplitude of the individual action potential is proportional to the diameter of the fiber;
- the number of muscle fibers of an individual motor unit in the detectable surrounding area of the electrode.

The last two factors have particular importance in clinical applications to identify morphological modifications of the MUAP shape resulting from modifications in the morphology of the muscle fibers (hypertrophy and atrophy) or the motor unit (loss of muscle fibers and regeneration of axons). Although usage of MUAP shape analysis is common practice among neurologists, interpretation of the results is not always straightforward and relies heavily on the experience and disposition of the observer.

The electrical manifestation of a MUAP is accompanied by a contractile twitch of the muscle fibers. To sustain a muscle contraction, the motor units must be activated repeatedly. The resulting sequence of MUAPs is called a motor unit action potential train (MUAPT). The waveform of the MUAPs within a MUAPT will remain constant if the geometric relationship between the electrode and the active muscle fibers remains constant, if the properties of the recording electrode do not change, and if there are no significant biochemical changes in the muscle tissue. Biochemical changes within the muscle can affect the conduction velocity of the muscle fiber and the filtering properties of the muscle tissue.

Therefore the final EMG signal is formed by adding several MUAPTs which can be detected by electrodes either located on the surface (skin) or inserted beneath it, using needle or wire electrodes. Both electrodes types can be used singularly (monopolar configurations) or, typically, in pairs (bipolar configuration).

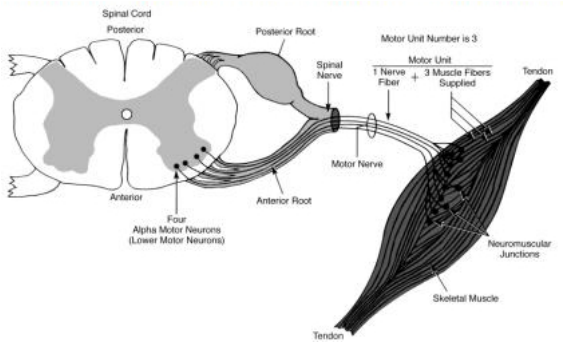

FIGURE 1.12: Structures responsible for promoting an EMG signal.

The electrical activity inside a muscle or on the surface of the skin outside a muscle may be easily acquired by placing an electrode with only one detection surface in either environment and detecting the electrical potential at this point with respect to a reference electrode located in an environment that either is electrically quiet or contains electrical signals unrelated to those being detected. Such an arrangement is called monopolar and is at times used in clinical environments because of its relative technical simplicity. This configuration has the drawback that it will detect all the electrical signals in the vicinity of the detection surface which includes unwanted signals from sources other than the muscle of interest.

The bipolar detection configuration overcomes this limitation. In this case, two surface electrodes are used to detect two potentials in the muscle tissue of interest each with respect to the reference electrode. The two signals are then fed to a differential amplifier which amplifies the difference of the two signals. Signals emanating from the muscle tissue of interest near the detection surface will be dissimilar at each detection surface because of the localized electrochemical events occurring in the contracting muscle fibers, whereas AC noise signals originating from a more distant source (50 or 60 Hz electromagnetic signals radiating from electronic devices) and DC noise signals (polarization potentials in the metal electrolyte junction) will be detected with an essentially similar amplitude at both detection surfaces. Therefore, they will be subtracted, but not necessarily nullified prior to being amplified.

EMG provides many important and useful applications, besides basic physiological (analysis of MUAP morphology or screening pathologies like dystrophy and muscle infection) and biomechanical studies (muscular load during a task, ergonomics studies), EMG is established as an evaluation tool for applied research, physiotherapy/rehabilitation, sports training and to generate control commands for human computer interfaces. Control systems based on the classification of EMG signals are used in two main potentials applications: powered upper-limb prostheses and electric powered wheelchairs. Most

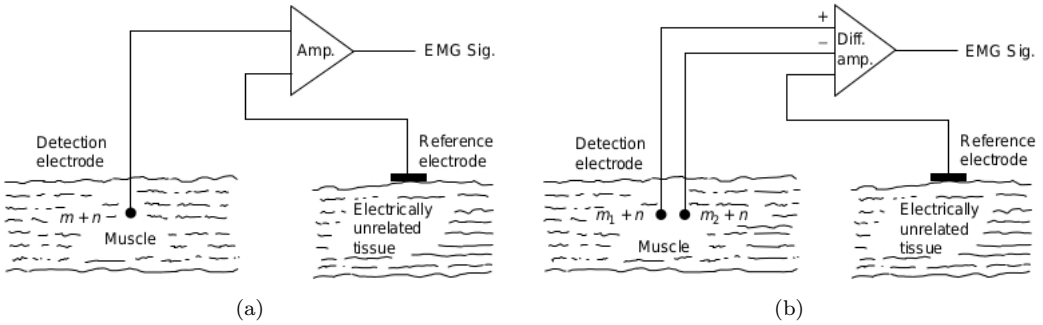

FIGURE 1.13: EMG detection using (a) monopolar configuration and (b) bipolar configuration.

commercial EMG based prostheses recognize the user's movements by comparing magnitude features of EMG signals with a predeterminated threshold generating a small number of control commands.

1.5 Motivation

This thesis attempts to use the several advantages of inkjet printing technology to develop devices and applications in biomedical field introducing new designs and features used to acquire EMG signals.

This thesis proposes the use of inkjet printing technology to develop non conventional electrodes for measuring physiological signals, particularly EMG signals introducing the electronic skin concept. The study for the thesis include the entire process of fabrication, optimizing printing conditions to each electrode type; designing studies, to extract the most advantages of each material; material cleaning and handling; visualization and comparison of the printed electrodes to the commercial ones.

From my knowledge, this is the first time that inkjet technology is used to fabricate electrodes for biomedical applications. Despite of the several applications and studies done using inkjet printing, this is the first study that combines the flexibility of the materials to the possibility of printing any conducting pattern to conceive devices to be in contact with the skin and extract physiological information.

Through the development of this thesis several ideas were thought and discussed and have potential to be continued as future work. I believe this is the first step to introduce a low cost and intuitive procedure to fabricate devices with innovative characteristics into biomedical world.

1.6 Outline

Chapter 1 introduces the inkjet printing technology explaining how it operates and advantages when compared with others fabrication techniques. It also includes an introduction to electrodes explaining the chemistry and electronics behind the conventional and non conventional electrodes showing the state-of-the-art for those devices. Chapter 1 also introduces electromyography, what it is and how can be recorded. Finally, presents the motivation for this work.

Chapter 2 describes the materials and fabrication procedures used to develop printed electrodes. It presents characteristics of each substrate, silver ink nanoparticle and also the designs of electrodes used in this work.

Chapter 3 contains the results of tests performed on printed electrodes. This results includes sheet resistant, resistivity and impedance measurements that allows a characterization of printed electrodes. Also contains the performance of printed electrodes in real electromyographic and electrocardiographic measurements.

Chapter 4 describes the methods implemented with *MatLab* used for post signal acquisition. This Chapter includes algorithms for movement detection, features extraction and a classification procedure to distinguish three different movements.

Chapter 5 starts to an introduction of a platform that enables the acquisition of biosignals. Then, it describes the fabrication procedures to reproduce some of the circuits presented before.

Chapter 6 makes the final conclusion remarks, presents possible applications for the work developed and discusses future work.

Chapter 2

Printed Electrodes

2.1 Materials

To fabricate printed electrodes was used a drop-on-demand *Fujifilm Dimatrix 2831 Materials Printer* (DMP-2831) which has a piezoelectric system for controlling the nozzles. DMP-2831 (see Figure 2.1)is a materials deposition system designed for micro-precision jetting, a variety of functional fluids onto several types of surface, including plastic, glass, ceramics, and silicon, as well as flexible substrates from membranes, gels, and thin films to paper products.

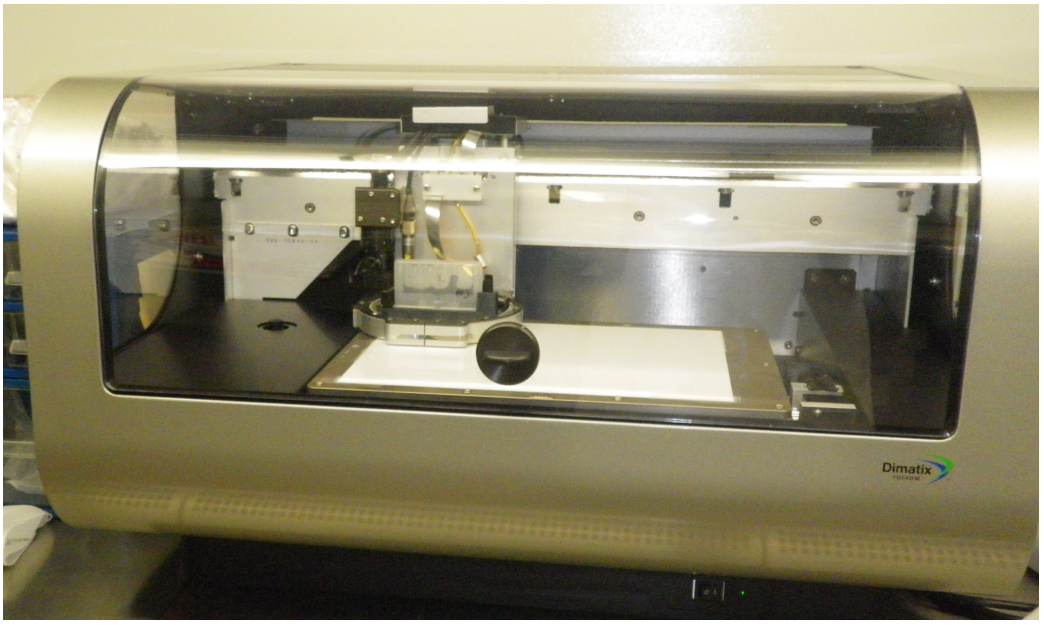

FIGURE 2.1: Fujifilm Dimatrix 2831 Materials Printer.

DMP-2831 is a useful machine that facilitates developing and testing manufacturing processes and product prototypes. The drop-on-demand system minimizes waste of

expensive fluid materials, thereby eliminating the cost and complexity. Besides, DMP-2831 fits within standard flow chamber which is the only lab material required to use it [3].

This printer allows the deposition of fluidic materials on 200 x 300 mm substrates and handles substrates up to 25 mm thick, utilizing a disposable piezoelectric inkjet cartridge. The temperature of the vacuum platen, which secures the substrate in place, can be adjusted up to 60°C. A waveform editor and a drop-watch camera system allows manipulation of the electronic pulses to the piezoelectric jetting device for optimization of the drop characteristics as it is ejected from the nozzle. This system enables easy printing of structures and samples for process verification and prototype creation. To minimize waste of expensive fluids, each cartridge reservoir has a capacity of 1.5 ml. Cartridges can easily be replaced to facilitate printing of a series of fluids. Each single-use cartridge has 16 nozzles linearly spaced at 254 microns with typical drop sizes of 10 picoliters. Cartridges with drop volume of 1 pL are also available. The printer's resolution permits printing any pattern at 5 - 254 μm dot pitch with a repeatability of $\pm 25\mu$m.

2.1.1 Ink

The application of inkjet printing for patterning several devices requires functional inks holding special properties. Different types of inks can be used including organometallic compounds in solution which can be converted to metal at low temperature, conductive polymers and suspensions of nanoparticles using many kind of metals (gold, silver and copper). Those inks typically contain other additives such as dispersants, adhesion promoters, surfactants, thickeners and others [29].

Among metal nanoparticles inks, silver has gained more interest in part due to its price and performance. The finely dispersed silver nanoparticle is gaining comprehensive applications, such as catalyst and active ink for electronics, due to the unique properties of chemical stability, catalytic activity and excellent electric conductivity. For successful application and commercialization, silver nanoparticles dispersion in water inks adopted by inkjet printing technique allows a simple and inexpensive method for nanoparticle preparation, ink formulation with a stable aqueous metal dispersion, and a printed pattern with high electric conductivity. Conductive silver inks which exhibit nearly Newtonian rheological behavior has excellent dispersion stability [4].

In addition to the electrical properties the materials printability plays critical roles in inkjet printing. Firstly, the ink must have the capability of being stable and accurately printed. Secondly, the ink has to meet strict physicochemical properties to achieve

the best printed patterning, optimal performance and reliability. The most important ink's properties that dictate its *printability* is fluid properties, namely, viscosity, surface tension and density [5]. Those factors will have a critical role on the size and shape of the deposited droplets and the existence or not of satellite drops. In one hand, the viscosity of the ink must be low enough to enable the refill of the cartridge and the expulsion of a drop out of the nozzle by the transient pressure pulse. In another hand, the surface tension must be high enough to prevent unwanted dripping from the nozzle but low enough such that the ejected droplet can break away from the nozzle. Also, structure at both molecular and nano scale will impact attributes such as morphology (surface roughness, grain size), adhesion, mechanical integrity, solubility, and chemical and environmental stability [4].

To achieve a good printing result, the key characteristics of a piezoelectric inkjet ink are the dynamic viscosity of less than 20 mPa.s, surface tension value below 80 $mN.m^{-1}$, stability of the ink in solution/suspension in the printhead, and the particle size of the ink constituents preferably much lower, by orders of magnitude, than nozzle orifice.

For those reasons, to develop printed electrodes it was used a silver nanoparticle ink from *SunTronic* in which silver nanoparticles with size of less than 150 nm were dispersed in 20 wt.% of organic solvents (ethanol and ethanediol). This ink has a viscosity of 10 to 13 mPa.s and a surface tension of 28.0 to 31 $mN.m^{-1}$, both characteristics in the range of values to obtain good printing results.

Finally, electric characteristics of this silver ink also depend on the sintering process (see Figure 2.2) because it requires a suitable transformation of the deposited ink layer to render it functional [30]. Sintering promotes a conductive path and grain growth, especially for metal nanoparticle inks which further improves electrical conductivity and mechanical adhesion. For silver nanoparticle ink, is necessary sintering to form connections between neighbour particles for achieving a better conductive film. This approximation of neighbour particles is due to the removal of organic coatings of nanoparticles therefore, at least, is required an application of a temperature capable of removing these organic materials. Although sintering is commonly carried out by heating, other techniques can be used, such as electrical, photonic and microwave sintering [29]. These factors, in turn, will affect device performance, notably electrical performance.

SunTronic silver ink used can achieve a volume resistivity of 5 to 30 $\mu\Omega$.cm after sintering at 150 to 300°C. However, thermal sintering is not suitable for all types of substrates, as the sintering temperature is between the values mentioned before, many polymer substrates cannot withstand such temperatures. In the electrode development, this temperature was changed for each type of substrate used to exploit the best features of both ink and substrate.

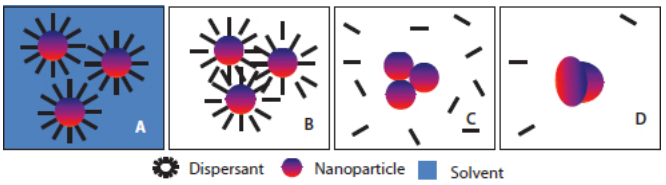

FIGURE 2.2: Sintering process of nanoparticles silver ink. (A) Nanoparticles dispersed in solvent; (B) solvent is evaporated due to heating; (C) Evaporation of dispersant and other additives; (D) sintering of nanoparticles [3].

2.1.2 Substrate

As mentioned earlier, inkjet printing itself does not depend on the substrate. It is possible to use a wide type of substrate: rigid, flexible, reinforced and non-reinforced. However, the interaction of the printed ink and the substrate plays a decisive role in determining the accuracy and robustness of the printed structure, and ink properties and substrate properties have to be well matched. As a result, the substrate surface is usually processed prior to printing in order to improve wetting and adhesion. Each substrate used in this work had a specific treatment that was optimized to their intrinsic characteristics.

2.1.2.1 Photographic paper

Paper is probably the cheapest and most widely used flexible substrate in daily life. When compared to plastic substrates such as polyethylene terephtalate (PET), polymide (PI) and others, its price is significantly lower. In addition to this, paper is also environmentally friendly and is more available. Recently, it has been considered as a potential substrate for low-cost flexible electronics, which motivate us to create paper electrodes to be used in biosignals acquisition. With this approach, the electrodes can have reduced costs, with potential to produce disposable electrodes.

The paper used as a substrate for printed electrodes is a common photographic paper 230 μm thick. This type of paper is commonly coated with certain compounds that grant qualities to the paper, such as surface smoothness and gloss, weight and inks absorption. Unlike common paper, photographic paper is a good substrate to use for inkjet printing due to its coating layers. Usually, most commercial photographic papers are coated with one or two layers of polyethylene layers making the paper base impermeable to liquids. It is also added a clear resin layer above an emulsion layer which protects it from physical damage. The layers added after the paper base improve dimensional stability, prevents the paper from curling upon drying, reduce drying times and makes the surface very smooth. Those characteristics make photographic paper a good substrate for printing conductive patterns of silver nanoparticles ink.

To perform the ink sinterization after the printing procedure it was necessary to measure the resistance of the photographic paper to high temperatures. A piece of photographic paper was placed on a heating plate and was registered that the maximum temperature that the paper resists is 120°C. However, to guarantee the non degradation of the photographic paper, the sinterization process was made at a maximum of 100°C.

Before the printing procedure and to ensure the success of it, the surface of photographic paper was clean with a jet of compressed air to remove dust particles.

2.1.2.2 Polydimethylsiloxane

As a substrate for printed electrodes, it was also used the elastomer polydimethylsiloxane (PDMS), a silicone rubber, which is known to be inexpensive, biocompatible, and amenable to molding micro scale, and to have excellent gas and water permeability [31].

Most polydimethylsiloxane fluids are non-volatile polymeric organosilicon materials consisting of $(CH_3)_2SiO$ structural units (see Figure 2.3), typically more than 4. The polymer backbones of polysiloxane is the same as glass like materials. It is the high flexibility around the oxygen atom in the siloxane backbone, and the low intermolecular forces that make the polymers very flexible. In silicone rubbers, organic groups are attached to the silicon atoms and methyl groups are the most abundant. To create silicone rubber, some methyl groups are exchanged with vinyl or phenyl groups which provide rubber like structures that are flexible at extreme low temperatures [32]. It is the cross-linking abilities of the vinyl groups that provide the means to create rubber or solid structures [33].

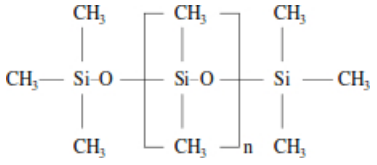

FIGURE 2.3: The chemical structure of PDMS with, typically, n¿4 [34].

Recently, the PDMS material is receiving increasing amount of attention from researchers from several activities, including microelectromechanical systems fabrication. The major advantages of this polymeric compound relies on its mechanical and chemical properties. Since PDMS is viscoelastic, it acts like a viscous liquid when is prepared and could cover any surface and mold to it and acts like an elastic solid similar to rubber after a curing process. The final form of the cured PDMS has a stabilized cross structure, which is non-soluble and stable at higher temperatures [35]. It is also transparent at least within the visible spectrum which can be used to monitor, for instance, fluid flow inside it. Besides, the chemical stability translates on interesting and strong mechanical

properties such as flexibility and stretchability. Due to the chemical properties of the silicone rubber, PDMS surfaces are hydrophobic and tends to remain that way. The bulk of silicone rubber contains small quantities of highly mobile low molecular weight chains and these PDMS oligomers continuously creep out and adsorb on top restoring the hydrophobic property of the material [32]. For that reason, PDMS is not easy substrate to print on, because the ink in contact with the surface has a contact angle of approximately 110° (see Figure 1.6-b). This means that if the PDMS surface is not treated, when a continuous line of silver ink is printed the result is several spaced dots non continuous (see Figure 2.4-b).

(a) (b)

FIGURE 2.4: Printed lines in a surface with a (a) hydrophilic and (b) hydrophobic surface [29].

The fabrication of PDMS requires no cleanroom facilities and was performed in a regular flow chamber. The preparation of PDMS (*Sylgard 184*) started by mixing the elastomer base with curing agent at a 10:1 weight ratio, and the mixture was placed into vacuum chamber at room temperature and vacuum for 30 minutes to let air bubbles rise out. A bulk PDMS substrate was cured in a piece of glass (10x5 cm) by baking it in a 60°C oven for two hours.

Due to its hydrophobic properties, the PDMS had an extensive solvents treatment before printing to prepare the surface for receive the ink. To achieve this propose the PDMS pieces were immersed in triethylamine (SIGMA) for 2 hours with gentle agitation, then immersed in ethylacetate (SIGMA) for 2 hours with gentle agitation and finally, immersed in acetone for 2 hours with gentle agitation. Each solution was replaced by a new one after 1 hour of treatment. Finally, the PDMS pieces were dry with air flow and dry, once more, in the oven at 65°C overnight. Immediately before the printing process, those PDMS pieces were plasma treated with two cycles of 3 minutes each, reducing significantly the surface hydrophobicity.

2.1.2.3 Biocellulose

Biocellulose (BC) is a pure form of cellulose naturally produced by the bacteria *Glucanacetobacter xylinus* in a continuous sheet (see Figure 2.5). After processing, has the appearance of butter paper. Its purity enables the use of BC in medical applications, mainly as artificial temporary skin for wounds and burn healing. Its cost is probably

still too high to compete with other substrates [for instance, poly(ethylene terephtalate) - PET] but it may reach competitive values as production volumes increase [36].

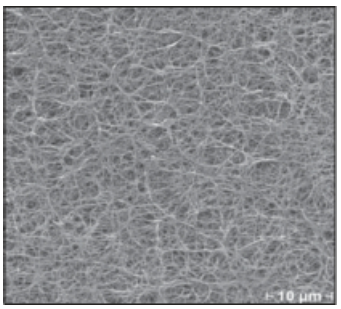

FIGURE 2.5: Nanofiber network of biocellulose [37].

BC is a pure substance, it has a continuous fibrous nanostructure with high dimensional stability and mechanical strength. It is biodegradable, renewable and its production is not dependable on petroleum derivates. It can be chemically modified, coated with other materials and incorporated in nanocomposites giving a variety of products for organic electronics, not only as substrate material but also as dielectric and as active conducting layer, with appropriate nanocomposites. Its surface energy and hydrophobic character can be controlled to enable the deposition of active layers.

The interest to use it as a substrate for fabrication of electronic components is the possibility to develop electronic circuits that can be biocompatible and flexible. The aim of using BC and BC-based materials as substrates derives from their resistance to high temperatures and high flexibility. BC has also the advantages of being renewable, biodegradable and ease to use. For inkjet printing proposes, BC sheets requires only a pre treatment with air flow to remove dust particles.

2.2 Design Characteristics

For developing printed electrodes, it was necessary to contribute with new designs for them. Each substrate have unique characteristics (flexibility, printability, physical resistance) therefore some electrodes were made to fit them. It was printed three major types of electrodes: flat discs, array of electrodes and spiked electrodes (see Appendix A).

The design characteristics of printed flat discs electrodes is similar to the commercial and standard wet electrodes. As comparison, we used BIOPAC circular electrodes with 3.5 cm diameter, which includes the adhesive and the contact part. These disposable electrodes are 1 mm thick and 1 cm diameter in surface area, whereas the surface in contact with skin is about 0.79 cm^2. These electrodes are also covered with an electrolite gel for improved electrical contact. The printed electrodes had similar dimensions

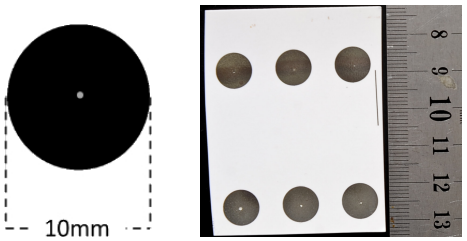

(a) (b)

FIGURE 2.6: Printed flat disc electrode. (a) Pattern used to print. (b) Six printed flat disc electrodes using silver ink on photographic paper.

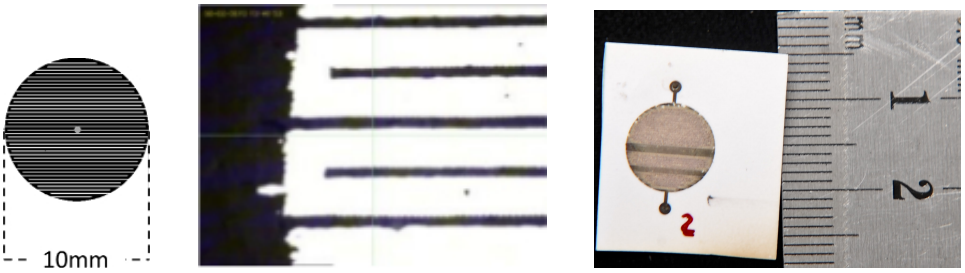

(a) (b) (c)

FIGURE 2.7: Printed electrode with one continuous filament. (a) Pattern used to print. (b) Detail of printed filament (printer's camera view). (c) Printed filament electrode using silver ink on photographic paper.

to BIOPAC's: 1cm diameter surface area for contact with the skin and $\sim 1\mu$m thick. Beside this standard dimensions, others were fabricated including an electrode with a rectangular shape with 3 cm width and 8 cm length.

A set of three electrodes were built to perform electromyography measurements as explained in section 1.4. This electrode set with shape of a armlet was one-time printed with two electrodes align and spaced with 8 cm and another electrode was placed between them but not aligned. The third electrode acts as a reference electrode and when the armlet is placed in the arm, this electrode is placed on the posterior part of the arm.

Another design for flat discs electrodes was considered with the aim of decrease the electrode resistance by electric sintering. This type of sinterization differs from the traditional method, of heating the device, because it's applied a difference of potential between two points. By applying this voltage, a current passes through it, originating heat and sinterizating the silver ink. To achieve this, was fabricated a electrode with one continuous filament with circle shape were a voltage was applied on both ends of the filament.

Arrays of electrodes were developed to fulfil the need of fabricating flexible electrodes. To accomplish that, silver ink was printed using PDMS as substrate because amongst all

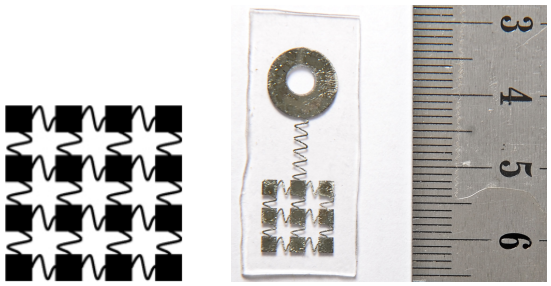

(a) (b)

FIGURE 2.8: Printed electrode array. (a) Pattern used to print. (b) Printed electrode array using silver ink on PDMS.

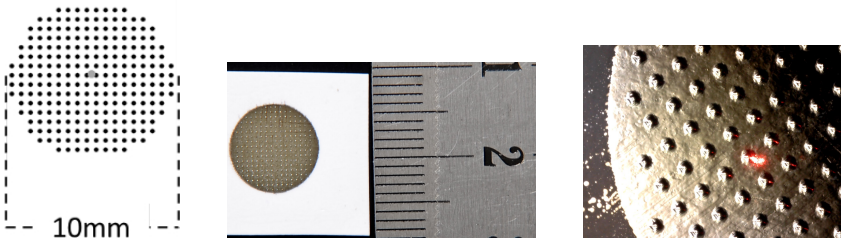

(a) (b) (c)

FIGURE 2.9: Printed spiked electrode. (a) Spikes' pattern with 5 pixels used to print. (b) Printed spiked electrode using silver ink on photographic paper. (c) Detail of spiked using Atomic Force Microscopy (AFM).

the substrates used, it is the most flexible. However, since the silver ink is not flexible, the solution found to achieve flexible electrodes was to design several tiny electrodes and connect them throw a serpentine shape line. This way, before the silver ink cracks, it expands according to the shape of the serpentine. Even if the serpentine line breaks, each tiny electrode has, at least, one more connection to other tiny electrode. This redundant system allows the electrode to be more flexible and more resistant to physical distortion of the substrate.

Other type of electrodes fabricated with inkjet technology were spiked electrodes. This spiked electrodes were made to allows the penetration of the most resistive layer of skin: the *Stratum corneum*. The spikes made by several printing layers of silver should be long enough to penetrate that layer but short enough not reach any nerve system, causing no pain. For that reason, printed spiked electrodes were fabricated to have $\sim 50\mu$m height, with a sharp edge and a strong base. The spikes were printed over a printed simple flat disc electrode mentioned before. Over that, approximately 230 spikes spaced with 250 μm were printed.

Besides those designs, electrodes for measure the galvanic resistance of the skin were fabricated. Since the main objective was to place the electrode on the index finger, two designs for this propose were made: a circular and a rectangular. The circular one

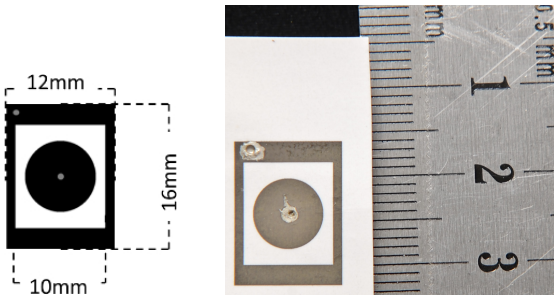

(a) (b)

FIGURE 2.10: Printed electrode for galvanic resistance measurements. (a) Pattern used to print. (b) Printed electrode using silver ink on photographic paper.

consisted on two circles, one smaller with diameter of 0.8 cm inside a ring with diameter of 1.3 cm. Both circle and ring have approximately the same area of 101.3 cm^2. The rectangular one had inside a circle with the similar dimensions as the last mentioned and a rectangle with dimensions of 16mm x 12mm.

2.3 Fabrication Procedure

The fabrication procedure of printed electrodes includes 5 main steps: pattern design, printing and sinterization procedure, AgCl layer production and assembley process.

The first step of the fabrication procedure is the design development. All designs of devices printed with the *Fujifilm Dimatrix 2831 Materials Printer* were accomplished using the software GIMP v2.8. The images must be in a format of 1 bit, i.e., must be black and white images. For a good design result, the resolution of the image developed with GIMP must be according to the resolution of the printer. For this work, it was used a printer resolution of 30 μm, which means that the minimum space (one pixel) between 2 consecutive drops of ink is 30 μm. The bitmap file of the design is then converted with DMP-2831 software for printing.

Once the design of the pattern is done, the second step is the printing procedure. This procedure includes a selection and optimization of nozzles, substrate placement, calibration of the print head, the printing procedure itself and the cleaning procedure. For a good print result with silver ink, the ink was inserted into the cartridge and then placed in the printer. To remove air bubbles, the cartridge remained at rest for 30 minutes. Since the printer is based on a piezoelectric system, the voltages of the nozzles were adjusted to achieve a drop velocity of 10 m/s and a firing frequency of 1 Hz. Although the print head had 16 nozzles, not always were possible to use it all, so it is necessary to select and configure the nozzles to obtain as many working nozzles as possible. The

advantage of this process is on one hand the guarantee of good printing results and on the other hand obtain a fast printing procedure which is proportional to the number of nozzles used. This process were sometimes lengthy due, especially, to the intensive usage of the same print head.

During the 30 minutes of waiting for eliminate air bubbles in the cartridge, the substrate was prepared and placed. Different substrates have different pre printing treatments as mentioned before (see Section 2.1.2). The substrate was then placed and fixed to the printer's plate due to a vacuum system integrated on the printer. Once the substrate is loaded, the cartridge is air bubbles free and the selected nozzles are working, the printing is started. First, it is printed a default pattern to calibrate the print head position and then the pattern developed before is printed on the substrate.

In all the electrodes fabricated, except for spiked electrodes, it was printed 4 layers of silver ink, one above another. The printing procedure for spiked electrodes was different than the other types of electrodes due to the spikes height. To accomplish the height of approximately 45 μm, the printing procedure was optimized. First, it was printed the base of the electrode with 4 layers, the same process as the simple flat discs electrodes. Then the spikes were fabricated by printing a pattern with the base of spikes (9 pixels) 15 times, then the pattern with spikes with 7 pixels, 5 pixels, 3 pixels and 1 pixel were printed 25, 30, 40 and 50 times, respectively. In sum, it was printed 160 layers to obtain spikes with height of 45 μm. The spikes fabrication was made with constant temperature of the printer's heating platen of 40°C and between each layer was waited 30 seconds for the ink to dry. This detail allowed to achieve more height because the ink had chance to dry between consecutive deposition of layers.

For electrodes printed on PDMS, the printing procedure of 4 layers was made with constant temperature of the printer's heating platen of 60°C.

The third step was the sinterization procedure. As mentioned before (see Section 2.1.1, silver ink needs to be sintered to form a continuous percolating structure that allows conduction. The sinterization procedure was made by two different methods: thermal and electric. Thermal sinterization was performed into all electrodes that had photographic paper as substrate. Due to the fragility of photographic paper to heat, the electrodes were placed in a heating plate at 85°C during 30 minutes. For electrodes printed on biocellulose and PDMS the sinterization procedure was similar, however it was used a temperature of 100°C and 150°C, respectively. The electric sinterization was only performed on electrodes constituted by one filament, by applying a voltage of 35 V and a damping current of 1 A after standard thermal sintering.

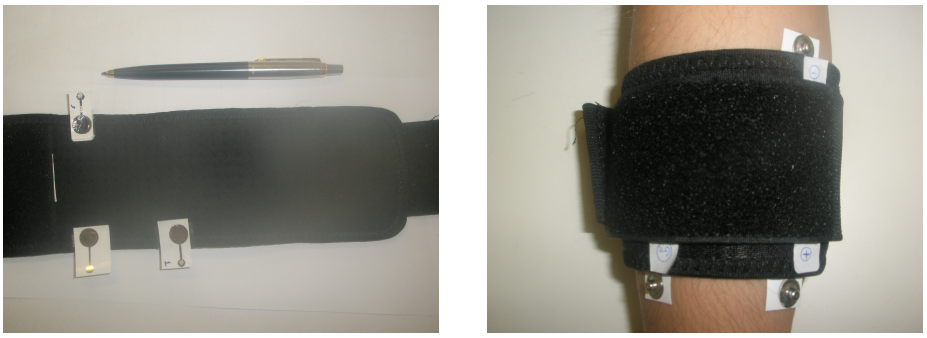

(a) (b)

FIGURE 2.11: (a) Electrodes placed on armlet and (b) the armlet placed on the arm.

The four step of the fabricating process was to produce a layer which enables the transduction of ionic concentrations measured by electrodes into electrical potentials. At the interface between the electrodes and the skin, the ionic signal (Cl^- ion transports the charge) is transformed into an electronic signal. Likewise, in common silver electrodes this layer is typically made of AgCl. The formation of this layer was achieved by adding Cl^- ions enabling a reaction between Ag and Cl to produce AgCl. However, due to the thin layer of silver and the fragility of the photo paper, the amount and the manner of introducing Cl^- ions is important. This process was optimized by using commercial bleach deposited by an airbrush at a distance of approximately 30 cm.

Finally, the fifth step in the production of these electrodes was ensuring a good, continuous and practical contact between the printed electrodes and the hardware. Usually, common electrodes have a metal and conductive snap to facilitate the connection of cables and make them practical to use. For the same reason, we use the same snap on printed electrodes. The snaps were placed in the back of the printed surface and the communication to the front was made through a hole filled with a conductive silver paste (*Agar Scientific*). The electrodes were then placed on a commercial armlet where the metallic snaps were placed outside of it for cables connection.

Chapter 3

Electrodes' characterization

3.1 Resistivity

Thin films resistance quantification is usually performed by measuring the surface ressistivity or sheet resistance (R_s) given in units of $\Omega/\square$. The sheet resistance is applicable to two-dimensional systems in which the thickness of the film is despised, so it is implied that the current flow is along the plane of the film. The sheet resistance is calculated using Equation 3.1. If the resistance of a square ($W = L$) is measured, that resistance is the sheet resistance. But if the film's thickness (e) is considered, the sheet resistance is inverse to e, assuming that the resistivity (ρ) in units Ω·cm is constant.

$$R_s = R\frac{W}{L} \tag{3.1}$$

This phenomenon of increasing the film's thickness to obtain small sheet resistance was proven using a resistivity test pattern. To accomplish an accurate measurement of silver's sheet resistance and, therefore, its resistivity, the four-probe technique was used. This is one of the most common methods of measuring the electrical resistivity of printed films because the contact and wiring resistances are negligible [29]. The operation is simple and consists in supplying current through the outer two probes and measuring the voltage across the inner two probes. To obtain more accurate results, the four probes be spaced equally between each other.

Two different patterns for measure the sheet resistance were used. The first one was used to verify the veracity of the relation between the thickness and the sheet resistance. The operation was performed in a printed square with four contacts (see Figure 3.1) and, as described above, current was injected in two probes and voltage was measured in the

Number of Layers	Thickness (cm)	Sheet Resistance ($\Omega/\square$)	Resistivity ($\mu\Omega$·cm)
One	1.1×10^{-5}	5.9	64.9
Two	2.3×10^{-5}	2.1	49.0
Three	3.4×10^{-5}	1.2	40.8
Four	5.5×10^{-5}	0.7	39.0

TABLE 3.1: Average values of sheet resistance and resistivity of printed squares.

other two. It was used the same square pattern with one, two, three and four layers to test the influence of the thickness. The ejected current varied between 0.2 mA to 1 mA and the results showed a sheet resistance difference between the number of layers, since with just one layer was measured a R_s of 5.9 $\Omega/\square$ and with two layers a value of 2.1 $\Omega/\square$ was obtained. It was observed that the sheet resistance decreases more than two times by increasing the pattern's thick in similar proportions. Although, continuing with the study of the influence of thickness in sheet resistance, the proportion between the increasing thick (number of printed layers) and decreasing R_s was no longer linear. Increasing the number of layers from two to three and from three to four, was achieved a sheet resistance of 1.2 and 0.7 $\Omega/\square$. This means that adding a layer, which is not necessary the double of thickness of the previous pattern, decreases the sheet resistance approximately 1.5 times.

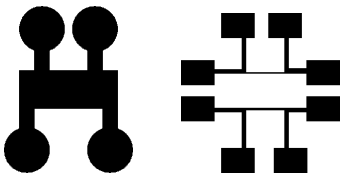

(a) (b)

FIGURE 3.1: Patterns used to measure silver's resistivity. (a) Square pattern and (b) line pattern.

Using both pattern's thickness and the data obtained measuring the sheet resistance, the bulk resistivity,ρ, was calculated by the formula $\rho = R_s \times e$, where e is the pattern thickness. The result (see Table 3.1) showed reasonably constant values for two, three and four layers patterns but a high value for one layer pattern. This can be due to failures during printing, since more than one layer originates a more homogeneous film and bridges possible printing failures. The small differences between resistivity values for other layers may be due to small sinterization differences or possible errors during patterns thickness measurements. For those measurements, it was used a printing procedure as described before and the sinterization was performed by placing the pattern printed in photographic paper in a heating plate for 30 minutes with a temperature of 100°C.

With other characteristics but with the same goal the resistivity of printed silver, it was performed a similar four-probe technique and measured the sheet resistance and the resistivity for thermal and electrical sintering. This time, it was used a line with different thickness and width and, once more, was applied a current through two probes and measured the voltage between the other two. The four probes were equally spaced in the pattern. The printed patterns consisted in two types of lines: a wide width line with 153 μm (W_w) and a short with 86.8 μm (W_w). Both had 3 mm (L) and were printed with two and four layers. This new pattern was selected to understand the influence of electrical sintering on printed patterns, which has to be made in a line with small width. If electrical sintering is applied, for instance, on a square, the current between the two probes will flow through the shortest path, therefore only a line will be sinterized.

For this propose, the printed pattern had four contacts for placing the probes and a line, within characteristics mentioned before, where the current will flow. After printing the silver on photographic paper, a first standard procedure of sinterization was used with 85°C during 30 minutes. This first step was needed to significantly reduce the resistance of the silver and prepare it for further electrical sintering. The results (see Table 3.2) showed that the average sheet resistance was larger for patterns with two layers, 1.7 Ω/□ and lower for patterns with four layers, 1.4 Ω/□. Although values of R_s were different when measured with a square and line pattern, both are in the same order of magnitude. Small differences may be due to changes in the temperature and/or time of sinterization, since lines patterns had a softer sinterization procedure. With those values for sheet resistance, the resistivity was calculated using the equation 3.2 and was obtained an average value of 39 $\mu\Omega$·cm and 76 $\mu\Omega$·cm for patterns with two and four layers, respectively. This time, the increase of film's thickness obtain small sheet resistance but not smaller resistivity, which can be justified by the small dimensions of the line in which the thickness (e) can not be despised. Also, in small printed lines like those ones, a small printing flaw might has a large impact on the film's conductivity, therefore, film's resistivity.

$$\rho = R \times \frac{W \times e}{L} \tag{3.2}$$

After measuring the sheet and resistivity of printed lines with only thermal sintering, it was tested the effect of electrical sintering. The test was performed on large lines printed with four layers since the other lines broke during the application of current through them. The results of electrical sintering were satisfied since the resistivity decrease, approximately 64% from 76 $\mu\Omega$·cm to 27.3 $\mu\Omega$·cm using a voltage of 8V. A new electrical sintering was performed on the same patterns decreasing 82% of the initial value, to a final resistivity of 13 $\mu\Omega$·cm, using a voltage of 10V.

Substrate	Sintering procedure	Number of Layers	Thickness, e (cm)	Resistance, R (Ω)	Sheet Resistance, R_s ($\Omega/\square$)	Resistivity, ρ ($\mu\Omega$·cm)
Photographic paper	Thermal (85°, 30 min)	Two	2.3×10^{-5}	43.2	1.7	38.5
Photographic paper	Thermal (85°, 30 min)	Four	5.5×10^{-5}	35.4	1.4	76.0
Photographic paper	Electrical (8V)	Four	5.5×10^{-5}	9.8	0.5	27.3
Photographic paper	Electrical (10V)	Four	5.5×10^{-5}	4.6	0.24	13.0
Biocellulose	Thermal (100°, 30 min)	Four	7.6×10^{-5}	10.4	0.4	31.7
PDMS	Thermal (150°, 30 min)	Four	7.3×10^{-5}	8.7	0.35	25.3

TABLE 3.2: Average values of sheet resistance and resistivity of printed lines using different substrates and sintering procedures.

It was proven that electrical sintering is a way for decreasing silver's resistivity and therefore the resistance of the device, however, the power needed to preform must not exceed 4 W. If that limit is exceeded the printed lines will broke and the film will no longer be conductive. Furthermore, some substrates as biocellulose do not stand electrical sintering since the thin substrate will burn and tear. Similar results were noticed when a electrical sintering was applied in patterns printed on PDMS since the poor adhesion between silver ink and the substrate makes the silver to rip and remove from it. However, the silver's resistivity for those substrates are smaller than for photographic paper because a stronger sinteriring procedure is used. It was measured a average resistivity of 31.7 $\mu\Omega$·cm and 25.3 $\mu\Omega$·cm with thermal sintering of 100°C and 150°C for biocellulose and PDMS substrates, respectively.

3.2 Impedance

The bioelectric potentials carried in electrolytic media in form of ionic currents, are transduced by the electrodes into electronic signals. This takes place by means of capacitive coupling (without net charge transfer) and by charges transfer reaction in which the electrodes and ions in the physiologic environment exchange electrons through oxidation-reduction reactions. To characterize the behaviour of the electrode interface, electrochemical impedance spectroscopy (EIS) was used to understand the behaviour of the electrode interface properties and the influence of AgCl amount in the electrode.

As explained in Chapter 2, electrodes have a top layer that enables the transduction of ionic concentrations measured by electrodes into electrical potentials. This top layer was obtained by depositing commercial bleach on top of the printed silver, however it was necessary to study the effects of the amount of bleach and the electrodes' electrical

behaviour on the interface. The tested electrodes were the printed flat discs electrodes which were compared to commercial, with similar surface area.

The first step was to guarantee that the bleach was, in fact, contributing to the formation of AgCl layer on top of the printed silver. To confirm this layer formation, it was used a potentiostat that maintained a voltage between two points of the electrode and compares it to a Ag/AgCl reference electrode. The result was that the difference between the printed silver electrode (without bleach) and the reference electrode started to be 50 mV but decrease to 20 mV after two hours. Comparing the difference between the printed silver electrode with bleach and the Ag/AgCl reference electrode, it started with a difference of 30 mV and two hours later the difference was less than 10 mV. This means that the bleach promotes the formation of AgCl layer and the printed electrode with bleach could be compared to a Ag/AgCl electrode.

The influence of the amount of bleach on printed electrodes was verify using EIS in which the impedance of electrode's interface was measured for signals with a frequency range from 5 Hz to 13 MHz. Using EIS device *4192A LF Impedance Analyzer, Hewett-Packard* it was registered the frequency, f (Hz), the impedance, $|Z|$ (Ω) and the phase angle, θ (rad) of the signal. With these values Nyquist plot (see Figure 3.2) was built achieving a semicircle, characteristic of a single RC equivalent circuit. The Nyquist plot is composed of a real (X axis) and an imaginary part (Y axis) from the impedance equation (see Equation 3.3). The left side of the plot represents low frequencies and the right side (near plot's origin) represents higher frequencies, however is not possible to tell what frequency was used to each point.

$$Z = |Z|(cos(\theta) + isin(\theta)) \tag{3.3}$$

Typically, for a perfect single RC circuit, the semicircle must start in the origin of the X axis. In the Nyquist plot for printed flat discs it was detected a equivalent circuit similar to a resistor in series with a RC circuit. The first resistor represents the electrolyte resistance and can be observed as the first zero of the semicircle. The electrolyte resistance consists the uniformity current distribution through a definitive electrolyte area. It was observed that the electrolyte resistance was 15 kΩ, 3 kΩ and 21 kΩ for commercial, printed with diluted bleach and printed with pure bleach. The difference of electrolyte resistance between both printed electrodes can be justified for imperfections on pattern's printing which can change the current flow.

The second semicircle's zero corresponds to the polarization resistance or the charge transfer resistance. Unfortunately, for commercial electrodes was not possible to measure the impedance at frequencies lower than 5 KHz but according with [21] and [38] its

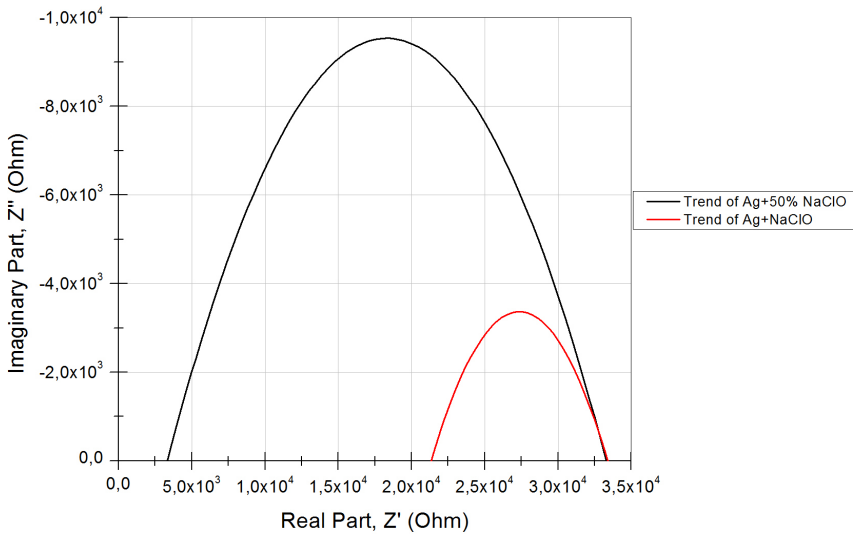

FIGURE 3.2: Nyquist plot for printed electrodes

impedances are between 350 and 450 Ω, approximately the same value of polarization and charge transfer resistance. The measurements for this resistance were 33 kΩ for both printed flat electrodes. The charge transfer resistance is smaller which means that the charge is easily transferred, electrons enter the metal and the metal ions diffuses into the electrolyte faster. However, the high value of polarization resistance for the commercial electrodes is an advantage since it allows the passage of current between the electrolyte solution and the electrode's metal without modifying the charge distribution of the solution nearby the electrode. Printed electrodes have a smaller polarization resistance which allows the passage of current between the solution and the electrode by means of a variation on charge distribution on the solution near the electrode. For that reason, with printed electrodes is more likely to occur motion artefact, so its important to establish a strong contact between skin and electrode.

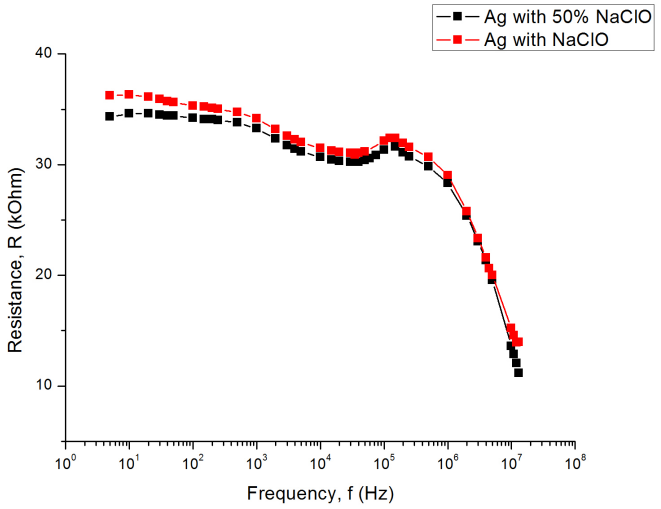

FIGURE 3.3: Plot of resistance according to frequency for printed electrodes.

Plotting the electrode resistance according to the frequency (see Figure 3.3), its observed that printed electrodes have smaller resistance, approximately 35 kΩ, compared with commercial, with values between 350 and 450 kΩ. Furthermore, printed electrodes have larger values of capacitance with, approximately 250 nF, compared to 20 nF for commercial electrodes.

3.3 ECG measurements

ECG signals are probably the most well known biosignals, and can be found in multiple applications in the medical and quality of life domain. It is typically used to measure the rate and regularity of heartbeats and the presence of any pathology in the heart.

The performance of the gelled, dry and printed inkjet electrodes (see Appendix A, EP2) were tested during the acquisition of ECG signals. The ECG signals were acquired in both hands, as illustrated in Figure 3.4 with two acquisition systems: BIOPAC and BITalino, described further in Chapter 5. It was performed four experiments using the three types of electrodes. Each experiment consisted of a 30 seconds recording done simultaneously with the BIOPAC and the BITalino using a sampling rate of 1000 Hz in both devices. It was collected ECG signals from 20 subjects in a static standing position, with the electrodes applied as shown in Figure 3.4.

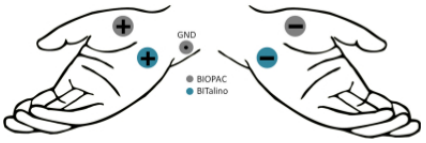

FIGURE 3.4: Electrode leads placement for ECG measurements.

Two features were employed for evaluation purposes, namely the signal-to-noise ratio (SNR) computed from the data collected with both devices for each experiment, and the Root Mean Square Error (RMSE), calculated with equation 3.4, of the difference between synchronized signals with the different electrodes.

$$RMSE(x,y) = \sqrt{\frac{\sum_{k=1}^{N}(x[k]-y[k])^2}{N}} \tag{3.4}$$

It was calculated the distribution of the SNR differences for all subjects and was considered the interest signal to be concentrated on the 5 - 20 Hz band of its frequency spectrum, and the remainder as noise.

The lowest value of SNR with the BITalino device was obtained in the experiment 4, when using the paper electrodes, obtaining a SNR of -1.87±2.14 dB and -3.80±2.66 dB

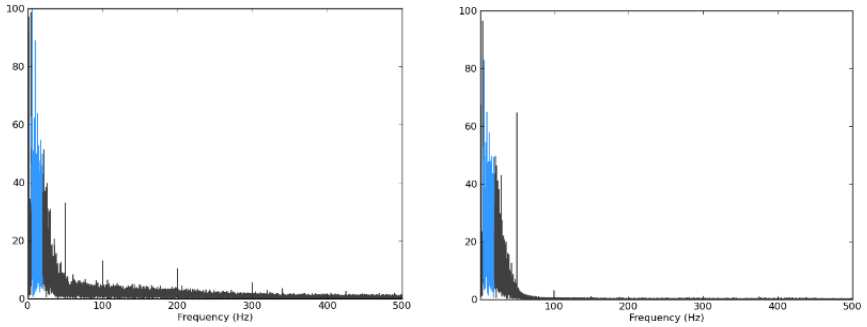

(a) BIOPAC (b) BITalino

FIGURE 3.5: ECG signal frequency spectrum for both acquisition devices. The blue region indicates the interest signal and the remainder the noise.

measured with BITalino and BIOPAC device, respectively. The SNR of BITalino was higher than BIOPAC, which was already expected due to the analogic filtering occuring in the BITalino ECG sensor.

In what concerns the ECG morphology, all the experiments have shown a high similarity between the ECG signals obtained from both devices. Despite the comparison between the two devices, it was interesting finding that the inkjet printed electrodes show a very good performance when compared to the other electrodes, with a reasonable RMSE value. For all the experiments, we verified very low RMSE values, indicating that the signals obtained from all three types of electrodes retain much of the waveform morphology.

Although the signals obtained with the paper-based electrodes present a lower signal-to-noise ratio, the ECG morphology is maintained, which results in a similar performance when compared to the conventional gelled Ag/AgCl electrodes used in clinical contexts.

3.4 EMG measurements

The detection of electromyographic signals was performed using two different data acquisition: BIOPAC MP45 data acquisition unit and the BITalino device that was further validated as a capable device for measuring biosignals. Before any recording, both data acquisitions devices were set with a sampling frequency of 500Hz.

To collect EMG signals, was used a bipolar approach using three electrodes, one for reference and two for effectively collect the activity. The two surface electrodes detects two potentials with respect to the reference electrode and the reading value is the difference of the two electrodes. The printed and standard electrodes were placed always in similar

positions, one electrode in the wrist as a reference electrode and the other two in the anterior part of the forearm, spaced with approximately 4 cm.

With BIOPAC data acquisition, it was collected signals from 4 subjects with age between 23 and 26 years old that used a forearm bandage with three printed spiked electrodes (one ground electrode) linked to a BIOPAC electrode lead set (SS2LA/L) fed into a MP45 data acquisition unit. The same experiment was performed using common BIOPAC disposable electrodes placed near the location of the previous electrodes. Before any recording, the system was calibrated for each electrode set and a sampling frequency of 500Hz was used. It was asked the subject to wait a few seconds and then to perform a series of four exercises of hand clench, release and wait. The subject began with a weak hand clench and then increased clenching intensity such that the fourth clench is at maximum strength.The same experience but using commercial electrodes was done simultaneously since BIOPAC allows the usage of a maximum of three channels at the same time. The result can be observed in Figure 3.6.

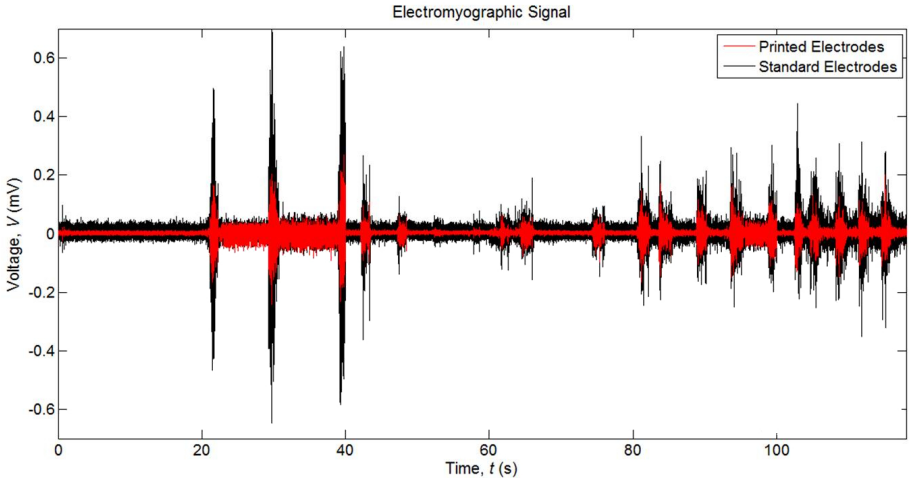

FIGURE 3.6: EMG signal recorded with commercial and spiked electrodes recorded at the same time.

With the collected data values of SNR were calculated using equation 3.5 where the root mean square (RMS) is calculated using the equation 3.6, N is the total number of points and $x[i]$ is the voltage of one point which results on the power of the EMG signal.

$$SNR_{dB} = 20log(\frac{RMS_{signal}}{RMS_{noise}}) \tag{3.5}$$

$$RMS = \sqrt{\frac{1}{N}\sum_{i=1}^{N}(x[i])^2} \tag{3.6}$$

Since the frequency band of interest for EMG signals is between 5 to 500 Hz, therefore approximately all the frequencies read by the data acquisition devices, it won't make sense to select from the frequency spectrum the frequencies of interest. To solve this problem of extracting the points referring to user's movements and the points referring to noise signal, it was developed a tool for find the movement's beginning. Thus, the RMS_{signal} was calculated from the points of extracted movements and RMS_{noise} was calculated from points where movements where not detected. It was asked to the subjects that waited, at least, 10 seconds before performing any movement for good perception of noise in EMG signals.

From the experiment perform with BIOPAC using commercial (BIOPAC) and printed spiked electrodes (silver onto photographic paper) at the same time, it was calculated several SNR values for both types of electrodes (see Figure 3.7). The figure shows values of SNR for different subjects where the height of the box plot indicates the degree of dispersion, the band inside the box represents the median and the bottom and top of the box are the first and third quartiles. The median value of SNR was higher for commercial electrodes (approximately 15 dB) than printed spiked electrodes (approximately 10 dB). The dispersion of values is slightly larger for printed electrodes and can be due to the contact between skin and electrode not be stable all the time. The time response, visible on Figure 3.7 for both electrodes when movements were performed was very reasonable.

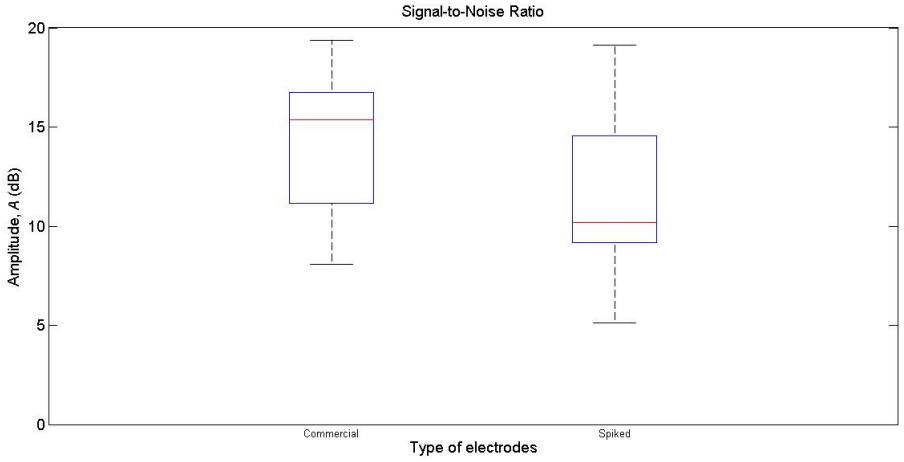

FIGURE 3.7: Signal-to-noise ratio of commercial and spiked electrodes, recorded at the same time.

Using BITalino as acquisition device, it was collected signals from 10 subjects with age between 16 and 52 years old in a static sit position with the elbow in contact with the table. These experiments were performed using different commercial and several types of printed electrodes, namely, flat discs, arrays and spiked on photographic paper; flat discs on biocellulose; and flat discs and arrays on PDMS. Due to the number of channels of BITalino, which is one, the experiments were performed one at a time and

not simultaneous as the experience before. The SNR calculation (see Equation 3.5) and the extraction of movements were similar to the ones used on BIOPAC's experience and are full explained in Chapter 4.

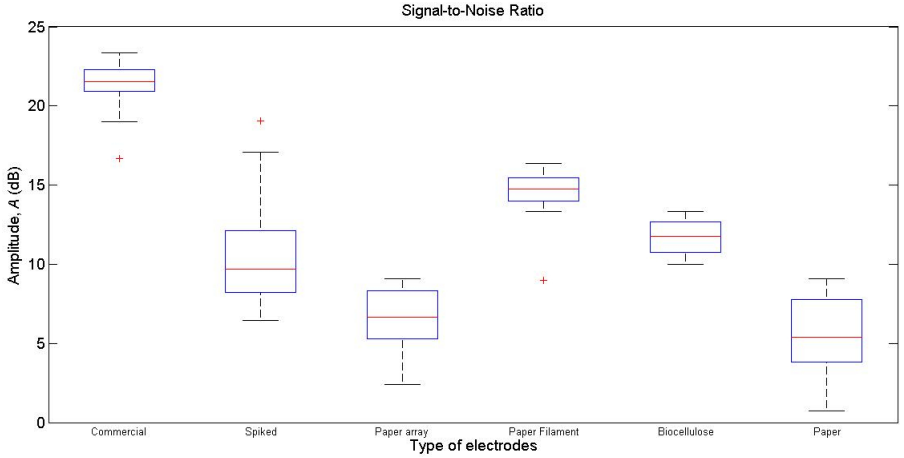

FIGURE 3.8: Signal-to-noise ratio of commercial and several print electrodes.

The results showed that commercial electrodes still have the best SNR, with median of approximately 22 dB when compared to printed electrodes, however, some types of printed electrodes have quite reasonable results. For spiked electrodes a more accurate experience was performed on BIOPAC's acquisition data unit where simultaneous acquisition was taken. Yet, in this experience similar results were obtained whereas the median SNR value for printed spiked electrodes were, again, approximately 10 dB and has a similar dispersion as the first experience. Spiked electrodes have demonstrated potential of being a useful type of printed electrodes for further use.

Flat discs and array electrodes printed in photographic paper have demonstrated similar results since de median for both is approximately 5 dB. These results showed that paper array may not introduce major advantages when printed on photographic paper because its main characteristic is the possibility stretchability which in paper in not very useful. However, if the array were bigger, increasing the number of small electrodes interconnected and increasing the area of contact, may bring advantages of material wasting. Since the data acquisition is similar to full printed electrodes, it would be interesting print array of electrodes where several small areas are in blank (with no ink).

An interesting finding was the electrode made with just one filament and small contact area but with reduce resistivity (13Ω·cm) have a SNR median value of approximately 15 dB and a small dispersion. This means that reducing the resistivity of silver ink after the printing procedure increase the performance of the electrode for measuring biosignals. This result make perfectly sense because reducing material's resistivity implies an increase of conductivity and the ability of conducting an electric current is also increase.

Biocellulose printed electrodes have also a low resistivity (∼31Ω·cm) due to high temperature sintering, therefore the EMG results showed SNR values of approximately 13 dB and a small dispersion. Another feature of biocellulose when measuring biosignals is that the sheet can be wet from the outside (surface not in contact with the skin). The physical behaviour of wet biocellulose in contact with the skin is similar to thin wet paper placed on the skin. When still wet, the contact between skin and electrode is strong and no damage is cause for electrode's ink or substrate. This feature is very interesting and commonly seen in thin films.

Similar results of biocellulose electrodes were expected for PDMS printed electrodes. Despite optimization of printing and sintering procedures and treatment of PDMS, when it has contact with the skin the ink is removed and clings to the skin. A strong contact with the skin and the PDMS electrode is difficult and a slight movement may cause ink's removal. To rectify and improve the adhesion between skin/PDMS and PDMS/ink is necessary further work, thereby decreasing the PDMS thickness and its hydrofobicity could be an option to achieve those goals. Yet, decreasing PDMS thickness increase it fragility and could rip more easily because a small hole is necessary to transmit information between both PDMS surfaces. In that spot, the hole weakens the whole structure and flexibility and stretchability are compromised. Nevertheless PDMS characteristics have tremendous advantages of being used in such devices as printed electrodes. During the resistivity tests and preparation of electrodes, namely arrays of electrodes in PDMS, it is verified that the conductivity of printed lines were kept even after deformation (stretching and bending) of the substrate. During large stretching, the conductivity were compromised but restored when the substrate returned to its initial state.

Chapter 4

Signal Processing

4.1 Movement detection

The SNR measurements were performed by comparing the power of both signal and noise of EMG biosignals. Therefore, an accurate tool for detect signals of interest (user's movement) was inserted in signal processing post-acquisition. For a correct extraction of movements, its critical the success of identification of the onset movement which indicates the instant that the movement began. If the identification of the onset movement is incorrectly detect, might result in a earlier detection which implies an inclusion of a big amount of noise or a late detection excluding the movement's beginning or even all movement.

There is two proper ways to identify the onset movement, which consists in a manual and a automatic manner. The manual way implies a personal signal examiner or the use of other physical measurement that must be performed at the same time as the movement, for instance, the use of an accelerometer that change drastically its value by shaking it when the movement is made. However, the automatic way its more comfortable, inexpensive and could be applied after signal's acquisition for every data.

Several detection algorithms have been introduced earlier by Lidierth [39], Hodges [40], Bonato [41], Abbink [42] and others. The mentioned algorithms have the same basic principle because they all are threshold based methods which are simpler than statistical methods. Statistical methods are generally better performing identification of onset movements but need more computational power therefore not suitable for real time processing. Amongst threshold based methods, it was choose for this work the Bonato due to its simple application, good results achievements for offline and real time applications and small SNR sensitivity when compared to other methods [43].

Bonato method for identification of onset movements was applied on EMG data acquired on experiences mentioned above. The method consists in first, transform the signal to raw data (absolute value of signal) followed by implementation of whitening filter which makes the noise similar to the white noise, attenuating high spectral components and enhancing low ones. The test function, g_k, is then determined by the sum of squared successive samples which divides by the baseline variance (σ_0^2). Usually, the initial 10 seconds of recording is movements free so this segment is used as background noise and its variance is obtained (see Equation 4.1).

$$g_k = \frac{1}{\sigma_0^2} \times (x_{i-1}^2 + x_i^2),\ for\ odd\ i,\ \ i \geqslant 1 \tag{4.1}$$

When g_k is higher than a threshold, h, the method produces t_a which is a estimation of the time that onset of movement occurs. However, the method accept the onset estimative, at least n out of m successive samples must exceed the threshold h, indicating the active state of the muscle. Furthermore, is considered that the muscle's active state must last for at least t_1 seconds. If all the thresholds were exceeded, the earliest beginning of active state is taken as the onset time, t_0. This double threshold scheme provides a high degree of freedom for selecting detection parameters and could be adjusted to different target data. However, the size of m samples dictates the test window that will be used and if it is small the accuracy of the test may be compromised, if its too large the computational time is increased.

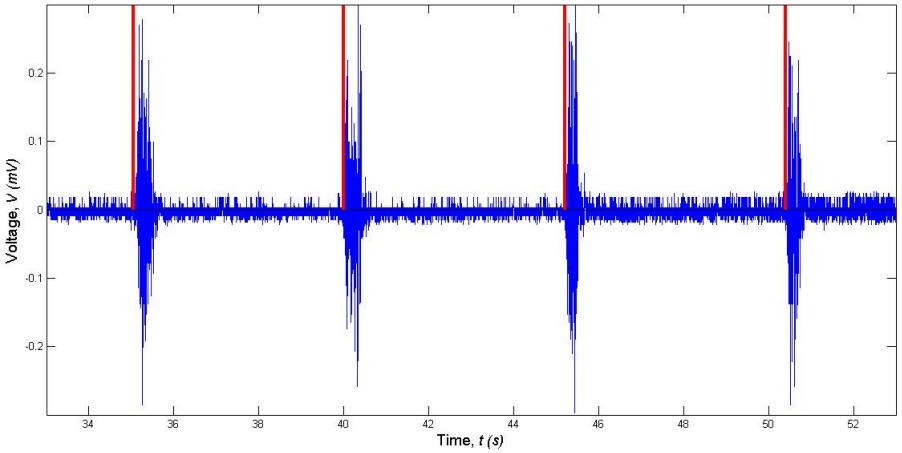

FIGURE 4.1: Onset times (red) using Bonato method in EMG measurements.

For Bonato application in EMG measurements (see Figure 4.1), the threshold values adopted were similar for different type of electrodes, however it was a need to sometimes slightly adjust them, namely, the value of h. The reason is the voltage measured with printed electrodes was smaller than the commercial ones, so in that cases, the threshold must decrease.

Since the movements were always similar, it was not adopted the Bonato method for detecting the end of movements. Therefore, the movements were assumed to last 1.5 seconds after the onset time. The result of movements extraction using printed electrodes on biovellulose is show in Figure 4.2.

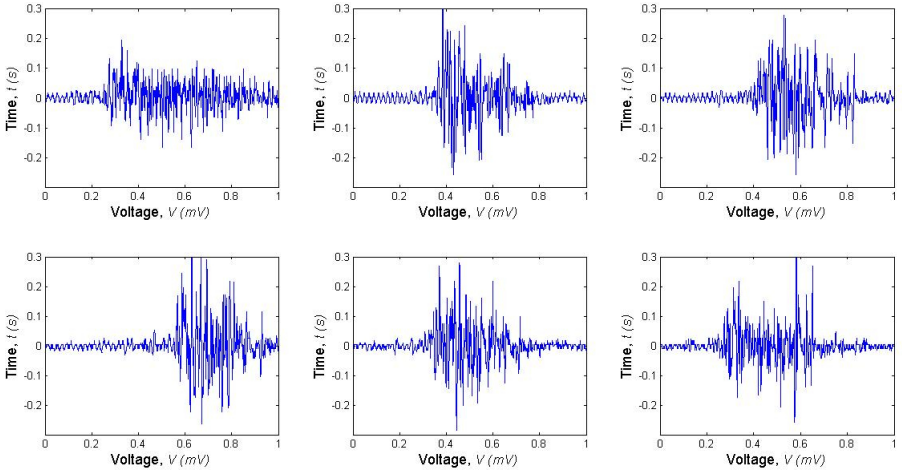

FIGURE 4.2: Movements extracted from a EMG experience using flat discs electrodes printed on biocellulose.

4.2 Feature extraction

Each EMG data acquire has at least one minute of recording with a sampling frequency of 1000 Hz which means that each EMG has approximately 60000 points. The feature extraction has as main task of reducing these amount of data elements to a set of features that distinguish one type of movement to another. The same number of features have been extracted from each type of movement done by one person using different printed electrodes. Despite of the possibility of using two types of features extraction, temporal and spectral, temporal approaches were mostly used. The reason is, once more, the easy implementation of algorithms and the efficiency of its results are well suited for further real time feature extraction without abuse of time and computational power. For this thesis, it was used six temporal approaches and one on frequency domain that are described bellow and which have demonstrated potentials when applied to EMG biosignals [44–46].

One of the extracted features was the movement's root mean square already mentioned in Chapter 3 which is calculated using Equation 3.6. It relates to standard deviation and represents features in time domain based on signal amplitude.

Two others features extracted from the signal is the integrated EMG, *iEMG*, which is calculated as the the sum of the absolute values of the EMG signal (see Equation 4.2),

where N represents the length of the signal (total number of samples) and x_i the voltage of a single sample. This feature is useful to calculate a similar one, the mean absolute value, *MAV*, which is calculated by taking the average of the absolute value of EMG signal (see Equation 4.3).

$$iEMG = \sum_{i=1}^{N} |x_i| \tag{4.2}$$

$$MAV = \frac{1}{N} \sum_{i=1}^{N} |x_i| \tag{4.3}$$

More features were used to fill a vector containing EMG information. The waveform length, *WL*, is the comulative length in amplitude between two consecutive samples. This means that for an entire EMG segment, *WL* represents the distance from the first sample to the last one, like if both ends were pull and straight. The waveform length is related with signal's amplitude, duration and frequency in just one equation (see Equation 4.4).

$$WL = \sum_{i=2}^{N} |x_i - x_{i-1}| \tag{4.4}$$

Zero crossing, *ZC* indicates a frequency of significant changes in EMG by counting the number of times that the amplitude value crosses the zero of Y-axis, switching from positive to a negative signal and vice-versa. Since this feature is sensible to noise, a threshold is implemented to reduce its influence. *ZC* is calculated using Equation 4.5 and 4.6.

$$ZC = \sum_{i=1}^{N-1} [sgn(x_i \times x_{i+1}) \cap |x_i - x_{i+1}| \geq threshold] \tag{4.5}$$

$$\text{where } sgn(x) = \begin{cases} 1, & \text{if } x \geq \text{threshold} \\ 0, & \text{otherwise} \end{cases} \tag{4.6}$$

The slope sign change (*SSC*) is a similar method to zero crossing that counts the number of changes between positive and negative slope among three consecutive samples. Once more, the feature is performed with a threshold that ensures that only significant changes are counted. This feature also represents frequency information of EMG signal and is calculated using Equations 4.7 and 4.8.

$$SSC = \sum_{i=1}^{N-1} [f[(x_i - x_{i-1}) \times (x_i - x_{i+1})]] \tag{4.7}$$

$$\text{where } f(x) = \begin{cases} 1, & \text{if } x \geq \text{threshold} \\ 0, & \text{otherwise} \end{cases} \tag{4.8}$$

Finally, the only frequency approach for feature extraction was the auto regressive coefficients, AR, which represents the linear combination of each sample to previous samples. In this thesis, was applied a sixth order AR [46] however similar results are obtained with orders of AR between the first and the tenth order [45, 47].

The several features extracted from EMG data of three types of movements recorded with different types of electrodes were grouped in a matrix with 12 rows, corresponding to extracted features (six dimensions from the first six features and six dimensions from AR) and several columns corresponding to the number of movements tested (at least 15 of each type).

4.3 Classification

Linear Discriminant Analysis (LDA) is a well-known method for characterize and separate two or more classes of objects which has been used in applications such as face recognition [48], text classification [49]. LDA takes as its input a set of high dimensional features grouped into classes and maximize the distance between classes whereas minimizes the distance within classes [46]. This way, is achieved maximum discrimination that can be used for EMG pattern recognition.

In this thesis, LDA method was used to prove that printed electrodes are good enough to distinguish three types of movements (see Figure 4.3) using printed flat discs electrodes on biocellulose, filamentary electrodes and array of electrodes printed on photographic paper. The measurements were performed with BITalino to one subject that performed at least 15 movements (in some cases, more than 20) for each type of movement and electrode.

For each data collected, the procedure since its acquisition was similar. Each movement was extracted using Bonato method, explained above, then features were extracted building a matrix with 12 features for each movement. Finally, the LDA method was applied analysing two classes twice, i.e., first a discrimination was performed between movement 1 (class 1) and the other two movements (class 0), see Figure 4.4; Second,

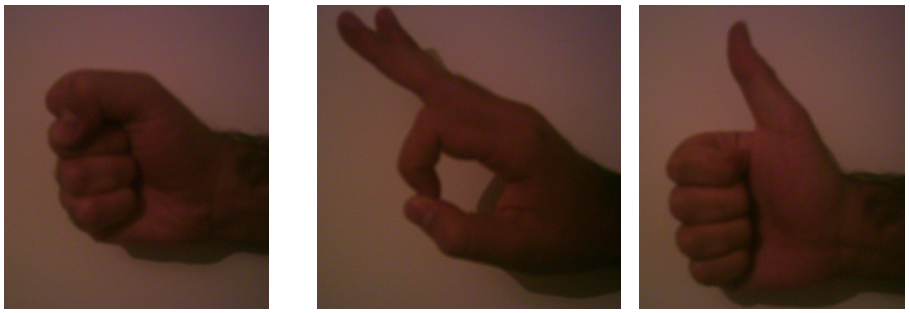

(a) Movement 1 (b) Movement 2 (c) Movement 3

FIGURE 4.3: Hand movement subjected to Linear Discriminant Analysis.

the discrimination was performed between movement 2 (class 1) and movement 3 (class 0), see Figure 4.5. The reason why was made two studies is because the first movement, hand's clench, is much stronger with higher voltages than the other two values. So, its expected that the discrimination between movement 1 versus movement 2 and 3 be more explicit. For both experiments, half of the data were used as training of LDA and the other half was used as testing. The training and testing session was performed 2000 times and the correct rate was performed in a box-and-whisker plot.

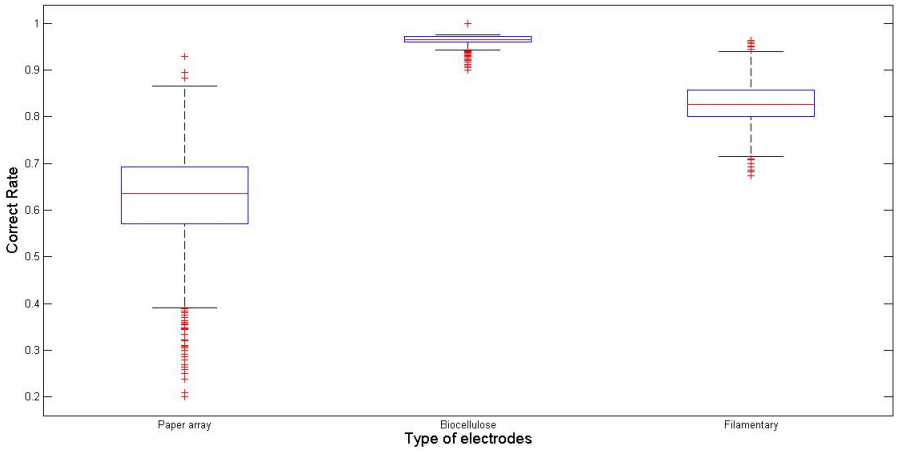

FIGURE 4.4: Linear Discriminant Analysis result for movement 1 versus movement 2 and 3

Fifty per cent of data that was not used on training, it was used for testing the LDA machine. The three types of printed electrodes tested, the filamentary electrode printed on photographic paper and the flat disc electrode printed on biocellulose and paper, showed that more than 60% of the data is correctly recognized. For printed electrodes on biocelullose, this value reach 96% value on distinguish correctly between movement 1 and the other two. However, for this type of electrode, the recognition between movement 2 and 3 is much lower due to similarity of patterns of both movements. The best recogninition between this both movements was performed by filamentary electrodes which have a correct rate of 80% in this experiment.

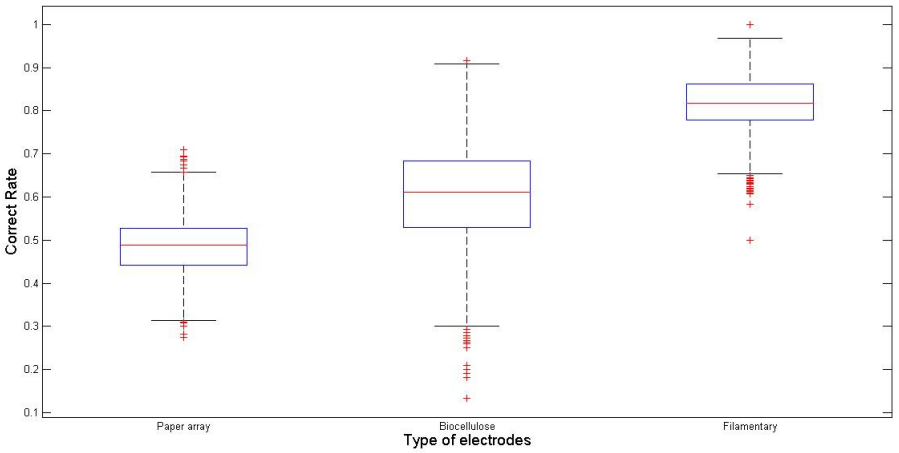

FIGURE 4.5: Linear Discriminant Analysis result for movement 2 versus movement 3

The low resistivity after electrical sintering have proved to be a great advantage for obtaining low SNR values and a high rate for distinguish different movemens, when its patterns are similar. The lowest correct rate measured was achieved by flat discs electrodes printed on photographic paper that showed a rate of 50% of correctly pattern recognition. This means that if the movement 2 or movement 3 is performed by the user, the machine system will just recognize correctly one out of two movements.

Chapter 5

Printed Circuits

A research group from *Instituto de Telecomunicações, Instituto Superior Técnico*, Lisbon developed a device, BITalino, that enables a real-time acquisition which its primary function is the use of ECG signal for integration in a biometric system. BITalino is a generic acquisition platform that enables the acquisition of multiple physiological signals, namely electrocardiography, electromiography, electrodermal activity (EDA), and accelerometry (ACC). Additionally, it also provides a light sensor and a light emitting diode (LED).

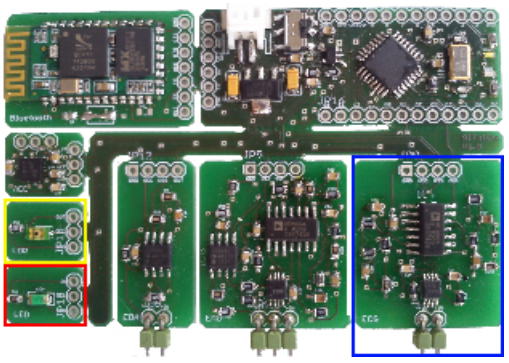

FIGURE 5.1: The BITalino platform highlighting the ECG (blue), the light sensor (yellow) and the LED (red) circuits.

The ECG sensor is based on voltage potential differential principles. Accordingly, to measure the low potential differences associated with these signals (in mV range), it includes a precision instrumentation amplifier and has low-noise high speed operational amplifiers to perform bandpass filtering and amplification. The ECG sensor was designed for 2-lead measurement of the bioelectrical activity of the heart and it is specially designed for hands electrode placement. However, it is also possible to place the electrodes in standard location (chest).

For this thesis, an attempt to reproduce some of these integrated circuits (ECG, light sensor and LED) by inkjet printing was performed. The objective was to print the same circuits design using silver ink as conductive material and photographic paper as substrate.

5.1 Fabrication Procedure

The firsts steps of the three printed circuits fabrication (ECG, LED and light sensor) were similar as those for electrodes, explained in section 2.3. The design used to inkjet print the circuit was similar to the used for standard printed circuit board (PCB) production, which in case of ECG circuit was a double layer circuit. Since the ECG circuit was much complex than the LED and light sensor, it requires the use of calibration marks for both layers be aligned.

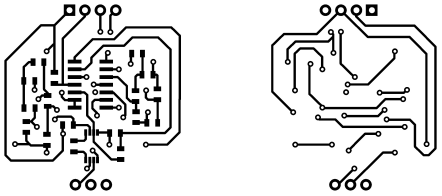

(a) (b)

FIGURE 5.2: Printed circuit patterns. (a) Front layer and (b) bottom layer.

As a substrate, it was used both sided photographic paper for printing both layers of the circuit. This paper was thinner ($\sim$130 μm) than the one used for electrodes development and more flexible. However, it *printability* was similar to the thickest photographic paper. After printing one side of the circuit, it was used a pin to make four holes in the calibration marks and the other layer of the circuit was aligned using those holes.

After printing both sides of the paper, the circuit ink was sintered by heating at 85°C during 30 minutes. Then, vias which are electrical connections between layers that goes through from the top layer to the bottom one, were made using a pin. The holes where filled with conductive silver paste (*Agar Scientific*) for ensure a good contact between layers. Finally, the electronic components were placed in the right places using the same silver paste, as intermediate between the printed circuit and the component.

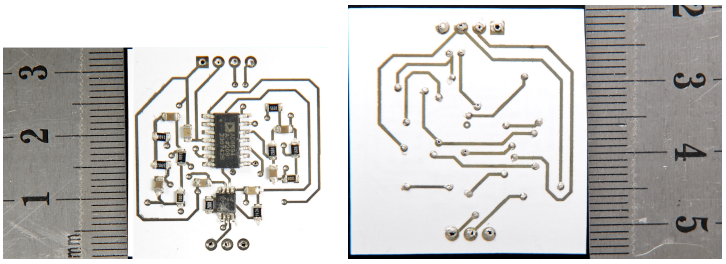

(a) (b)

FIGURE 5.3: ECG printed circuit. (a) Front layer and (b) bottom layer.

5.2 Circuit performance

Unfortunately the ECG printed circuit wasn't successful accomplished. Despite several attempts to connect the printed ECG sensor to BITalino almost all were unsuccessful. The reason was due to a high fragility of the printed system because the placement of many rigid components, such as resistors, capacitors and integrated circuits, into a flexible substrate as the double sided photographic paper, made the whole structure very delicate to handling. Due to the reduce size of surface-mount technology components, the use of silver glue was limited for causing no short circuits therefore the components were weakly attached to the paper. Yet, the major difficulty was to glue the integrated circuits, especially the responsible for signal filtration because its pads were spaced with approximatery 200 μm.

The components glued with conductive silver glue were often removed unintentionally just by handling the device. In some attempts, the printed circuit was sealed with a thin plastic (parafilm) and submitted to a brief heating with air at 250°C to melt the plastic and encapsulate the circuit. However, a resistor was removed by connecting the circuit to perform tests. So, further work will be necessary to achieve a strong and permanent contact between the components and the paper. An interesting option might be the use of a flexible electric insulator, such as PDMS, to encapsulate the circuit after placing the electronic components.

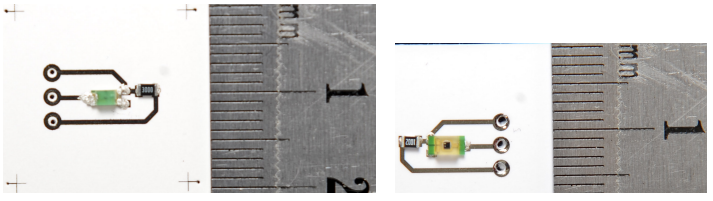

(a) LED (b) Light sensor

FIGURE 5.4: Light sensor and LED printed circuit

Yet, the simpler printed devices such as the LED and the light sensor (see Figure 5.4) worked perfectly when integrated with the BITalino fabricated with standard methods. Those circuits were only composed by two components: a LED plus a resistor or a light sensor plus a resistor. The substrate used was the typical photographic paper which is thicker and less flexible than the one used for printed ECG sensor.

Chapter 6

Conclusions

6.1 Main results

Inkjet technology has advantages as a fabrication method when compared to other conventional procedures. Inkjet technology allows the deposition of several materials directly with non contact with it, mask-less and the possibility of printing over a previous printed pattern. Due its versatility of inks (conductive, polymers and organic) and substrates, direct deposition of materials with high precision ($\sim$5 μm) using simple methods, this technique shows a high potential as a fabrication method. Despite the wide range of applications of inkjet printing in electronics, a lack of intend for printing devices for collecting biosignals. The subject of the work presented was the first step towards the development of a inkjet device for a close contact with skin for collecting biosignals.

The versatility of inkjet printing allowed to print electrodes, using a inkjet printer DMP-2831, onto substrates that included photographic paper, biocellulose and PDMS and test the performance of different designs: standard flat discs, spiked, filamentary and serpentine array of small electrodes. The study consisted in optimizing substrate treatments, printing and sintering (thermal and electrical) procedures to take high advantage of each one. Results of this optimization procedures showed an advantage of using electrical sintering to minimize the resistivity of silver ink by reducing it, approximately 82% of its initial value, from 76 $\mu\Omega$·cm to 13 $\mu\Omega$·cm. However, not all the designs and substrates tolerate electrical sintering. The changes of silver ink resistivity were due, exclusively to sintering procedure and printing quality.

A comparison between similar commercial and printed electrodes showed that both acts as an RC equivalent circuit despite of the difference on resistor component for low frequencies signals (higher for commercial electrodes). The printed electrodes were

tested by collecting EMG signals from ten subjects, measuring signal-to-noise ratios to understand the quality of the signal. Like expected, commercial electrodes had the best SNR values, of 22 dB, followed by filamentary electrodes printed onto photographic paper (15 dB), biocellulose electrodes (13 dB) and spiked electrodes using paper as substrate (10 dB). Tests performed on PDMS electrodes showed a poor adhesion between the substrate and ink. When the electrodes were in contact with the skin, a slight movement cause ink's removal and the electrode could not be used again. Although the firsts seconds of recorded signal seemed to be reasonable wasn't possible to record data using those electrodes.

For ECG measurements, larger and thicker printed electrodes were used on hands and the results showed a SNR difference between commercial and printed electrodes of only -3.80 dB. This can be explained by the contact of printed electrodes with the skin. In ECG measurements it asked to subjects to hold printed paper-based electrodes in their hand tightly. In EMG measurements, however, electrodes were placed on a armlet and the contact with the skin was probably weaker.

Although the performance of printed electrodes has been slightly weaker than commercial ones, it was performed a linear discriminant analysis to understand if the printed electrodes can be used for pattern recognition of movements. This experience was performed on one subject that performed three different hand movements (see Figure 4.3) at least 15 times. Since the first movement is stronger (hand clench) than the other two, it was performed a discrimination of movement one versus movement two and three and then between movement 2 versus movement 3. Results showed that its possible to recognize isolated movements even weak movements (movement two and three).

This work also included the development of printed electronic circuits in photographic paper to further integration of printed electrodes. The objective of this part of the work was to reproduce three BITalino modules: the light sensor, the LED and the ECG sensor. The most complex of the three modules was, indeed, the ECG sensor that included analogic amplification and filtration of ECG biosignals. However, this circuit wasn't successful accomplished. Despite of several attempts, the introduction of many rigid components (resistors, capacitors and integrated circuits) into a flexible substrate as the photographic paper made the whole structure very delicate to handling. The components glued with conductive silver paste were often removed unintentionally by just handling the device. Further work will be necessary to achieve a strong and permanent contact between the components and the paper. Yet, the simpler printed devices such as the LED and the light sensor worked perfectly when integrated with the BITalino fabricated with standard methods.

6.2 Applications

The development of this thesis is the first step towards the development of a inkjet devices for a close contact with skin for collecting biosignals, so all the advantages that inkjet printing technology hold can be used to develop solutions in biomedicine.

Inkjet printed electrodes, namely for EMG measurements, have a wide range of possible applications especially for hand/forearm rehabilitation procedures, brain-computer interfaces and simple use in clinical environment. The use of the printed electrodes presented in this work might be a low cost option to conventional commercial electrodes. When printed in thin sheets like biocellulose, it performs a strong contact with the skin making it comfortable to use. Also the use of flexible substrates lead to better accordance with the shape of the body's region that is increased with the decrease of sheet thickness. Also, the use of spiked electrodes introduce the possibility of a gel free electrodes for a more practical use.

For brain-computer interfaces, printed electrodes could have a interesting advantage by adjusting the electrodes' design to the region or function to be monitored. Inkjet printing provides the possibility of different patterns easily and quickly. For instance, it can be developed simultaneous small or large electrodes that fits perfectly in desire regions in the forearm to extract measurements of those exactly muscles. Once acquired those data, it could be applied to control games on a computer based on movements recognition. In computer games industry, the use of biosignals is one major priority. Biosignals allows a closely interaction between the player and the game making it more appealing.

Another application consists in using movements recognition for monitoring hand rehabilitation process. Hand rehabilitation is usually long but especially boring for those who must perform it. The introduction of printed electrodes could permit the usage of rehabilitating movements to interact with a software which the subject enjoy to interact. This way, hand rehabilitation could become less boring and the data of movements performed by the subject can be recorded and showed to a physician which evaluates his progress.

6.3 Future Work

In this work, the first step of collecting biosignals with inkjet printing devices was made. Further work must include an optimization of PDMS printability and adhesion. PDMS is

a remarkable substrate for fabricating flexible electronic devices, therefore an optimization of PDMS treatment and/or in the sinterization of silver must be done to improve the adhesion of silver to the substrate. Another solution is to use different substrate with similar characteristics, such as polyimide, namely krapton. Krapton is a polyimide film which remains stable across a wide range of temperatures and has demonstrated applications in flexible electronics, namely on electronic skin.

Further work on inkjet printing circuits must also be done. The use of elastic conductive glue might be an interesting solution to overcome the problem of substrate flexibility and components hardness. However, a practical solution can be test which includes the encapsulation of printed electronic circuit. The idea is to maintain the process of printing and paste the components with conductive glue on photographic paper (not elastic) and then encapsulate it with a flexible insulator like PDMS. If the PDMS does not pressure electronic components to move when it is shed above it, when it became dry and solid perhaps the circuit become more stable and flexible to handling.

More complex research can be done to towards this work achieving an electronic skin device (see Figure 1.10). This will be possible if the cables were removed from the electrodes and sensors by adding wireless components to the flexible substrates. Wireless powering via inductive effects represents an appealing option to inductively power the device. Optimizing the power efficiency of wireless link is imperative to minimize the size of external energy source, heating dissipation in the tissue and interferance with other devices. Coils geometries are the most important factor in defining the link power efficiency therefore is a need to study and optimize different designs of wireless power coils, such as square shaped and circumferential printed spiral coils.

For total cable removal from the flexible device capable of measuring biosignals, future work must include a development of antennas to transmit data using, for instance, radio frequencies. Radio frequency identification (RFID) has been demonstrated as an developing tool in printed electronics for sending information using specified band frequencies. This device can be used to build wireless electrodes in which the current that flows through the tag change the frequency of the transmitted signal proportional to collected biosignal.

Bibliography

[1] Bok Yeop Ahn, Steven B Walker, Scott C Slimmer, Analisa Russo, Ashley Gupta, Steve Kranz, Eric B Duoss, Thomas F Malkowski, and Jennifer a Lewis. Planar and three-dimensional printing of conductive inks. *Journal of visualized experiments*, (58):1–8, January .

[2] Krishna Balantrapu, Meaghan Mcmurran, and Dan V Goia. Inkjet Printing of Silver Nanoparticles for Electronic Applications. *Advanced Materials Processing*.

[3] Thomas Blaudeck, Reinhard R Baumann, and Aslok Sridhar. Inkjet Printing as a Key Enabling Technology for Printed Electronics. *Material Maters*, 6:1–8, 2011.

[4] ZhouPing Yin, YongAn Huang, NingBin Bu, XiaoMei Wang, and YouLun Xiong. Inkjet printing for flexible electronics: Materials, processes and equipments. *Chinese Science Bulletin*, 55(30):3383–3407, November 2010.

[5] Madhusudan Singh, Hanna M Haverinen, Parul Dhagat, and Ghassan E Jabbour. Inkjet printing-process and its applications. *Advanced materials (Deerfield Beach, Fla.)*, 22(6):673–85, February 2010.

[6] Paul Calvert. Inkjet Printing for Materials and Devices. *Chemistry of Materials*, 13(10):3299–3305, October 2001.

[7] Herman Wijshoff. The dynamics of the piezo inkjet printhead operation. *Physics Reports*, 491(4-5):77–177, June 2010.

[8] G D Martin, S D Hoath, and I M Hutchings. Inkjet printing - the physics of manipulating liquid jets and drops. *Journal of Physics: Conference Series*, 105: 012001, March 2008.

[9] By Jolke Perelaer, Antonius W. M. de Laat, Chris E. Hendriks, and Ulrich S. Schubert. Inkjet-printed silver tracks: low temperature curing and thermal stability investigation. *Journal of Materials Chemistry*, 18(27):3209, 2008.

[10] Sungjune; Jung. *Fluid characterisation and drop impact in inkjet printing for organic semiconductor devices.* PhD thesis, University of Cambridge, 2011.

[11] Emine Tekin, Patrick J. Smith, and Ulrich S. Schubert. Inkjet printing as a deposition and patterning tool for polymers and inorganic particles. *Soft Matter*, 4(4): 703, 2008.

[12] Jurgen Brunahl. *Physics of Piezoelectric Shear Mode Inkjet Actuators*. PhD thesis, Royal Institute of Technology, 2003.

[13] Jürgen Brünahl and Alex M. Grishin. Piezoelectric shear mode drop-on-demand inkjet actuator. *Sensors and Actuators A: Physical*, 101(3):371–382, October 2002.

[14] Joseph D. Bronzino. Biopotential Electrodes. In *The Biomedical Engineering Handbook: Second Edition*, chapter 48. CRC Press, second edi edition, 2000.

[15] C. de Luca. Electromyography. In J. G. Webster, editor, *Encyclopedia of Medical Devices and Instrumentation*, pages 98 – 109. Wiley-Interscience, 2006.

[16] L A Geddes, L E Baker, and A G Moore. Optimum electrolytic chloriding of silver electrodes. *Med. & Biol. Eng.*, 7(July 1968):49–56, 1969.

[17] R. S. C. Cobbold. Transducers for biomedical measurements: Principles and applications. *Wiley*, 1974.

[18] Clifford D. Ferris. *Introduction to Bioelectrodes*. Plenum Publishing, 1974.

[19] Herman P. Schwan. Determination of biological impedances. In William Nastuk Gerald Oster, editor, *Physical Techniques in Biological Research*, pages 322–405. Academic Press, 1963.

[20] John W. Clark, Michael R. Neuman, Walter H. Olson, Robert A. Peura, and Frank P. Primiano. *Medical instrumentation: application and design*. John Wiley & Sons, inc, fourth edi edition, 2009.

[21] Yu Mike Chi, Tzyy-ping Jung, and Gert Cauwenberghs. Dry-Contact and Noncontact Biopotential Electrodes: Methodological Review. *IEEE*, 3:106–119, 2010.

[22] Patrick Griss and Heli K Tolvanen-Laakso. Characterization of micromachined spiked biopotential electrodes. *IEEE transactions on bio-medical engineering*, 49 (6):597–604, June 2002.

[23] Nuno Sérgio Dias, João Paulo Carmo, Paulo Mateus Mendes, and José Higino Correia. Wireless instrumentation system based on dry electrodes for acquiring EEG signals. *Medical engineering & physics*, 34(7):72–81, September 2012.

[24] Zhenqiang Ma. An electronic second skin. *Science (New York, N.Y.)*, 333(6044): 830–1, August 2011.

[25] Dae-Hyeong Kim, Nanshu Lu, Rui Ma, Yun-Soung Kim, Rak-Hwan Kim, Shuodao Wang, Jian Wu, Sang Min Won, Hu Tao, Ahmad Islam, Ki Jun Yu, and Tae-il Kim. Epidermal electronics. *Science (New York, N.Y.)*, 333:38–43, August 2011.

[26] B. Kumar, H.S. Tan, N. Ramalingam, and S.G. Mhaisalkar. Integration of ink jet and transfer printing for device fabrication using nanostructured materials. *Carbon*, 47(1):321–324, January 2009.

[27] E. Menard, R. G. Nuzzo, and J. a. Rogers. Bendable single crystal silicon thin film transistors formed by printing on plastic substrates. *Applied Physics Letters*, 86(9), 2005.

[28] Seungjun Chung, Jaemyon Lee, Hyunsoo Song, Sangwoo Kim, Jaewook Jeong, and Yongtaek Hong. Inkjet-printed stretchable silver electrode on wave structured elastomeric substrate. *Applied Physics Letters*, 98(15):110–153, 2011.

[29] Gerard Cummins. Inkjet printing of conductive materials: a review. *Circuit World*, 38(4):193–213, 2012.

[30] Tomasz Falat, Bartosz Platek, and Jan Felba. Sintering Process of Silver Nanoparticles in Ink-Jet Printed Conductive Microstructures - Molecular Dynamics Approach. pages 1–5, 2012.

[31] Ju-Yeoul Baek, Jin-Hee An, Jong-Min Choi, Kwang-Suk Park, and Sang-Hoon Lee. Flexible polymeric dry electrodes for the long-term monitoring of ECG. *Sensors and Actuators A: Physical*, 143(2):423–429, May 2008.

[32] Carola Essö. *Modifying Polydimethylsiloxane (PDMS) surfaces*. PhD thesis, 2007.

[33] Liang Guo, Gareth Guvanasen, Christopher Tuthill, T. Richard Nichols, and Stephen P. DeWeerth. A low-cost, easy-fabricating stretchable microneedle-electrode array for intramuscular recording and stimulation. *2011 5th International IEEE/EMBS Conference on Neural Engineering*, pages 562–565, April 2011.

[34] Xiameter. An Overview of Polydimethylsiloxane (PDMS) Fluids in the Environment. Technical report.

[35] M Waleed Shinwari, David Zhitomirsky, Imran a Deen, P R Selvaganapathy, M Jamal Deen, and D Landheer. Microfabricated reference electrodes and their biosensing applications. *Sensors (Basel, Switzerland)*, 10(3), January 2010.

[36] Ana T Pereira, João Martins, Jorge Morgado, and Hugo A Ferreira. Applications of Inkjet Printing for Organic Electronics Organic Thin-Film Transistors and Electrodes for Electromyography. 2013.

[37] Paul Gatenholm and Dieter Klemm. Paul Gatenholm and Dieter Klemm. 35 (March):208–214, 2010.

[38] Wendy Franks, Iwan Schenker, Patrik Schmutz, and Andreas Hierlemann. Impedance characterization and modeling of electrodes for biomedical applications. *IEEE transactions on bio-medical engineering*, 52(7), July 2005.

[39] M. Lidierth. A computer based method for automated measurement of the periods of muscular activity from an emg and its application to locomotor emgs. *Electroenceph. Clin. Neurophysiol.*, 1986.

[40] P. W. Hodges and B. H. Bui. A comparison of computer-based methods for determination of onset of muscle contraction using electromyography. *Electroenceph. Clin. Neurophysiol.*, 1996.

[41] P. Bonato, T. D'Alession, and M. Knaflitz. A statistical method for the measurement of muscle activation intervals from surface myoelectric signal during gait. *IEEE Trans. Biomed. Eng.*, pages 287–298, 1998.

[42] J. H. Abbink, A. van der Bilt, and H. van der Glas. Detection of onset and termination of muscle activity in surface electromyograms. *Journal Oral Rhab.*, 1998.

[43] Gerhard Staude. Onset Detection in Surface Electromyographic Signals: A Systematic Comparison of Methods. 2001(2):67–81, 2001.

[44] M Hamedi, A M Noor, T T Swee, and I K Afizam. Comparison of Different Time-domain Feature Extraction Methods on Facial Gestures' EMGs. pages 1897–1900, 2012.

[45] Angkoon Phinyomark, Chusak Limsakul, and Pornchai Phukpattaranont. A Novel Feature Extraction for Robust EMG Pattern Recognition. 1(1):71–80, 2009.

[46] A. Phinyomark, H. Hu, P. Phukpattaranont, and C. Limsakul. Application of Linear Discriminant Analysis in Dimensionality Reduction for Hand Motion Classification. *Measurement Science Review*, 12(3):82–89, January 2012.

[47] Omry Paiss and Gideon F Inbar. Autoregressive Modeling of Surface EMG and Its Spectrum with Application to Fatigue. *IEEE transactions on biomedical engineering*, 34(10):761–770, 1987.

[48] Xiaogang Wang and Xiaoou Tang. Random sampling LDA for face recognition. *Proceedings of the 2004 IEEE Computer Society Conference on Computer Vision and Pattern Recognition, 2004. CVPR 2004.*, 2:259–265, 2004.

[49] Peg Howland, Moongu Jeon, and Haesun Park. Structure Preserving Dimension Reduction for Clustered Text Data Based on the Generalized Singular Value Decomposition. *SIAM Journal on Matrix Analysis and Applications*, 25(1):165–179, January 2003.

Appendix A

Electrode data sheet

Ag/AgCl Printed Electrodes Data Sheet

Name	Info	Sketch	Photo
EP1	**Substrate:** Photo Paper, 230µm thick **Ink:** *SunTronic* Jettable Silver **Sintering:** 85°C, 30min. **Shape:** Planar, circle **Dimensions:** 10mm diameter, ≈0.55µm thick **Area:** 73.9 mm^2 **Contact:** Metallic snap with silver paste (Agar Scientific) **Top Layer:** Gel and commercial bleach	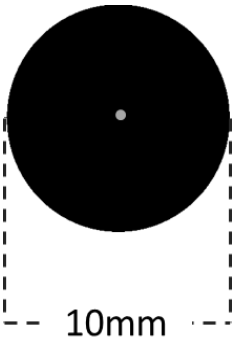	
EP2	**Substrate:** Photo Paper, 230µm thick **Ink:** *SunTronic* Jettabble Silver **Sintering:** 85°C, 30min. **Shape:** Planar, rectangle **Dimensions:** 80mm x 30mm x ≈1µm **Area:** 2400mm^2 **Contact:** Metallic snap with silver paste (Agar Scientific) **Top Layer:** Commercial bleach	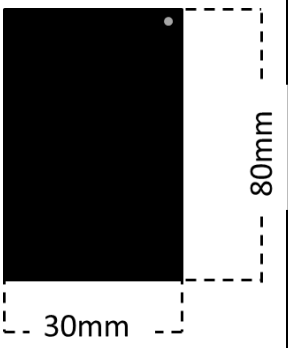	Not Available
EP3	**Substrate:** PDMS, variable thickness **Ink:** *SunTronic* Jettabble Silver **Sintering:** 150°C, 30min. **Shape:** Planar, circle **Dimensions:** 10mm diameter, ≈0.55µm thick **Area:** 73.9mm^2 **Resistance:** **Contact:** Metallic snap with silver paste (Agar Scientific) **Top Layer:** Commercial bleach	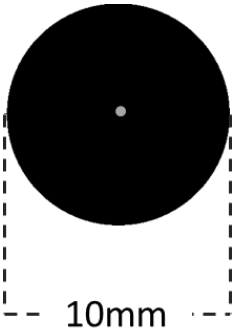	

EP4	**Substrate:** Biocellulose, 50µm thick **Ink:** *SunTronic* Jettabble Silver **Sintering:** 100°C, 30min. **Shape:** Planar, circle **Dimensions:** 10mm diameter, ≈0.55µm thick **Area:** 73.9mm^2 **Contact:** Metallic snap with silver paste (Agar Scientific) **Top Layer:** Commercial bleach	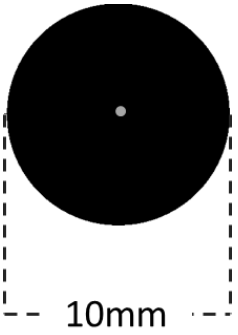	
EP5	**Substrate:** Photo paper, 230µm thick **Ink:** *SunTronic* Jettabble Silver **Sintering:** 85°C, 30min. **Shape:** Planar, circle **Dimensions:** 23.3mm x 10mm x ≈0.55µm **Resistance:** ≈35kΩ **Contact:** Metallic snap with silver paste (Agar Scientific) **Top Layer:** Commercial bleach	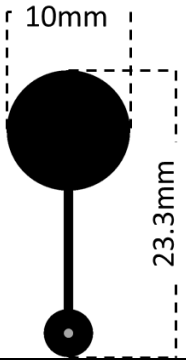	Not Available
EP6	**Substrate:** Photo paper, 230µm thick **Ink:** *SunTronic* Jettabble Silver **Sintering:** 85°C, 30min then electrical sintering with 35V. **Shape:** One continuous filament, planar, circle **Dimensions:** 10mm diameter, ≈0.55µm thick **Area:** 50.1 mm^2 **Contact:** Metallic snap with silver paste (Agar Scientific) **Top Layer:** Commercial bleach	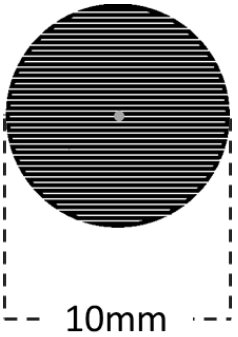	

ES1	**Substrate:** Photo paper, 230µm thick **Ink:** *SunTronic* Jettabble Silver **Sintering:** 85°C, 30min. **Shape:** Spiked, circle **Dimensions:** 10mm diameter, ≈40µm height (spike height) **Contact:** Metallic snap with silver paste (Agar Scientific) **Top Layer:** Commercial bleach **Additional information:** Spiked array with approximately 244 spikes spaced with ≈270µm. Spikes with pyramid shape. Each spike has a bottom layer of ≈270µm diameter and a top layer of ≈30µm diameter	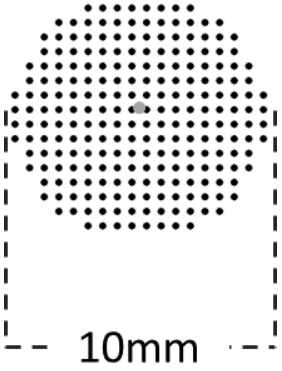	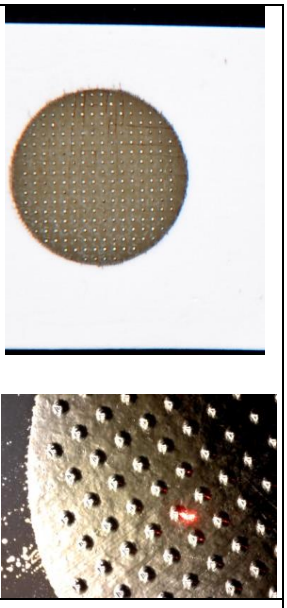
EGR1	**Substrate:** Photo paper, 230µm thick **Ink:** *SunTronic* Jettabble Silver **Sintering:** 85°C, 30min. **Shape:** Planar, circle **Dimensions:** 13mm diameter, ≈0.55µm thick **Area:** 101.3mm^2 **Contact:** Metallic snap with silver paste (Agar Scientific) **Top Layer:** Commercial bleach	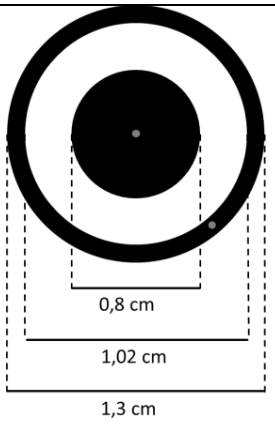	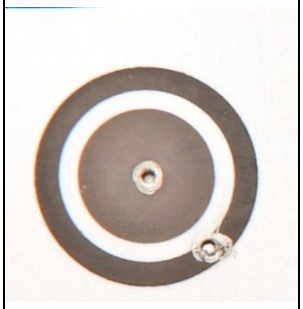
EGR2	**Substrate:** Photo paper, 230µm thick **Ink:** *SunTronic* Jettabble Silver **Sintering:** 85°C, 30min. **Shape:** Planar, rectangle **Dimensions:** 16mm x 12mm x ≈0.55µm **Area:** 128.8mm^2 **Contact:** Metallic snap with silver paste (Agar Scientific) **Top Layer:** Commercial bleach	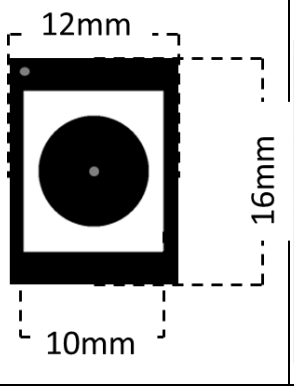	

EGR3	**Substrate:** Photo paper, 230µm thick **Ink:** *SunTronic* Jettable Silver **Sintering:** 85°C, 30min. **Shape:** Planar, circle **Dimensions:** 18.8mm x 12.8mm x ≈0.55µm **Contact:** Metallic snap with silver paste (Agar Scientific) **Top Layer:** Commercial bleach	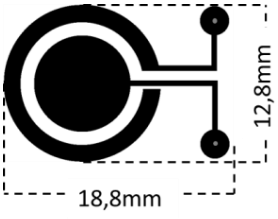	Not Available
EGR4	**Substrate:** Photo paper, 230µm thick **Ink:** *SunTronic* Jettable Silver **Sintering:** 85°C, 30min. **Shape:** Planar, rectangle **Dimensions:** 18.4mm x 16mm x ≈0.55µm **Contact:** Metallic snap with silver paste (Agar Scientific) **Top Layer:** Commercial bleach	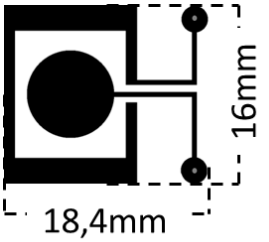	Not Available
EA1	**Substrate:** PDMS, variable thickness **Ink:** *SunTronic* Jettable Silver **Sintering:** 150°C, 30min. **Shape:** Planar, rectangle **Dimensions:** 18mm x 18mm x ≈0.55µm **Area:** ≈74.6mm^2 **Contact:** Metallic snap with silver paste (Agar Scientific) **Top Layer:** Commercial bleach	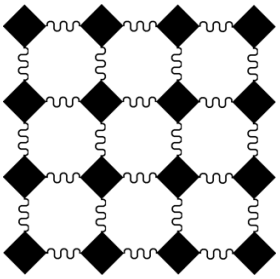	Not Available
EA2	**Substrate:** Photo paper, 230µm thick **Ink:** *SunTronic* Jettable Silver **Sintering:** 85°C, 30min. **Area:** ≈84.2mm^2 **Shape:** Planar, rectangle **Dimensions:** 14mm x 14mm x ≈0.55µm **Contact:** Metallic snap with silver paste (Agar Scientific)	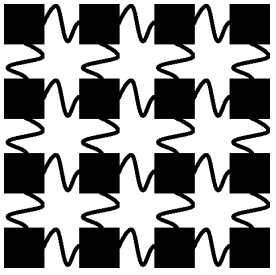	
EA3	**Substrate:** PDMS, variable thickness **Ink:** *SunTronic* Jettable Silver **Sintering:** 150°C, 30min. **Area:** ≈84.2mm^2 **Shape:** Planar, rectangle **Dimensions:** 14mm x 14mm x ≈0.55µm **Top Layer:** Commercial bleach	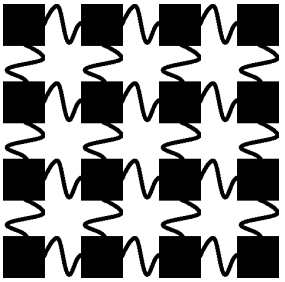	

Appendix B

MATLAB code

MATLAB FUNCTIONS FOR IMPLEMENTATION OF BONATO METHOD, MOVEMENT EXTRACTION AND FEATURES EXTRACTION

```
%%%%%%%%%%%%%%%%%%%%%%%%%%%%%%%%%%%%%%%%%%%%%%%%%%%%%%%%%%%%%%%%%%%%%%%%%%%%%%%
% BONATO METHOD
%%%%%%%%%%%%%%%%%%%%%%%%%%%%%%%%%%%%%%%%%%%%%%%%%%%%%%%%%%%%%%%%%%%%%%%%%%%%%%%
function [ Onset ] = Bonato( signal, time )
%%Bonato - This function finds the movement beginning and gives
%%back the first instant of the movement
%%   INPUT: EMG signal
%%          time vector
%%
%%   OUTPUT: Onset times
restVar = var(signal(1:10000));
dt = 1e-3;
%Ta stores g values
ta=zeros(ceil(length(signal)/2),2);
linha=1;
%Calculate Bonato values
for k=1:2:length(signal)-1
    g = 1/restVar*(signal(k)^2+signal(k+1)^2);
    ta_time(linha) = time(k);
    ta(linha,1) = k;
    ta(linha,2) = g;
    linha = linha +1;
end
ta_time(linha)=time(k+1);
h = 15; %Threshold
n =5; %Number of samples that must exceed threshold
m = 500; %In m successive samples
T1=0.1; %seconds
S1 = T1/dt+dt; %Sample number
%firstOnset=ta;
Onset=[];
index=1;
activeCount=0;
firstK=zeros(length(ta),1);
i=1;
onsetFound = false;
% Executes while Onset is being found in the entire segment
while index+m<length(ta)
    countK=0;
    % Loop through m samples to check threshold
    for k=index:index+m-1
        if ta(k,2)>=h
            countK=countK+1;
            if activeCount==0 && countK==1
                firstK = ta(k,1);
            end
        end
    end
    index=index+m;
    if countK >= n
        activeCount = activeCount+1;
    else
        activeCount=0;
    end
```

```
    if activeCount*m >= S1
        Onset(i) = firstK;
        i=i+1;
        onsetFound=true;
    end
end
%Selects the minimum onset, corresponding to movements beginning
firstOnset = min(Onset);
[junk,index] = unique(Onset,'first');
Onset = Onset(sort(index));
amp = zeros(length(Onset),1);
amp = amp+4000;
OnsetTime=(Onset'+1)*dt;
end

%%%%%%%%%%%%%%%%%%%%%%%%%%%%%%%%%%%%%%%%%%%%%%%%%%%%%%%%%%%%%%%%%%%%%%%%%%%%%%%
% MOVEMENT EXTRACTION
%%%%%%%%%%%%%%%%%%%%%%%%%%%%%%%%%%%%%%%%%%%%%%%%%%%%%%%%%%%%%%%%%%%%%%%%%%%%%%%
function [ Mov, MovTime ] = EMG_Movement( signal, Onset )
%EMG_Movement extract the movements done in a window with windowsT
seconds
%   INPUT: Signal
%          Onset
%   OUTPUT: Matrix with length(Onset) columns and windowS raws (Mov)
%           Vector with movements time (MovTime)
Fs=1000; %Hz
dt=1/Fs; %sec
windowT = 1; %seconds
windowS = windowT/dt+dt; %Sample number
Mov = [];
% Select signals segment corresponding to movements
if Onset(1)-ceil(windowS/4) < 1
    windowS = length(signal(1:Onset(1)+ceil(windowS/4)));
elseif Onset(end)+ceil(3*windowS/4) > length(signal)
    windowS = length(signal(Onset(end)-ceil(3*windowS/4):end));
end

for i=1:1:length(Onset)
    Mov = [Mov signal(Onset(i)-
ceil(windowS/4):Onset(i)+ceil(3*windowS/4))];
end
MovTime = 0:dt:dt*length(Mov)-dt;
end

%%%%%%%%%%%%%%%%%%%%%%%%%%%%%%%%%%%%%%%%%%%%%%%%%%%%%%%%%%%%%%%%%%%%%%%%%%%%%%%
% WAVEFORM LENGTH
%%%%%%%%%%%%%%%%%%%%%%%%%%%%%%%%%%%%%%%%%%%%%%%%%%%%%%%%%%%%%%%%%%%%%%%%%%%%%%%
function [ WL ] = EMG_WL( Mov )
%EMG_WL gives the waveform length for each movement
%   INPUT: Vector with movements (Mov)
%
%   OUTPUT: WL of each movement (WL)
Fs=1000; %Hz
dt=1/Fs; %sec
WL = zeros(1,size(Mov,2));
for k=1:1:size(Mov,2)
    for i=1:1:size(Mov,1)-1
```

```
        interm = abs(Mov(i+1,k)-Mov(i,k));
        WL(1,k) = WL(1,k) + interm;
    end
end
end

%%%%%%%%%%%%%%%%%%%%%%%%%%%%%%%%%%%%%%%%%%%%%%%%%%%%%%%%%%%%%%%%%%%%%%%%%%%%%%%
% ZERO CROSSING
%%%%%%%%%%%%%%%%%%%%%%%%%%%%%%%%%%%%%%%%%%%%%%%%%%%%%%%%%%%%%%%%%%%%%%%%%%%%%%%
function [ ZC ] = EMG_ZC( Mov, threshold)
%EMG_ZC gives the zero crossings over a threshold
%   INPUT: Vector with movements (Mov)
%          Zero-Crossing threshold (default 0.1)
%
%   OUTPUT: Zero-Crossing vector (ZC)
Fs=1000; %Hz
dt=1/Fs; %sec
ZC = zeros(1,size(Mov,2));
MovTime = 0:dt:dt*length(Mov)-dt;
figure
p=1;
for k=1:1:size(Mov,2)
    sgn = 0;
    for i=1:1:size(Mov,1)-1
        sgn = Mov(i,k)*Mov(i+1,k);
        if sgn < 0
            sgn = true;
            if abs(Mov(i,k) - Mov(i+1,k)) >= threshold
                ZC(1,k) = ZC(1,k)+1;
            end
        else
            sgn = false;
        end
    end
end
end

%%%%%%%%%%%%%%%%%%%%%%%%%%%%%%%%%%%%%%%%%%%%%%%%%%%%%%%%%%%%%%%%%%%%%%%%%%%%%%%
% SLOPE SIGN CHANGES
%%%%%%%%%%%%%%%%%%%%%%%%%%%%%%%%%%%%%%%%%%%%%%%%%%%%%%%%%%%%%%%%%%%%%%%%%%%%%%%
function [ SSC ] = EMG_SSC( Mov, threshold )
%EMG_SSC gives the slope sign changes
%   INPUT: Vector with movements (Mov)
%          Slope Sign Changes threshold (default 0.01 or 0.05)
%
%   OUTPUT: SSC of each movement (SSC)
Fs=1000; %Hz
dt=1/Fs; %sec
SSC = zeros(1,size(Mov,2));
MovTime = 0:dt:dt*length(Mov)-dt;
figure
p=1;
for i=2:1:size(Mov,1)-1
        if ((Mov(i,k) - Mov(i-1,k)) * (Mov(i,k) - Mov(i+1,k))) >=
threshold
                SSC(1,k) = SSC(1,k)+1;
        end
```

```
end
end

%%%%%%%%%%%%%%%%%%%%%%%%%%%%%%%%%%%%%%%%%%%%%%%%%%%%%%%%%%%%%%%%%%%%%%%%%%%%
% ROOT MEAN SQUARE
%%%%%%%%%%%%%%%%%%%%%%%%%%%%%%%%%%%%%%%%%%%%%%%%%%%%%%%%%%%%%%%%%%%%%%%%%%%%
function [ rms ] = EMG_rms( Mov )
%EMG_rms gives the root mean square of each movement
%   INPUT: vector with movements (Mov)
%
%   OUTPUT: Vector with rms values of each movement (rms)
Fs=1000; %Hz
dt=1/Fs; %sec
rms = zeros(1,size(Mov,2));
for k=1:1:size(Mov,2)
    rms(1,k)=sqrt(1/size(Mov,1)*sum(Mov(:,k).^2));
end

%%%%%%%%%%%%%%%%%%%%%%%%%%%%%%%%%%%%%%%%%%%%%%%%%%%%%%%%%%%%%%%%%%%%%%%%%%%%
% MEAN ABSOLUTE VALUE
%%%%%%%%%%%%%%%%%%%%%%%%%%%%%%%%%%%%%%%%%%%%%%%%%%%%%%%%%%%%%%%%%%%%%%%%%%%%
function [ Mav ] = EMG_MAV( Mov )
%EMG_MAV gives the Mean Absolute Value of each movement
%   INPUT: Vector with movements (Mov)
%
%   OUTPUT: Mean Absolute Value of each movement (Mav)
Mav = zeros(1,size(Mov,2));
for k=1:1:size(Mov,2)
        Mav(1,k) = 1/length(Mov)*sum(abs(Mov(:,k)));
end
end

%%%%%%%%%%%%%%%%%%%%%%%%%%%%%%%%%%%%%%%%%%%%%%%%%%%%%%%%%%%%%%%%%%%%%%%%%%%%
% INTEGRATED
%%%%%%%%%%%%%%%%%%%%%%%%%%%%%%%%%%%%%%%%%%%%%%%%%%%%%%%%%%%%%%%%%%%%%%%%%%%%
function [ iEMG ] = EMG_int( Mov )
%EMG_int gives the integrated EMG
%   INPUT: Vector with movements (Mov)
%
%   OUTPUT: Vector with integrated EMG values (iEMG)
Fs=1000; %Hz
dt=1/Fs; %sec
iEMG = zeros(1,size(Mov,2));
for k=1:1:size(Mov,2)
    for i=1:1:size(Mov,1)
        interm = abs(Mov(i,k));
        iEMG(1,k) = iEMG(1,k) + interm;
    end
end
end

%%%%%%%%%%%%%%%%%%%%%%%%%%%%%%%%%%%%%%%%%%%%%%%%%%%%%%%%%%%%%%%%%%%%%%%%%%%%
% AUTO REGRESSIVE COEFFICIENTS
%%%%%%%%%%%%%%%%%%%%%%%%%%%%%%%%%%%%%%%%%%%%%%%%%%%%%%%%%%%%%%%%%%%%%%%%%%%%
function [ ar_coeffs ] = EMG_AR( Mov, order )
%EMG_AR gives a order number of auto regressive coefficients
```

```
%   INPUT: vector with movements (Mov)
%          Order of AR model (order)
%
%   OUTPUT: Auto Regressive Coefficients (ar_coeffs)
ar_coeffs = zeros(order,size(Mov,2));
for k=1:1:size(Mov,2)
    for i=1:1:order
        interm = arburg(Mov(:,k),order)';
        ar_coeffs(:,k) = interm(2:end);
    end
end
end

%%%%%%%%%%%%%%%%%%%%%%%%%%%%%%%%%%%%%%%%%%%%%%%%%%%%%%%%%%%%%%%%%%%%%%%%%%%%%%%
% FEATURE VECTOR
%%%%%%%%%%%%%%%%%%%%%%%%%%%%%%%%%%%%%%%%%%%%%%%%%%%%%%%%%%%%%%%%%%%%%%%%%%%%%%%
function [ features ] = EMG_feature( Mov, ZC_threshold, SSC_threshold,
AR_order )
%EMG_feature gives all the features of each movements
%   INPUT: Vector with movements
%          Zero-Crossing threshold (default 0.1)
%          Slope Sign Changes threshold (default 0.01)
%          Auto Regressive Order (default 6)
%
%   OUTPUT: Vector with 8 features and dim 13
%               -Line 1: Waveform Length (EMG_WL)
%               -Line 2: Integrated (EMG_int)
%               -Line 3: Zero-Crossing (EMG_ZC)
%               -Line 4: Slope Sign Changes (EMG_SSC)
%               -Line 5: Root Mean Square (EMG_rms))
%               -Line 6: Mean Absolute Value (EMG_MAV)
%               -Line 7:end: Auto Regressive Coefficients (EMG_AR)
close all;
features = zeros(12, size(Mov,2));
features(1,:) = EMG_WL( Mov );
features(2,:) = EMG_int( Mov );
features(3,:) =EMG_ZC( Mov, ZC_threshold);
features(4,:) =EMG_SSC( Mov, SSC_threshold );
features(5,:) =EMG_rms( Mov );
features(6,:) =EMG_MAV( Mov );
features(7:end,:) =EMG_AR( Mov, AR_order );
end
```

Appendix C

CONFTELE paper

Applications of Inkjet Printing for Organic Electronics

Organic Thin-Film Transistors and Electrodes for Electromyography

Ana T. Pereira, Jorge Morgado, Luís Alcácer
Instituto de Telecomunicações,
Instituto Superior Técnico
Av. Rovisco Pais,
P-1049-001 Lisboa, Portugal

João Martins, Hugo A. Ferreira
Instituto de Biofísica e Engenharia Biomédica, Faculdade de Ciências da Universidade de Lisboa
Campo Grande
P-1749-016 Lisboa, Portugal

***Abstract*—This paper presents examples of inkjet printing applications for organic electronics. Two applications developed are presented in detail: organic thin-film transistors fabricated on biocellulose and electrodes for electromyography deposited on photo paper.**

Keywords— inkjet printing, organic electronics, biocellulose, organic thin-film transitors, electromyography,

I. INTRODUCTION

Direct printing of functional materials has several advantages as a patterning technique. This is a noncontact patterning, maskless, low temperature process, which is low cost and compatible with large area and high-throughput processing. It allows additive patterning, with the possibility of using both organic and inorganic materials, and is compatible with the use of flexible substrates, Inkjet printing offers these capabilities having potential to simplify fabrication processes and decrease their costs [1].

Inkjet printing enables direct patterning and deposition of solution-processable materials, thereby enabling low material consumption. It has excellent compatibility with organic and inorganic materials. Since it is based on digital data, microstructures can be easily and rapidly designed and fabricated. Furthermore, scalability to large area manufacturing is possible. In 2008 the Organic Electronics Association predicted that the organic and printed electronics market will exceed $300 billion over the next 20 years [2].

Applications of inkjet printing in electronics vary in a wide range. Detailed reviews about inkjet printing of electronics may be found in references [1] and [2]. In this paper a variety of application examples are presented to demonstrate the possibilities available for this printing technique. A key active element for implementing organic circuits is the organic thin-film transistor (OTFT). All inkjet-printed transistors have been fabricated using a self-aligning process [3]. Another example couples inkjet printing with other fabrication techniques such as lithography to fabricate transistor arrays in flexible substrates [4]. Examples of sensors fabricated by inkjet printing are carbon-nanotubes gas sensors [5], phenolic compounds sensor [6], and humidity sensor [7]. Inkjet-printed grids are used to replace indium-tin oxide (ITO) contacts in solar cells [8], [9]. Examples of silver grids are presented in Figure 1. Printing of indium–zinc–tin-oxide [10] is also used to replace the ITO layer in solar cells. Enhancement of multicrystalline solar cells efficiency is achieved by inkjet printing of quantum dots [11]. Radio-frequency identification (RFID) antennas are fabricated by inkjet printing [12], [13], and an example is shown in Figure 1. An inkjet-patterned, flexible organic memory array was also demonstrated [14]. Active laser arrays were created by inkjet deposition of self-assembled photonic structures [15]. Inkjet printing was used to make a parallel study of the influence on the emission color of pi-conjugated semiconducting polymers varying side chains, film thicknesses and thermal treatment of organic light-emitting diodes (OLED) [16]. High efficiency phosphorescent OLEDs, based on small molecules commonly used in vacuum processes, are fabricated by inkjet printing with performance very close to vacuum deposited devices with similar structure [17]. Quantum dot–polymer composites were inkjet-printed for full-color displays [18]. Finally, the selective inkjet printing of conductors for displays has also been demonstrated [19].

In this paper we present two applications of inkjet printing developed in our group: OTFTs and electrodes for electromyography. OTFTs were fabricated on biocellulose and the electrodes for electromyography were deposited on photo paper.

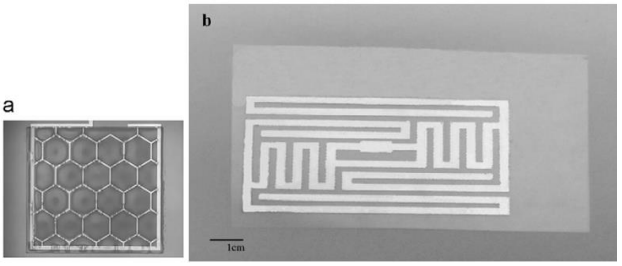

Figure 1. Example of inkjet printed applications: *a*, inkjet printed Ag current collecting grid covered by an inkjet printed layer of PEDOT:PSS (a conducting polymer) [8]; *b* Photograph of inkjet printed radio-frequency identification (RFID) antenna on PET (a common plastic) substrate [13].

We thank FCT for financial support under the contracts PTDC/CTM/102144/2008 and PEst-OE/EEI/LA0008/2011.

A Fujifilm Dimatix 2831 Materials Printer was used for inkjet printing silver and an insulating polymer, poly(vinylphenol) (PVP) inks. This technology consists on a drop-on-demand system controlled by a piezoelectric transducer. When a voltage pulse is applied to the piezoelectric, a drop is ejected. The cartridge emits drops with 10 pL that when printed result in a 30 µm diameter spot. Printing resolution is limited by the size of the drop, which depends ultimately on jetting conditions, the ink, surface energy of substrate, and nozzle diameter.

II. OTFTS FABRICATED ON BIOCELLULOSE

Biocellulose (BC) is a pure form of cellulose naturally produced by the bacteria *Glucanacetobacter xylinus* [20]. Its purity enables the use of BC in medical applications, mainly as artificial temporary skin for wounds and burn healing. The interest to use it as a substrate for fabrication of electronic components is the possibility to develop electronic circuits that can be biocompatible, flexible and low cost. The aim of using BC and BC-based materials as substrates derives from their insulating electronic properties, resistance to high temperatures and high flexibility. BC has also the advantages of being renewable and biodegradable.

A. Fabrication process

The first step of OTFTs fabrication is the planarization of biocellulose. For that, poly(vinylphenol),PVP, is dissolved in hexanol (7.6% (w/v)). Poly(melamine-co-formaldehyde), which acts as cross-linker is added to this solution (in a 0.6 % (v/v)). This solution is deposited by spin coating on the biocellulose substrate. The PVP cross-linking occurs at 200 °C, which renders the PVP film insoluble. Then, for the gate contact, silver nanoparticles ink (SunTronic) is printed and cured at ~150°C. The next step is the printing of the PVP dielectric layer, using the above solution with cross-linker, followed by a thermal annealint at 200 °C to promote the cross-linking reaction. For the source and drain contacts silver is printed and cured at ~150°C. Finally, the organic semiconducting layer of pentacene is thermally evaporated. A scheme of the OTFT, comprising the 5 layers of materials, is shown in Figure 2. Figure 2. also shows a photo of an OTFT fabricated on biocellulose highlighting its flexible properties.

B. OTFT Characterization

The transistors characterization was made under nitrogen dry atmosphere. Output and transfer curves were measured using a HP 4140B pA Metter/DC voltage source. OTFT measured curves are shown in Figure 3. for a transistor with channel width of 3350 µm and length of 135 µm. The calculated mobility is 7×10^{-5} $cm^2/V.s$ and the on/off ratio is 15. The low on/off ratio is attributed to leakage current through the dielectric.

III. ELECTRODES FOR EMG

Biomedical engineering is another field where inkjet printing can be applied. The fabrication of devices used to measure physiological processes is one of example. Electromyography (EMG) signals are formed by physiological variations in the state of muscle fiber membranes which produce an electrical potential difference between two points that can be measured using electrodes. These signals are then analyzed and used as an evaluation tool for medical research or rehabilitation [21].

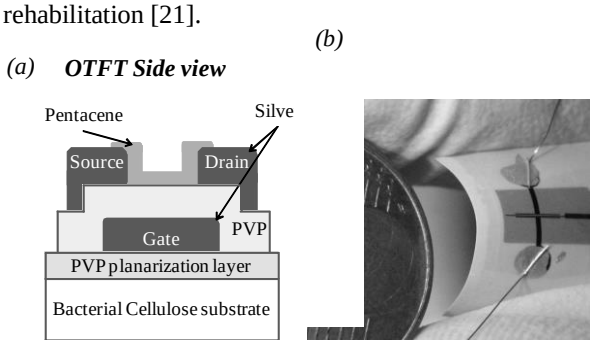

Figure 2. *(a)* Schematic representation of the OTFT structure. *(b)* Photo of OTFT fabricated on biocellulose.

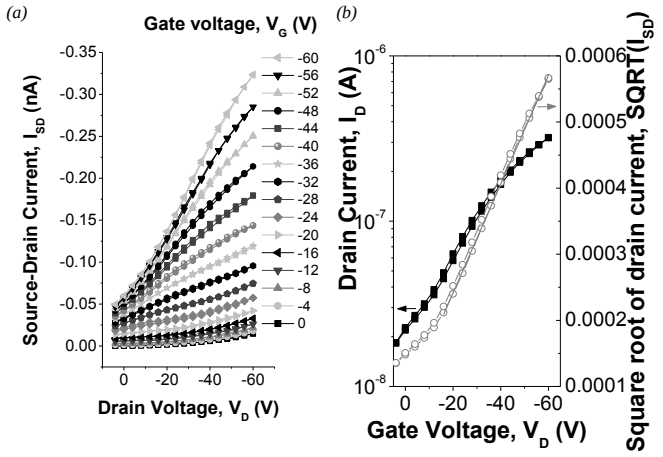

Figure 3. *(a)* Output curve of an OTFT on biocellulose. *(b)* Transfer curve aquired at saturation voltage of 60 V and respective square root curve.

Producing electrodes by inkjet printing enables the use of thin and flexible substrates that may also be biocompatible, as polydimethylsiloxane (PDMS) or biocellulose. On the other hand, low-cost paper-like substrates such as photo paper can be used as substrate and several inks for the conductive part of the electrode (silver, gold or the conductive polymer PEDOT:PSS) can be tested.

A. Fabrication process

The first step was teh selection of a design for electrodes that could be comparable to the commercial and standard wet electrodes used in clinical environment. As comparison, we used BIOPAC circular electrodes with 3.5 cm diameter, which includes the adhesive and the contact part. These disposable electrodes are 1 mm thick and 1 cm diameter in surface area, whereas the surface in contact with skin is about 0.79 cm^2. These electrodes are also covered with an electrolite gel for improved electrical contact.

Our printed electrodes had similar dimensions to BIOPAC's: ~1µm thick and 1cm diameter surface area for contact with the skin. We fabricated electrodes using photo

paper as substrate because it is flexible, cheap, thin (230 µm thickness) and easy to acquire and use. The conductive material used was commercial printable silver ink (SunTronic) composed by silver nanoparticles which provide good electrical conductivity for electronic applications.

Electrodes were printed with four silver layers and subjected to heat treatment during 20 minutes at a temperature of 100ºC.

The second step of the fabricating process was to produce a layer which enables the transduction of ionic concentrations measured by electrodes into electrical potentials. At the interface between the electrodes and the skin, the ionic signal (Cl^- ion transports the charge) is transformed into an electronic signal. Likewise, in common silver electrodes this layer is typically made of AgCl [22]. The formation of this layer was achieved by adding Cl^- ions enabling a reaction between Ag and Cl to produce AgCl. However, due to the thin layer of silver and the fragility of the photo paper, the amount and the manner of introducing Cl^- ions is important. This process was optimized by using commercial bleach deposited by an airbrush at a distance of approximately 30 cm.

The third step in the production of these electrodes was ensuring a good, continuous and practical contact between the printed electrodes and the hardware. Usually, common electrodes have a metal and conductive snap to facilitate the connection of cables and make them practical to use. For the same reason, we use the same snap on printed electrodes. The snaps were placed in the back of the printed surface and the communication to the front was made through a hole filled with a conductive silver paste (Agar Scientific).

The fourth step of the fabricating process is the addition of a new thin top layer of electrolytic gel (KCl gel) that dried at ambient temperature. This gel functions as a protective layer for both skin and electrode and diminishes the impedance of the skin-electrode interface.

Finally, three electrodes were placed on an elastic bandage according to the standard scheme for measuring EMG signals at the forearm, as illustrated in Figure 4.

Figure 4. Printed electrodes set placed on an elastic bandage. Three electrodes are needed to measure an EMG: negative (top left), positive (bottom left) and ground (bottom right).

B. Results

The study of printed electrodes for EMG started with the analysis of the characteristics of a single electrode. In the second part of the study the fabricated electrodes were used to obtain electromyography signals and the results compared with signals obtained from commercial electrodes.

It was observed that the resistivity of the electrode decreases with increasing number of silver layers printed. The electrodes were fabricated by printing 4 layers. An electrode resistivity of 0.142Ω/□ was measured. Impedance studies showed that the magnitude of resistance for common electrodes [23] is approximately $350 \times 10^3\ \Omega$ while for printed electrodes it is approximately $35 \times 10^3\ \Omega$. Analyzing the Nyquist plot (Figure 5) we can verify that the quantity of bleach used on the top layer of electrodes modifies the characteristics of it equivalent circuit. A comparison between commercial and printed electrodes shows that the first have higher resistance but smaller capacitance than the second ones.

The second part of the study involved a real measurements on a subject (male, 22years old) using the forearm bandage with three printed electrodes (one ground electrode) linked to a BIOPAC electrode lead set (SS2LA/L) fed into a MP45 data acquisition unit. The same experiment was performed using common BIOPAC disposable electrodes placed near the location of the previous electrodes.

Before any recording, the system was calibrated for each electrode set and a sampling frequency of 500Hz was used. It was asked the subject to wait a few seconds and then to perform a series of four exercises of hand clench, release and wait. The subject began with a weak hand clench and then increased clenching intensity such that the fourth clench is at maximum strenght.

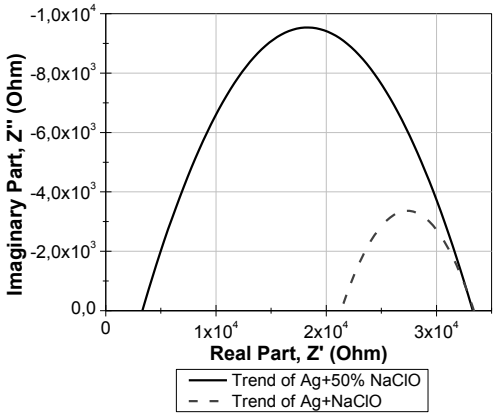

Figure 5. Trend curves of impedance measurements of printed electrodes with pure and diluted bleach.

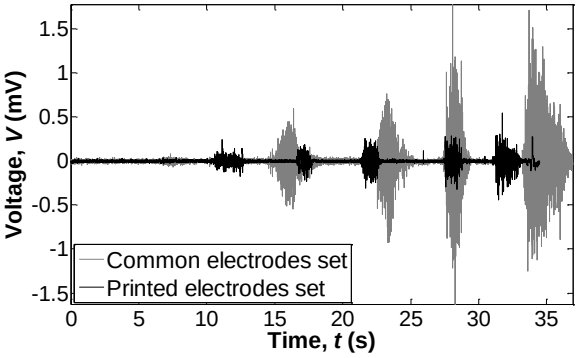

Figure 6. Measurements of EMG signals. Comparison between common and printed electrodes set used on the same subject.

An increase in signal amplitude was observed for both electrode types from the first to the last hand clenching exercise, as shown in Figure 6. Commercial electrodes afforded higher amplitude signals (≈1.5 mV on maximum clench) than printed electrodes (≈0.4 mV on maximum clench). Analyzing the frequency spectrum it was observed that both electrodes sets have similar responses to similar stimulus showing the same noise spikes in in the range of 50 Hz harmonics, except on 100 Hz where printed electrodes have higher amplitude than commercial ones. EMG signals showed similar frequency patterns for both electrode types.

IV. Conclusions

Two different applications of inkjet printing are presented. OTFTs were fabricated by printing contacts and dielectric layers over biocellulose. The OTFTs obtained present a mobility of 7×10^{-5} $cm^2/V.s$ and an on/off ratio of 15. Improvements in OTFT performance are expected upon optimization of the PVP dielectric layer.

Electrodes were printed to be used in electromyography measurements. Compared with common commercial electrodes, a similar measurement of the electromyography signal was obtained, however signal amplitudes are lower. Future steps include a study on the electrodes size. Decreasing the size of the electrodes would enable the fabrication of a higher number of electrodes in the same area, which would increase signal resolution.

Inkjet printing has proven to be a technique proper for depositing materials for a wide range of applications. New applications are expected to be developed in the future such as memories, OLEDs and organic photovoltaic solar cells.

Acknowledgment

The authors acknowledge Carmen Freire from CICECO for the bacterial cellulose films.

References

[1] Z. Yin, Y. Huang, N. Bu, X. Wang, and Y. Xiong, "Inkjet printing for flexible electronics: Materials, processes and equipments," *Chinese Science Bulletin*, vol. 55, no. 30, pp. 3383–3407, Nov. 2010.

[2] M. Singh, H. M. Haverinen, P. Dhagat, and G. E. Jabbour, "Inkjet printing-process and its applications.," *Advanced materials (Deerfield Beach, Fla.)*, vol. 22, no. 6, pp. 673–85, Mar. 2010.

[3] H.-Y. Tseng and V. Subramanian, "All inkjet-printed, fully self-aligned transistors for low-cost circuit applications," *Organic Electronics*, vol. 12, no. 2, pp. 249–256, Feb. 2011.

[4] H. Chen, C. Kung, W. Houng, Y. Peng, Y. Hsien, C. Chou, C.-J. Kao, T.-H. Yang, and J. Hou, "Polymer Inverter Fabricated by Inkjet Printing and Realized by Transistors Arrays on Flexible Substrates," *Journal of Display Technology*, vol. 5, no. 6, pp. 216–222, Jun. 2009.

[5] H. Lee, G. Shaker, K. Naishadham, S. Member, X. Song, M. Mckinley, B. Wagner, M. Tentzeris, and A. Carbon, "Carbon-Nanotube Loaded Antenna-Based Ammonia Gas Sensor," vol. 59, no. 10, pp. 2665–2673, 2011.

[6] R. S. J. Alkasir, M. Ornatska, and S. Andreescu, "Colorimetric paper bioassay for the detection of phenolic compounds.," *Analytical chemistry*, vol. 84, no. 22, pp. 9729–37, Nov. 2012.

[7] H. Andersson, A. Manuilskiy, T. Unander, C. Lidenmark, S. Forsberg, and H.-E. Nilsson, "Inkjet Printed Silver Nanoparticle Humidity Sensor With Memory Effect on Paper," *IEEE Sensors Journal*, vol. 12, no. 6, pp. 1901–1905, Jun. 2012.

[8] Y. Galagan, E. W. C. Coenen, S. Sabik, H. H. Gorter, M. Barink, S. C. Veenstra, J. M. Kroon, R. Andriessen, and P. W. M. Blom, "Evaluation of ink-jet printed current collecting grids and busbars for ITO-free organic solar cells," *Solar Energy Materials and Solar Cells*, vol. 104, pp. 32–38, Sep. 2012.

[9] J.-S. Yu, I. Kim, J. Kim, J. Jo, T. T. Larsen-olsen, R. R. Søndergaard, H. Markus, D. Angmo, F. C. Krebs, M. Hösel, and M. Jørgensen, "Silver front electrode grids for ITO-free all printed polymer solar cells with embedded and raised topographies, prepared by thermal imprint, flexographic and inkjet roll-to-roll processes.," *Nanoscale*, vol. 4, no. 19, pp. 6032–40, Sep. 2012.

[10] J. Kim, S.-I. Na, and H.-K. Kim, "Inkjet printing of transparent InZnSnO conducting electrodes from nano-particle ink for printable organic photovoltaics," *Solar Energy Materials and Solar Cells*, vol. 98, pp. 424–432, Mar. 2012.

[11] X. Pi, L. Zhang, and D. Yang, "Enhancing the Efficiency of Multicrystalline Silicon Solar Cells by the Inkjet Printing of Silicon-Quantum-Dot Ink," *The Journal of Physical Chemistry C*, vol. 116, no. 40, pp. 21240–21243, Oct. 2012.

[12] K. Koski, E. Koski, J. Virtanen, T. Björninen, L. Sydänheimo, L. Ukkonen, and A. Z. Elsherbeni, "Inkjet-printed passive UHF RFID tags: review and performance evaluation," *The International Journal of Advanced Manufacturing Technology*, vol. 62, no. 1–4, pp. 167–182, Dec. 2011.

[13] X. Nie, H. Wang, and J. Zou, "Inkjet printing of silver citrate conductive ink on PET substrate," *Applied Surface Science*, vol. 261, pp. 554–560, Nov. 2012.

[14] T. N. Ng, B. Russo, B. Krusor, R. Kist, and A. C. Arias, "Organic inkjet-patterned memory array based on ferroelectric field-effect transistors," *Organic Electronics*, vol. 12, no. 12, pp. 2012–2018, Dec. 2011.

[15] D. J. Gardiner, W.-K. Hsiao, S. M. Morris, P. J. W. Hands, T. D. Wilkinson, I. M. Hutchings, and H. J. Coles, "Printed photonic arrays from self-organized chiral nematic liquid crystals," *Soft Matter*, vol. 8, no. 39, p. 9977, 2012.

[16] E. Tekin, H. Wijlaars, E. Holder, D. a. M. Egbe, and U. S. Schubert, "Film thickness dependency of the emission colors of PPE?PPVs in inkjet printed libraries," *Journal of Materials Chemistry*, vol. 16, no. 44, p. 4294, 2006.

[17] S.-H. Jung, J.-J. Kim, and H.-J. Kim, "High performance inkjet printed phosphorescent organic light emitting diodes based on small molecules commonly used in vacuum processes," *Thin Solid Films*, vol. 520, no. 23, pp. 6954–6958, Sep. 2012.

[18] V. Wood, M. J. Panzer, J. Chen, M. S. Bradley, J. E. Halpert, M. G. Bawendi, and V. Bulović, "Inkjet-Printed Quantum Dot-Polymer Composites for Full-Color AC-Driven Displays," *Advanced Materials*, vol. 21, no. 21, pp. 2151–2155, Jun. 2009.

[19] R. Ramakrishnan, N. Saran, and R. J. Petcavich, "Selective Inkjet Printing of Conductors for Displays and Flexible Printed Electronics," *Journal of Display Technology*, vol. 7, no. 6, pp. 344–347, Jun. 2011.

[20] S. J. L. R. Édison Pecoraro, Danilo Manzani, Younes Messaddeq, "Bacterial Cellulose from Glucanacetobacter xylinus: Preparation, Properties and Applications," in *Monomers, Polymers and Composites from Renewable Resources*, Mohamed Naceur Belgacem and Alessandro Gandini, Ed. Amsterdam: Elsevier, 2008, pp. 369–383.

[21] C. de Luca, "Electromyography," in *Encyclopedia of Medical Devices and Instrumentation*, J. G. Webster, Ed. Wiley-Interscience, 2006, pp. 98–109.

[22] M. R. Neuman, "Biopotential Electrodes," in *The Biomedical Engineering Handbook: Second Edition*, E. Bronzino, Ed. CRC Press, 2000.

[23] Y. M. Chi, T.-P. Jung, and G. Cauwenberghs, "Dry-contact and noncontact biopotential electrodes: methodological review.," *IEEE reviews in biomedical engineering*, vol. 3. pp. 106–19, Jan-2010.

Appendix D

Phycs paper

Experimental Study and Evaluation of Paper-based Inkjet Electrodes for ECG Signal Acquisition

Ana Priscila Alves[1], João Martins[2], Hugo Plácido da Silva[1], André Lourenço[1,3], Ana Fred[1] and Hugo Ferreira[2]

[1]*Instituto de Telecomunicações, Instituto Superior Técnico, Avenida Rovisco Pais, 1, 1049-001 Lisboa, Portugal*

[2]*Instituto de Biofísica e Engenharia Biomédica, Faculdade de Ciências da Universidade de Lisboa, Alameda da Universidade, 1649-004 Lisbon, Portugal*

[2]*Instituto Superior de Engenharia de Lisboa, Rua Conselheiro Emídio Navarro, 1, 1959-007 Lisboa, Portugal*

{*anapriscila.alves, hsilva, afred*}*@lx.it.pt, alourenco@deetc.isel.ipl.pt, joaopedr.martins@gmail.com, hhferreira@fc.ul.pt*

Keywords: Electrodes, Paper, Inkjet, Electrocardiography, Device.

Abstract: Applications involving biosignals, such as Electrocardiography (ECG), are becoming more pervasive with the extension towards non-intrusive scenarios helping targeting ambulatory healthcare monitoring, emotion assessment, among many others. In this study we introduce a new type of silver/silver chloride (Ag/AgCl) electrodes based on a paper substrate and produced using an inkjet printing technique. This type of electrodes can increase the potential applications of biosignal acquisition technologies for everyday life use, given that there are several advantages, such as cost reduction and easier recycling, resultant from the approach explored in our work. We performed a comparison study to assess the quality of this new electrode type, in which ECG data was collected with three types of Ag/AgCl electrodes: i) gelled; ii) dry iii) paper-based inkjet printed. We also compared the performance of each electrode when acquired using a professional-grade gold standard device, and a low cost platform. Experimental results showed that data acquired using our proposed inkjet printed electrode is highly correlated with data obtained through conventional electrodes. Moreover, the electrodes are robust to high-end and low-end data acquisition devices.

1 INTRODUCTION

Pervasive healthcare applications are becoming an invaluable tool for regular and non-intrusive monitoring. Biosignals play an important role in this kind of applications since they give information about the state of several vital organic tissues. Electrocardiographic (ECG) signals are probably the most well-known biosignals, and can be found in multiple applications in the medical and quality of life domains. It is commonly used to assess the overall cardiac function, measure the rate and regularity of heartbeats, and detect the presence of any pathology in the heart. The classical acquisition methods used in clinical or research studies typically recur to gelled silver/silver chloride (Ag/AgCl) electrodes. Given that ECG data acquisition has become more pervasive and inexpensive, enabling an easy access to continuous monitoring of the cardiac function, new and cheapest solutions have been proposed, with more practical electrodes and acquisition setups (Silva et al., 2011; Silva et al., 2013).

Paper has several advantages for ECG data acquisition in daily life scenarios; it enables: a) lower production costs; b) easier recycling; and c) simpler production, especially when considering the possibility of inkjet printing. When compared to plastic substrates such as polyethylene terephtalate (PET, ≈ 2 cent dm^{-2}) and polymide (PI, ≈ 30 cent dm^{-2}), paper has significantly lower production costs (≈ 0.1 cent dm^{-2}). In addition to this, considering the active disassembly design principles (Chiodo and Ijomah, 2012), paper is a good choice due to its environmentally friendly characteristics. Recently, it has been considered as a potential substrate for low-cost flexible electronics (Siegel et al., 2010; Leenen et al., 2009), which motivated us to do research on the possibility of using paper-based electrodes for biosignals acquisition. With such an approach and its ready availability, the electrodes can even be produced by the user himself or his caregivers.

The deposition of the conductive part of the electrodes to the paper substrate can be made recurring to photo-lithography, vacuum processes or printing

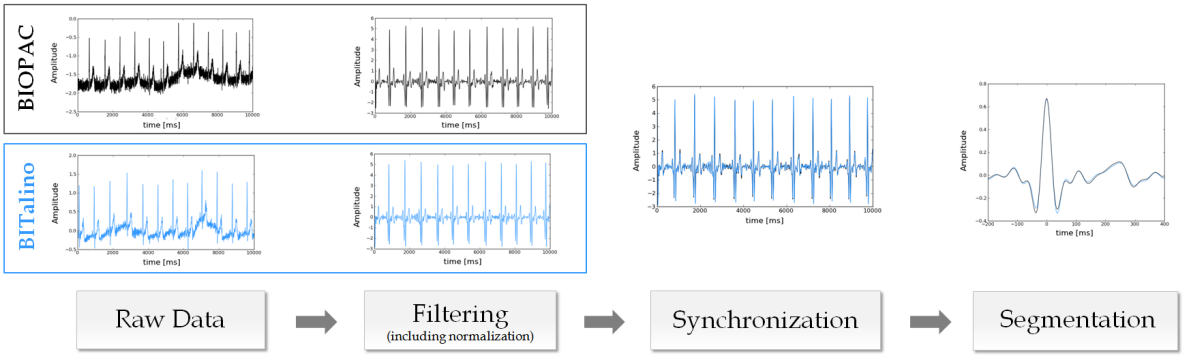

Figure 1: Block diagram of the pre-processing steps we have performed, to compare the signals acquired from both devices. The curves plotted in black were acquired using the BIOPAC while the blue ones with the BITalino

techniques. The use of printing techniques for fabricating electronics has several advantages over laboratory scale and subtractive batch processes (Tobjörk and Österbacka, 2011); printing is fast, low-cost, and widely used. In particular digital inkjet printing, which has been used as a research tool, is facilitating initial explorations of various aspects of printed electronics targeting the consumer market (Singh et al., 2010). The focus of this work was to explore the potential use of paper-based inkjet printed electrodes for ECG signal acquisition.

The most commonly used type of electrode is the gelled Ag/AgCl electrode; however, to make an acquisition setup more convenient for everyday use applications, other alternatives are emerging. Previous work from our group has started to explore the use of dry Ag/AgCl electrodes (Silva et al., 2011), which usually leads to signals with lower signal-to-noise ratio, although still suitable for monitoring or other non-intrusive applications. Thus, to study the characteristics of the paper-based inkjet printed electrodes, we perform a comparative study against the most common alternatives: i) gelled; ii) dry.

The remainder of the paper is organized as follows: in Section 2 we describe the proposed electrodes, focusing on their production and main characteristics; Sections 3 and 4 present the methodology applied in the comparison of the different electrode types and their quantitative evaluation; and finally, in Sections 5 and 6 we provide a summary of the experimental results and outline the main conclusions.

2 PAPER-BASED INKJET PRINTED ELECTRODES

The possibility of printing materials using inkjet technology brought several advantages to the conventional manufacturing procedures used, such as photolithography, transfer printing, among others. Comparing with those standard techniques for patterning thin films with high precision, some differences stand out. The appeal of inkjet technology lies in the fact that it is based on contactless deposition, which implies a lesser risk of contaminating the material, it is a maskless approach that makes an intuitive procedure, and it is an additive procedure, i.e., it is possible to print over a previous printed pattern (Singh et al., 2010).

Producing electrodes by inkjet printing enables the use of thin and flexible substrates that may also be biocompatible, examples of which are polydimethylsiloxane (PDMS) or biocellulose. On the other hand, low-cost paper-like substrates such as photo paper can be used as an alternative substrate and several conductive inks can already be used, such as silver, gold or conductive polymer (Calvert, 2001)).

We fabricated the electrodes using photo paper as substrate, due to its flexibility, availability, reduced thickness (230 μm) and easy maneuverability. To create the conductive part of the electrode we used a commercial printable silver ink from SunTronic, which is composed of silver nanoparticles and has been shown to provide good electrical conductivity for electronic applications.

The electrodes devised in the scope of our work were designed as a flat rectangle shape, with dimensions of 8 cm length, 3 cm width and approximately 1 μm thick. Each electrode has a total of 24 cm^2 of area in contact with the skin. The electrodes were first printed with four silver layers and aftwerwards subjected to heat treatment during 20 minutes at a temperature of 85 °C. With this heat treatment, we obtained a silver resistivity of $1.68 \times 10^{-6} \Omega.m$.

The second step of the fabrication process was to produce a layer which enables the transduction of ionic concentrations measured by electrodes into

electrical potentials. At the skin-electrode interface, the ionic signal (Cl^- ion transports the charge) is transformed into an electric signal. Likewise, in common silver electrodes this layer is typically made of AgCl (Clark et al., 2009). The formation of this layer was achieved by adding Cl^- ions, enabling a reaction between Ag and Cl to produce AgCl. However, due to the thin layer of silver and the fragility of the photo paper, the amount and the manner of introducing Cl^- ions is important. This process was optimized by using commercial bleach deposited by an airbrush at a distance of approximately 30 cm.

The third step in the production of these electrodes was focused on ensuring a good, long lasting, and practical contact between the electrodes and the acquisition hardware. To facilitate the connection of cables and make the electrodes practical for regular use, we use a metal stud and conductive snap. The snaps were placed in the back of the printed surface and the communication to the front was made through a hole filled with a conductive silver paste from Agar Scientific.

We estimated that each electrode produced with the procedure described would cost, approximately, 0.03€.

3 METHODOLOGY

We benchmarked the performance of our paper-based inkjet printed electrodes for ECG data acquisition, comparing them both to standard pre-gelled Ag/AgCl electrodes, and to the dry electrodes approach that we have been recently following (Silva et al., 2011). Reference data was collected using a BIOPAC biosignal acquisition unit, which has seen extensive use in the research domain and is considered to be a gold standard in biomedical research. However, this system has restricted operations and experimenting new customized solutions can damage the device. As such, we have used a BITalino acquisition system (Alves et al., 2013; Guerreiro et al., 2013), which give us a higher control over the system to try different experimental setups.

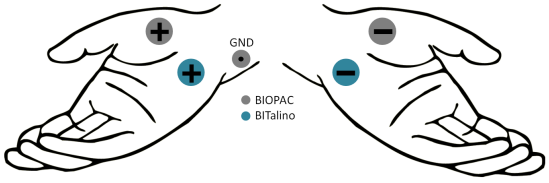

Figure 2: Electrode leads placement

This work is aligned with our research towards off-the-person ECG sensing (Silva et al., 2013), reason for which the ECG signals were acquired in the palmar region of the left and right hands, as illustrated in Figure 2. The electrodes used for data acquisition with the BIOPAC were always the pre-gelled Ag/AgCl, while with the BITalino we tested the previously mentioned 3 types of electrodes.

We devised our comparative study in two objectives:

1. comparison of the BITalino performance with a gold standard acquisition system, the BIOPAC;
2. comparison of electrodes for ECG acquisition.

The BITalino acquisition device adopts the 2-electrode approach with virtual ground, while the BIOPAC system is designed to collect data with the ground electrode. In order to inquire the BIOPAC performance after removing the ground electrode, we performed two experiments, with and without the ground electrode. To evaluate the performance of the dry, and paper-based inkjet electrodes in the ECG acquisition, we did 2 experiments in which we compared them with the pre-gelled ones. The experiments are summarized in Table 1.

Table 1: Summary of the experiments

Experiment	**BIOPAC**		**BITalino**
	type	GND	
1	Gel	Yes	Gel
2	Gel	No	Gel
3	Gel	No	Dry
4	Gel	No	Paper

Each experiment consisted of a 30 seconds recording performed simultaneously with the BIOPAC and the BITalino; we used a sampling rate of $1000\,Hz$ in both devices and a 12-bit resolution for the BIOPAC, whereas the BITalino has a 10-bit resolution. The BIOPAC raw data was reduced to 10 bits, to be at the same resolution as the BITalino signals. We have collected raw ECG data from 20 subjects in a static standing position, with the electrodes applied as shown in Figure 2

The data obtained by each device was pre-processed in three main steps, as represented in Figure 1. Taking the raw data as input, the baseline wander was corrected through a two-stage median filter, as proposed by (De Chazal et al., 2004), and the signals were filtered using a Finite Impulse Response (FIR) bandpass filter with a Hamming window of $300\,ms$, and cutoff frequencies of $5-20\,Hz$. The filtered signals were normalized to their maximum and minimum amplitudes, where the original signal

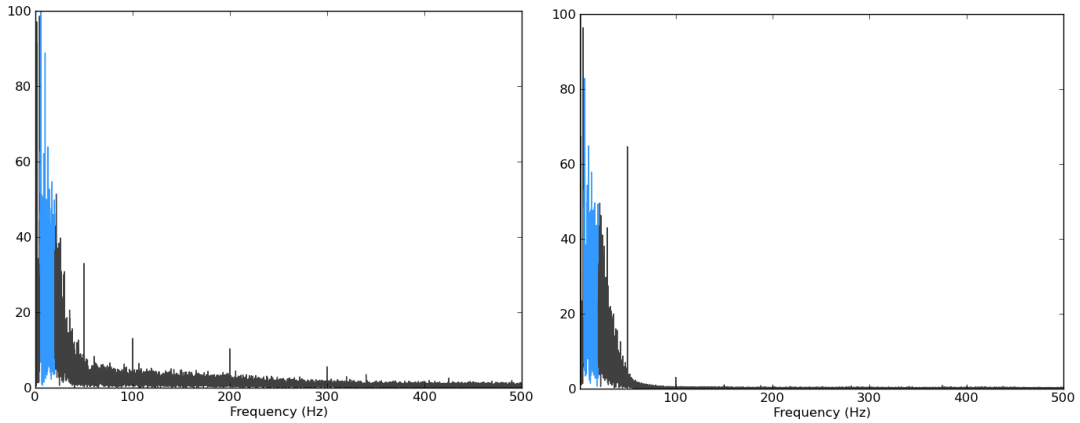

(a) BIOPAC (b) BITalino

Figure 3: Example of the ECG signal frequency spectrum for data collected with each acquisition device in one of the recording sessions. The blue region shows the interest spectral band and the remainder the noise

is subtracted of its mean, and divided by its standard deviation.

To prevent any possible electrical interference between the devices prone to bias the results and resulting from a hard wired connection between both devices, we chose to do the synchronization using the RR time intervals. Given that the comparison of the ECG data obtained from two independent systems can only be correctly performed for data expressed in the same time base, our synchronization method consists on the following steps:

1. Detection of the QRS complex in each independent signal, using the method proposed by (Engelse and Zeelenberg, 1979)
2. Let $RR_{BIOPAC} = \{RR_{BIOPAC_0}, ..., RR_{BIOPAC_n}\}$ and $RR_{BITalino} = \{RR_{BITalino_0}, ..., RR_{BITalino_m}\}$ be a set of RR time intervals for the n and m heartbeat waveforms detected respectively in the BIOPAC and BITalino ECG time series.
3. Construct a matching matrix, M, in which the entry $M(i, j)$ corresponds to the absolute value of the difference between the RR time intervals extracted from the BIOPAC and BITalino ECG time series, that is:
$$M(i, j) = |RR_{BITalino_i} - RR_{BIOPAC_j}| \quad (1)$$
4. Let $\#M$ be the number of items where $M(i, j) \leq RR_{th}$
5. If $\#M > Sync_{th}$, the synchronization is complete. Otherwise, go to next step.
6. Consider $RR_{BITalino}(k) = \{RR_{BITalino_k}, ..., RR_{BITalino_m}\}$. Repeat steps 3 and 4 for each value of $k \in \{1, ..., m\}$ and compute each value of $M(i, j) = |RR_{BITalino_i}(k) - RR_{BIOPAC_j}|$.
7. Find the k value where $\#M$ is higher
8. Synchronize the signals by applying a delay of k samples to the BITalino signal.

The acquisition was always initiated first with the BITalino, so it has the higher time series. We defined 2 thresholds in the synchronization method, $Sync_{th}$ and RR_{th}. The $Sync_{th}$ value applied was 20, since it is approximately the minimum number of heartbeats expected in a 30 seconds ECG signal. The RR_{th} threshold represents the minimum difference of RR time intervals, from different acquisitions, where the R peaks are considered to match in the time domain. Since the acquisitions were performed by two different systems, it is expected a small deviation between the instants where the same R peaks occur. Therefore, we considered that $5\,ms$ is the maximum value where the R peaks are considered to occur in the same instant. Finally, the individual heartbeat waveforms were segmented and scaled between 0 and 1; we consider the heartbeat waveform to be the $[-200; 400]\,ms$ interval around the R peak instant.

4 EVALUATION METRICS

Two metrics were employed for numerical evaluation purposes, namely the Signal-to-Noise Ratio (SNR) computed from the data collected with both devices for each of the 4 experiments, and the Root Mean Square Error (RMSE) of the cosine distance, to assess the morphological correlation between the heartbeat waveforms obtained with the BIOPAC and the BITalino, when using each type of electrodes. For the SNR calculation, we considered the interest signal to be concentrated on the $5 - 20\,Hz$ band of its

frequency spectrum, and the remainder as noise. For each record we calculated the difference between the SNR obtained from BITalino and BIOPAC acquisition.

Figure 3 illustrates an example of the frequency spectrum of ECG data acquired in both devices, for one of the test subjects in the experiment 1. The 50 Hz power line interference is visible in both signals; however, since the BITalino ECG sensor has an analog band pass filter from 0.5 to 40Hz, the higher frequencies are almost eliminated, contrary to what happens with the BIOPAC.

For the cosine distance calculation, the synchronized signals were segmented into individual heartbeat waveforms, and the distance between a given segment in the BIOPAC time series and the matching segment in the BITalino time series was calculated. The cosine distance, D_{cos}, between the signals x and y is given by Equation 2

$$D_{cos}(x,y) = 1 - \frac{\sum_{k=1}^{m} x[k]y[k]}{\sqrt{\sum_{k=1}^{m} x[k]^2 \sum_{k=1}^{m} y[k]^2}}, \quad (2)$$

The reason why we have calculated the cosine distance for each heartbeat, instead of using the entire signal, is due to the fact that we were only interested in the ECG waveform shape, which is comprised in the heartbeat region. To validate the similarity between the signals acquired from the two devices, we compute the RMSE, as defined in Equation 3

$$RMSE(x,y) = \sqrt{\frac{\sum_{j=1}^{N} \left(D_{cos_j}(x,y)\right)^2}{N}} \quad (3)$$

5 EXPERIMENTAL RESULTS

The results obtained for each experiment in the 20 subjects are represented in Figure 4.

The box plots display the distribution of the SNR differences across all the subjects. The height of the box plot indicates the degree of dispersion, the band inside the box represents the median, and the bottom and top of the box are the first and third quartiles. The smallest SNR difference between devices was obtained in the experiment 1, where the median value is lower and the degree of dispersion is reduced. This was already expected since the presence of the ground electrode in the BIOPAC device and the use of gelled electrodes in both systems correspond to the best case scenario in which the amount of captured noise is minimal. The higher dispersion obtained was in the experiment 4, due to higher noise presence in the signals.

Table 2 summarizes the results obtained for the signals collected using each device. In all the experiments, the SNR of BITalino was higher than BIOPAC, which was already expected due to the analogic filtering occuring in the BITalino ECG sensor.

Table 2: Experimental Results from BIOPAC and BITalino ECG signals acquisition, in the 4 experiments

Experiment	RMSE	SNR [dB] BITalino	SNR [dB] BIOPAC
1	0.0043 ± 0.0053	-1.02 ± 2.04	-2.04 ± 2.31
2	0.0042 ± 0.0039	-1.19 ± 1.84	-3.35 ± 2.45
3	0.0063 ± 0.0055	-1.62 ± 2.21	-3.69 ± 2.54
4	0.0042 ± 0.0043	-1.87 ± 2.14	-3.80 ± 2.66

The lowest value of SNR with the BITalino device was obtained in the experiment 4, when using the paper electrodes, indicating a higher noise presence. In what concerns the morphological correlation between waveforms, all the experiments have shown a high similarity between the ECG signals obtained from both devices. The signals acquired have a good approximation to the well known prototypical ECG waveform, providing an easy identification of the characteristic P-QRS-T complexes. Figure 5 presents an overlay with all the individual heartbeat waveforms collected in one of the recording sessions, showing the median and standard deviation of all the segments obtained from both devices in the four experiments. As we can see, the waveform morphology is maintained throughout the experiments and is virtually indistinguishable between devices and materials.

From the cosine distance results, we have calculated the Root-Mean-Square Error (RMSE), and the results are described in Table 2. For all the experiments, we verified very low RMSE values, indicating that the signals obtained from all three types of

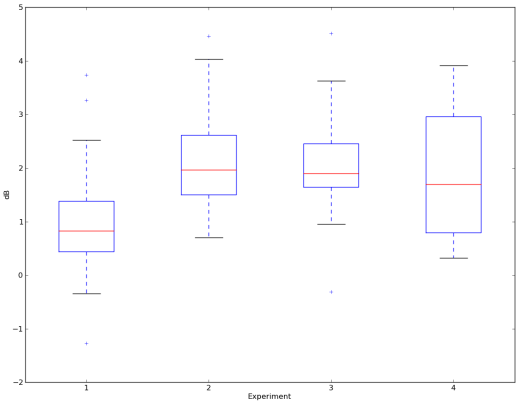

Figure 4: Boxplot of the difference between BITalino and BIOPAC Signal-to-Noise Ratio for each experiment

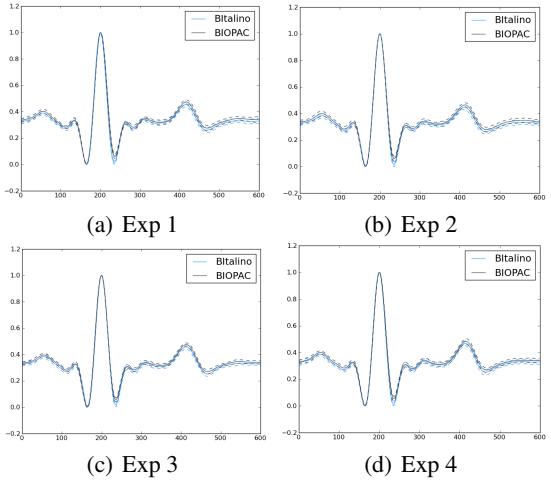

(a) Exp 1 (b) Exp 2

(c) Exp 3 (d) Exp 4

Figure 5: Segmented heartbeat waveforms from the BITalino (blue) and the BIOPAC (grey); the solid wave represents the mean, and dashed line the standard deviation.

electrodes retain much of the waveform morphology when compared to the signals obtained with the gold standard BIOPAC setup. An interesting finding is that the inkjet printed electrodes shows a very good performance when compared to the other electrodes, with a RMSE of 0.0042, while with the dry electrodes we obtained the worst results, with a RMSE of 0.0063. Although the signals obtained with the paper-based electrodes present a lower signal-to-noise ratio, the ECG morphology is maintained, which results in a similar performance to that found for the case in which standard clinical-grade pre-gelled Ag/AgCl electrodes are used. Moreover, the signals acquired with the BITalino device are highly correlated to those obtained with the BIOPAC, actually exhibiting lower noise levels in raw ECG signals.

6 CONCLUSIONS

In this paper we have proposed and evaluated paper-based inkjet printed electrodes for ECG data acquisition. We presented the fabrication steps, and benchmarked our electrodes against standard clinical-grade pre-gelled Ag/AgCl electrodes, and dry electrodes. Data acquisition was performed using a BIOPAC system, considered to be a gold standard within the biosignal research community, although due to the fact that it is a closed system, we have also supported our analysis on the BITalino, a physiological computing platform first introduced by our team.

The collected data was evaluated using the Signal-to-Noise Ratio (SNR), and a morphological waveform correlation index based on the Root Mean Square Error (RMSE). Experimental results have shown that the proposed approach explored in this work achieves comparable performance when compared with a reference sensor. Our evaluation has revealed that the heartbeat waveforms measured through the proposed approach are nearly identical to those obtained with the gold standard equipment.

This approach opens new possibilities in the field of biosignals, enabling people (e.g. patients and/or caregivers) to have easier access to consumables in continuous ambulatory monitoring scenarios. We believe our approach to have the threefold advantage of reducing production costs, being easier to recycle, and being more accessible when compared to conventional approaches.

REFERENCES

Alves, A. P., Silva, H., Lourenço, A., and Fred, A. (2013). BITalino: A Biosignal Acquisition System based on Arduino. In *Proceeding of the 6th Conference on Biomedical Electronics and Devices (BIODEVICES)*.

Calvert, P. (2001). Inkjet Printing for Materials and Devices. *Chemistry of Materials*, 13(10):3299–3305.

Chiodo, J. and Ijomah, W. (2012). Use of active disassembly technology to improve remanufacturing productivity: automotive application. *International Journal of Computer Integrated Manufacturing*, 0(0):1–11.

Clark, J. W., Neuman, M. R., Olson, W. H., Peura, R. A., and Primiano, F. P. (2009). *Medical instrumentation: application and design*. John Wiley & Sons, inc, fourth edition.

De Chazal, P., O'Dwyer, M., and Reilly, R. (2004). Automatic classification of heartbeats using ECG morphology and heartbeat interval features. *IEEE Transactions on Biomedical Engineering*, 51(7):1196–1206.

Engelse, W. A. H. and Zeelenberg, C. (1979). A single scan algorithm for QRS-detection and feature extraction. *Computers in Cardiology*, 6:37–42.

Guerreiro, J., Silva, H., Lourenço, A., Martins, R., and Fred, A. (2013). BITalino:A Multimodal Platform for Physiological Computing. In *Proceeding of the 10th International Conference on Informatics in Control, Automation and Robotics (ICINCO)*.

Leenen, M. A. M., Arning, V., Thiem, H., Steiger, J., and Anselmann, R. (2009). Printable electronics: flexibility for the future. *physica status solidi (a)*, 206(4):588–597.

Siegel, A. C., Phillips, S. T., Dickey, M. D., Lu, N., Suo, Z., and Whitesides, G. M. (2010). Foldable printed circuit boards on paper substrates. *Advanced Functional Materials*, 20(1):28–35.

Silva, H., Carreiras, C., Lourenço, A., and Fred, A. L. N. (2013). Off-the-person electrocardiography. In *International Congress on Cardiovascular Technologies (CARDIOTECHNIX)*.

Silva, H., Lourenço, A., Lourenço, R., Leite, P., Coutinho, D., and Fred, A. (2011). Study and evaluation of a single differential sensor design based on electro-textile electrodes for ECG biometrics applications. In *Proceedings of the IEEE Sensors Conference*, pages 1764 – 1767.

Singh, M., Haverinen, H. M., Dhagat, P., and Jabbour, G. E. (2010). Inkjet printing-process and its applications. *Advanced Materials*, 22(6):673–685.

Tobjörk, D. and Österbacka, R. (2011). Paper electronics. *Advanced Materials*, 23(17):1935–1961.